SYNTHESIS OF ANGIOGENESIS INHIBITORS AND THEIR CONJUGATION TO MACROMOLECULES

by

Gamze TANRIVER

B.S., Chemistry, Ondokuz Mayıs University, 2007

Submitted to the Institute for Graduate Studies in
Science and Engineering in partial fulfillment of
the requirements for the degree of
Master of Science

Graduate Program in Chemistry
Boğaziçi University

2010

To my family and my friends

ACKNOWLEDGMENTS

I would like to express my most sincere gratitude to my thesis supervisor Assist. Prof. Rana SANYAL for her endless attention and scientific guidance throughout this study. I appreciate her support and useful comments throughout my laboratory work.

I wish to express my thanks to Assist. Prof. Amitav Sanyal for his careful and constructive review of the final manuscript and for his care and help during my masters program.

I would extend my thanks to Assoc. Prof. Işıl Aksan Kurnaz for her helpful discussions regarding all my research in this laboratory and for her help during my masters program.

I would like to thank to Ayla Türkekul, Burcu Selen Çağlayan for running a large number of NMR.

I would like to express my gratitude to my former and present labmates, Özgül, Melike, Gönül, Hikmet, Tuğba, Duygu, Eun Ju, Nuray, Tuğçe, Elif, Saltuk, Sebla, Nergiz, Mehmet, Sezin, Serap, Gülen, Merve, Ece, Oyuntuya, İpek, Pınar, Pelin, Güven and my friends for their enjoyable company and friendship. I would like to thank all my friends and all the members of the faculty in the Chemistry Department.

Finally, my deepest thanks go to my whole family for their endless love, support and encouragement throughout these years.

This research has been supported by Boğaziçi University BAP 09S107 and TÜBİTAK 107T623 & 108T898.

LIST OF SYMBOLS/ ABBREVIATIONS

J	Coupling constant
υ	Frequency

ATRP	Atom transfer radical polymerization
CA-4	cis - combretastatin A-4
CA4P	Combretastatin A-4 phosphate
$CDCl_3$	Deuterated chloroform
CH_2Cl_2	Dichloromethane
DMAP	4-Dimethylaminopyridine
EtOAc	Ethyl Acetate
FT-IR	Fourier Transform Infrared
GPC	Gel Permeation Chromotography
HUVEC	Human Umbilical Vein Endothelial Cells
Hz	Hertz
MeOH	Methanol
MAC	Methacryloyl chloride
NMR	Nuclear Magnetic Resonance
PT	Polymer Therapeutics
PEG	Poly(ethylene glycol)
PEGMA	Poly(ethylene glycol) monomethyl ether methacrylate
PPX	Poly-L-glutamic acid-paxlitaxel conjugate
TEA	Triethylamine
THF	Tetrahydrofuran

ABSTRACT

SYNTHESIS OF ANGIOGENESIS INHIBITORS AND THEIR CONJUGATION TO MACROMOLECULES

Angiogenesis is a term used for formation of new blood vessels from pre-existing vessels. Normally, angiogenesis process is essential for wound healing yet, unregulated angiogenesis plays a pivotal role on tumor growth and metastasis. Anti-angiogenesis agents are widely used in combination therapy for cancer. Selectivity toward newly formed and disorganized blood vessels around the tumor is an attractive tool for reduced toxicity. Cell cycle inhibitors, the more commonly used anticancer agents, target fast reproducing cells: tumor cells and others such as erythrocytes and leukocytes, frequently causing hemoglobin deficiency and neutropenia, respectively. This on mechanism action of the anti-cancer agents render them less effective since the dose has to be reduced where the toxic side effects are tolerable. Many angiogenesis inhibitors entering the market in recent years, have proven successful in the clinic, with reduced side effects as well as shrunk tumor size.

Polymer conjugates – covalent combination of a macromolecule with a small molecule – have been attractive tools for drug delivery. Conjugation of the small molecule to a polymer provides water solubility, reduced toxicity and prolonged half life owing to the slower clearance. Furthermore accumulation in the tumor due to the large size of the molecule is an important driving force for utilization of polymer therapeutics for cancer chemotherapy. This thesis will focus on modification of an anti-angiogenesis agent and conjugation to a biocompatible and biodegradable polymer.

ÖZET

ANJİYOJENEZ İNHİBİTÖRLERİNİN SENTEZİ VE MAKROMOLEKÜLLERLE BİRLEŞTİRİLMESİ

Anjiyojenez önceden varolan damarlardan yeni kan damarları oluşumu için kullanılan bir terimdir. Normalde, anjiyojenez prosesi yaraların iyileşmesi için gereklidir fakat kontrolüz anjiyojenez tümör büyümesi ve yayılmasında büyük önem taşır. Anti-anjiyojenez ajanlar yaygın olarak kanser için birleştirilmiş terapide kullanılır. Yeni oluşan ve organize olmayan tümör etrafındaki kan damarları toksisitenin azaltılması için ilgi çekici bir araçtır. Daha çok anti-kanser ajanı olan hücre çemberi inhibitörleri hızlı üreyen hücreleri hedefler; tumor hücreleri ve diğerleri; sırasıyla genellikle hemoglobin eksikliği ve netrofeniyle sonuçlanan eritrosit ve lekosit. Toksik etkilerin tolere edilebildiği yerde dozun azaltılması gerektiği için anti-kanser ajanların mekanizmaları onları daha az etkili kılar. Son yıllarda markete giren anjiyojenez inhbitörleri azaltılmış yan etkilerin yanı sıra tümör boyutlarının küçültülmesi ile klinikteki başarısını kanıtladı.

Polimer konjugasyonları (makromoleküllerin küçük moleküllerle kovalent kombinasyonları) ilaç teslimi için ilgi çekici bir araçtır. Küçük moleküllerin polimer konjugasyonu daha yavaş temizlendiği için suda çözünürlük, azaltılmış toksisite ve uzatılmiş yarı ömrü sağlar. Ayrıca, büyük boyutta molekül olduğundan dolayı tümördeki birikmesi kanser kemoterapi için polimer tedavi edicilerin kullanımı açısından önemli bir itici güçtür. Bu tez anti-anjiyojenez ajanın modifikasyonu ve biyobozunur ve biyouyumlu polimer ile konjugasyonunu içerir.

TABLE OF CONTENTS

LIST OF FIGURES

LIST OF TABLES

INTRODUCTION

1.1. Cancer

Cancer is described as a disease of cell which loses its normal growth control. Cancer cells do not know how to die, which is called apoptosis. Therefore, uncontrolled growth of cells and metastasis which means dissemination of cancer cells to other parts of the body are formed [1]. The process of angiogenesis plays a crucial role on these conditions.

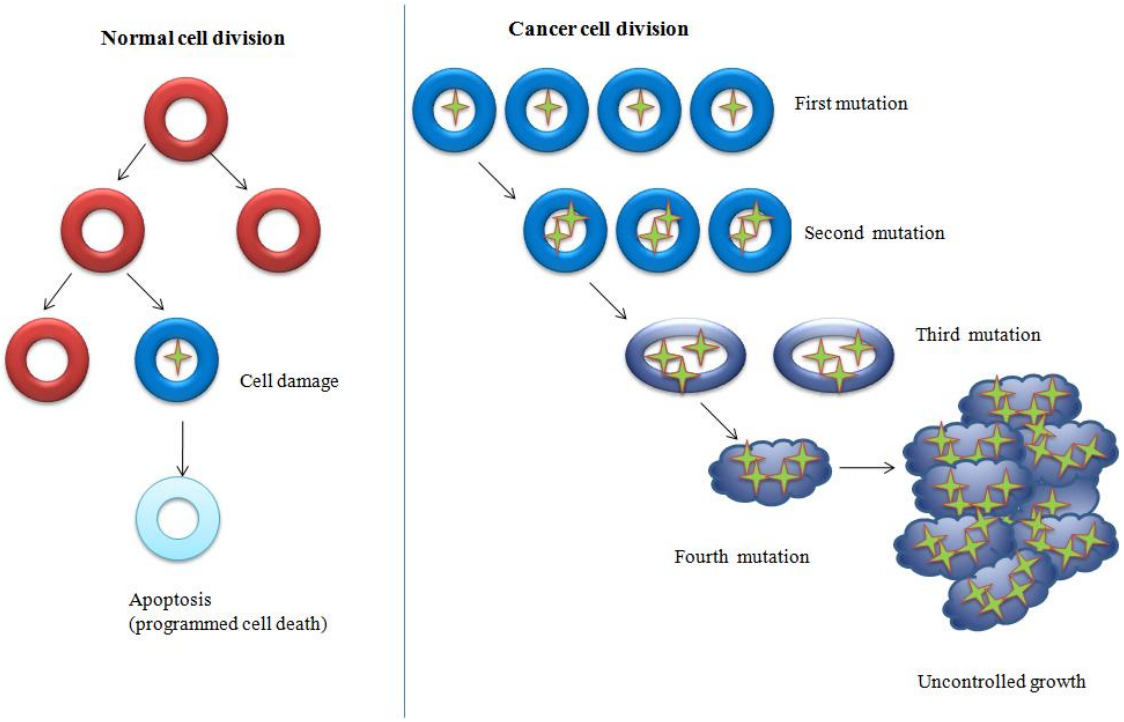

Figure 1.1. Cell divisions of normal and cancer cell [1]

1.2. Angiogenesis

In 1971, Judah Folkman firstly proposed anti-angiogenic therapy might be a useful route to treat cancer. Angiogenesis is a term used for formation of new blood vessels from pre-existing vessels [2]. Normally, angiogenesis process is essential for wound healing yet, unregulated angiogenesis plays a pivotal role on tumor growth and metastasis.

Angiogenesis process consists of complex steps. Since tumor cells need oxygen and nutrients to grow and spread when tumors reach clinically detectable mass or steady state,

tumors send a signal to express angiogenic inducers including growth factors, chemokines, angiogenic enzyme, endothelium specific receptors and adhesion molecules for growth of more vessels. After expressing angiogenic inducers, neovascularization facilitates that cancer cells penetrate the blood stream and spread to other organs or tissues. When clarifying angiogenesis process, it is important to stress that VEGF guides vascular permeability that is important for tumor growth and metastasis. Hypoxia (oxygen deficiency) expresses VEGF (vascular endothelial growth factor) and its receptor via HI-1a [3]. Figure 1.2 displays how tumor progress can switch with angiogenesis.

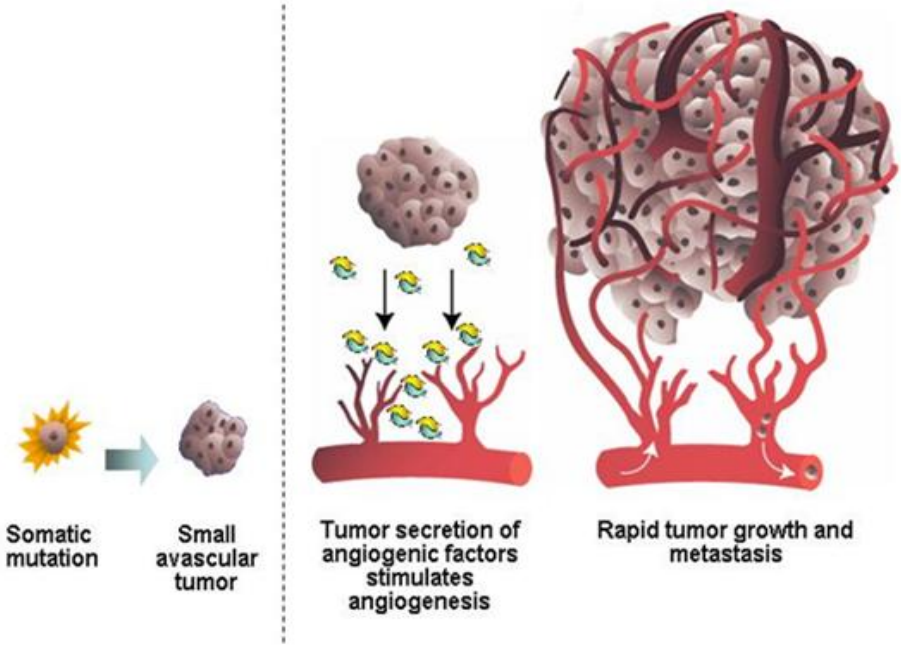

Figure 1.2. Summary of angiogenesis [4]

The angiogenic inhibitiors remarkably offer specific targeting opportunity. Nowadays, vast of anti-angiogenic drugs are in clinical trials and in markets. For instance, bevasicumab (Avastin), Iressa (Gefitinib), Sorafenib (Bay 43-9006, Nexavar), Sunitinib (SU-11248, Sutent), Tarceva (Erlotinib) got FDA (Food and Drug Administration) approvals [2]. When compared to conventional chemotherapy, anti-angiogenic therapy provides selective targeting, less side effects and safer toxicity profile. Additionally, in contrast with genetic instability of tumors, endothelial cells have rare spontaneous mutations. Anti-angiogenic agents affect endothelial cells that are directly contact with

blood circulation. On the contrary, tumor cells are far away from tumor tissue and accessibility of chemotherapy drugs to tumor cells is lesser. Turnover of tumor endothelial cells might be 50 higher than endothelial cells in health tissue [3].

1.3. Chemotherapy

Conventional chemotherapy is a way to treat cancer by delivering anticancer agent to tumor. Chemotherapy drugs affect rapidly dividing cell including both tumor growing fast and healthy tissue with high growth fraction indiscriminately and accordingly selectivity of the drugs are poor. Besides, toxicity is dose limiting in this system since vast of adverse side effects are observed such as, bone marrow toxicity (decrease in white blood cells (WBC) and red blood cells (RBC), hair loss, cardiotoxicity, nausea, gastrointestinal and skin problems and vulnerability to illness. That is why the amount of drugs given to patient is restricted. In addition to that, genomic instability of tumor cells leads to drug-resistant by decreasing activity of chemotherapy drugs [3], [5], and [6]. To combat undesired side effects, polymer therapeutics is a novel way because many chemotherapy drugs are open to be improved their pharmacokinetic profiles.

1.4. Polymer Therapeutics (PT)

Polymer therapeutics (PT) has been one of the most attractive drug delivery techniques over past decades in term of remarkable potential in medicine, nanotechnology and therapeutic applications. PT is a comprehensive term including polymeric drugs, polymer-drug conjugates, polymer-protein conjugates and polymeric micelles. In 1975, Ringsdorf first introduced the concept of polymer-drug conjugates and opened an important gate to PT and also Duncan and coworkers are pioneers of PT [7].

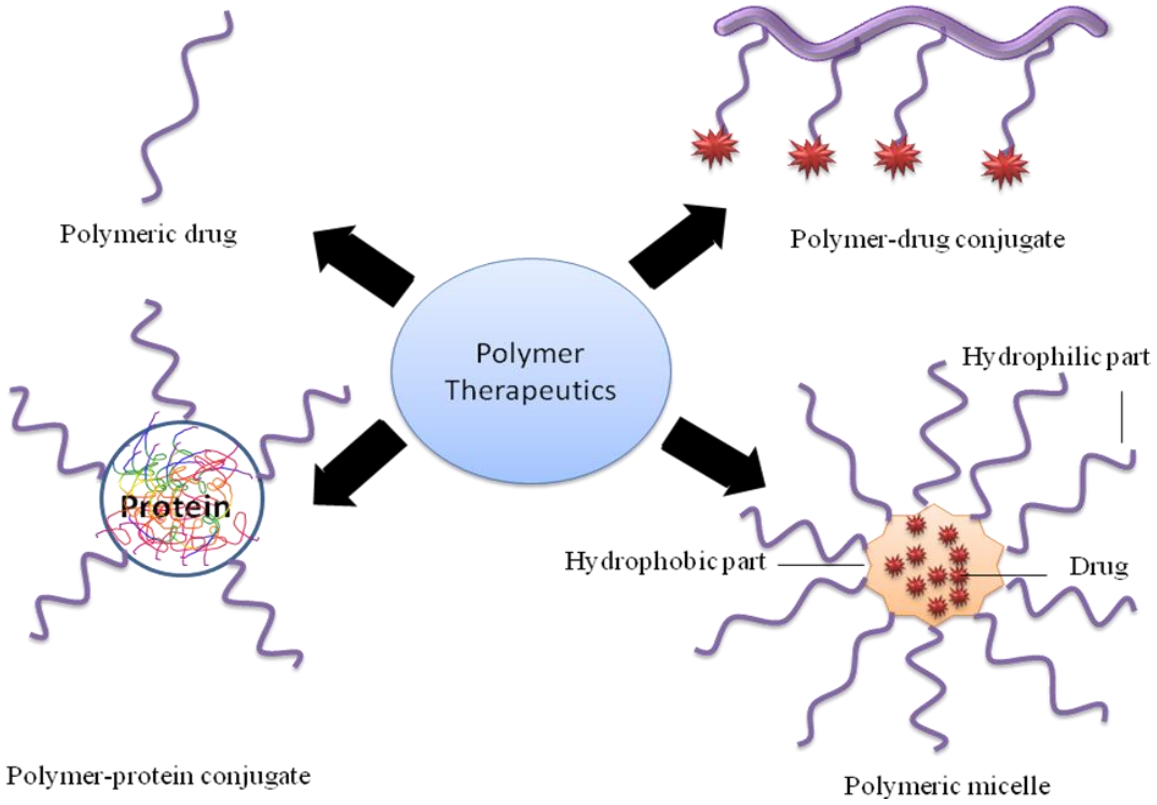

Figure 1.3. Schematic representation of PT [8]

Polymer-drug conjugates which are covalently attached to each other outweigh small molecules and offer significant opportunities due to controlled delivery of drug, increased drug efficiency. Clearly, polymer-drug conjugates improve drug solubility, reduce toxicity and undesired side effects, prolong drug residence in tumor thanks to EPR effect and provide slow body clearance, increase blood circulation time, and overpass drug resistance.

Moreover, compared to small molecule, polymers have higher molecular weight, can carry multiple copies of drug leading to less frequent dose application and load different type of drugs on the same polymer. It is important to stress that choice of polymer is very important owing to fulfilling some fundamental requirements such as biocompatibility, stability under physical conditions, non-immunogenic, non-toxic and reduced side effects. Thanks to living polymerization method desired polymeric structures can be prepared [7]. Novel polymeric architectures that are used in PT are graft, star shaped, branched, dendrimer and dendronized polymer [8] [Figure 1.4].

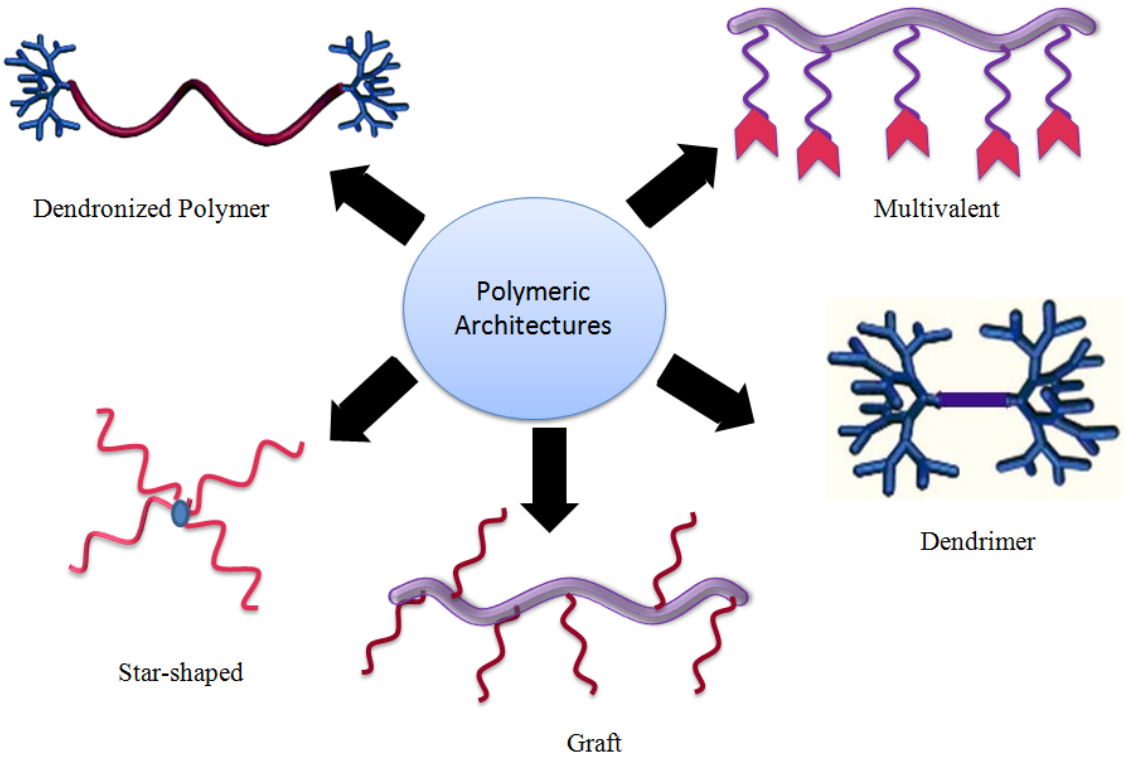

Figure 1.4.Schematic representation of novel polymeric architectures [8]

Drug release from polymeric structure can be manipulated by pH, enzyme, temperature, net charge to enhance drug efficiency by increasing local concentration of drug molecule at desired area [7].

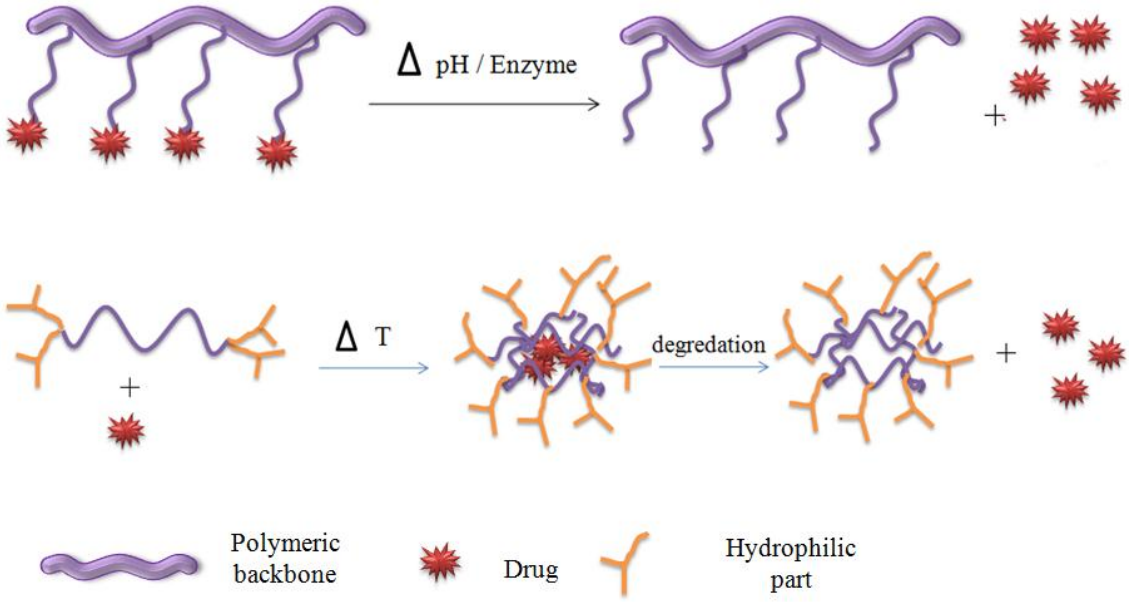

Figure 1.5. Schematic representation of cleavage type of polymer-drug conjugates [7]

By taking all advantages, anti-angiogenic agents can be conjugated with polymers having ideal linker to cleave by pH, enzyme, temperature, net charge to improve pharmacokinetic profile of anti-angiogenic agents.

As come to today, more than fourteen polymer-drug conjugates are in clinical trial [9]. Figure 1.7 demonstrates some of polymer-drug conjugates accepted as anti-cancer agents designed for passive targeting through the EPR effect.

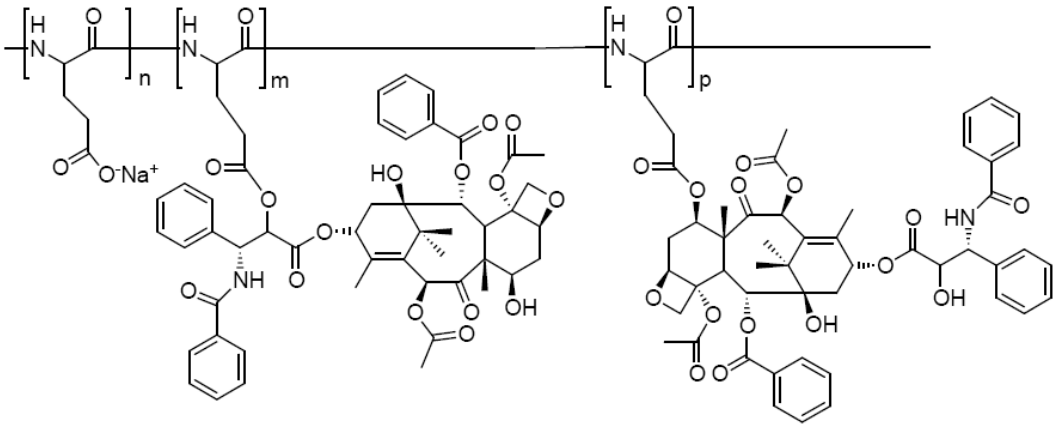

OPAXIO®

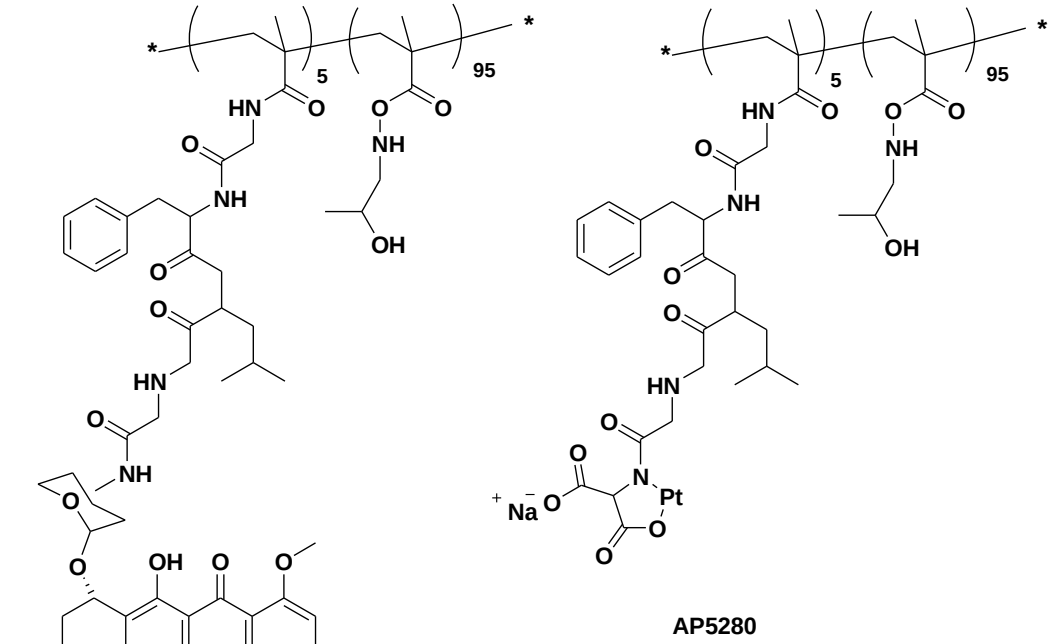

AP5280

PK1

Figure 1.6. Polymer–drug conjugates being accepted as anticancer agents.

Poly-L-glutamicacid–paclitaxel conjugate (OPAXIO, CT-2103); N-(2-hydroxypropylmethacrylamide (HPMA) copolymer–doxorubicin (PK1; FCE28068); HPMA copolymer–platinate (AP5280) [8].

Poly-L-glutamicacid(PGA)-paclitaxel conjugate (PPX), known as OPAXIO® which is accepted the most advanced anticancer polymer-drug conjugate has undergone phase III clinical trial for treatment of patients with non-small lung cancer (NCLC). PPX can be used both a single agent and combined with other drugs or radiotherapy to improve anti-cancer efficiency. By taking advantage of EPR effect, PPX accumulates on tumor more, stays in the body longer, prolongs tumor exposure and offers less toxic treatment opportunity. According to result of combination with carboplatin, patient with advanced stage III/ V primary ovarian cancer gave 98 % response [8].

Paclitaxel alone is one of widely used clinically active cytotoxic drug by inducing mitotic arrest, and apoptosis. According to study of Jack W. Singer, PPX (48 kDa) was devised to improve pharmacokinetic profile of paxlitaxel owing to hydrophobicity of paclitaxel and adverse side effects. Poly-L-glutamicacid (PGA), highly charged polymer is biodegradable and water soluble polymer. Paclitaxel conjugates on PGA by ester linkage in the body this bond is cleaved by lysosomal enzymes (cathepsin B) and 2' hydroxyl of paclitaxel which is inactive when conjugated is a pivotal for tubulin binding. Plasma C_{max} and AUC values for PPX and paclitaxel alone demonstrate that PPX stays in the plasma longer than standard paclitaxel (nearly 3 fold and 1000 fold respectively) and release active agent at negligible rate. These results lead to higher amount of PPX will reach targeted site and accumulate in the tumor vasculature.

Plasma concentration vs. Time graph shows that free paclitaxel declines fast. This means toxicity. On the contrary, PPX is stable in the plasma and less release of active agents is observed and in three weeks after administration of PPX, drug is still detectable [Figure 1.7].

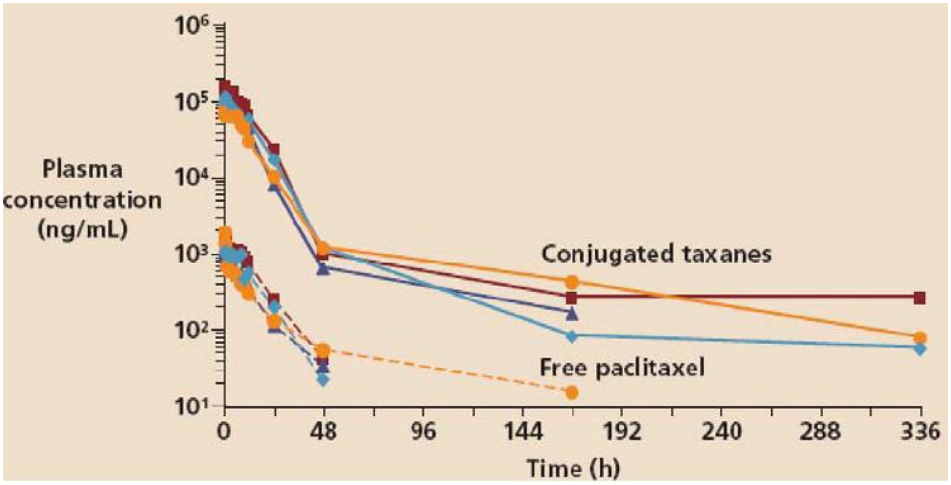

Figure 1.7. Plasma concentrations of conjugated taxanes and free paclitaxel after the first administration of PPX in four representative patients [10]

PPX shows a constant release and prolongs tumor exposure. In addition, half life of PPX is longer than paclitaxel and also accumulates on the tumor more. Paclitaxel alone has less tumor exposure and short half-life.

In brief, PPX is water soluble macromolecule version of paclitaxel. PPX has small volume of distribution, longer half-life and longer elimination phase and targets tumor tissue specifically via EPR effect as compared to paclitaxel [10].

1.4.1 EPR Effect

In 1986, Maeda and Matsuma introduced a phenomenon, named 'Enhanced Permeability and Retention Effect' (EPR effect) for controlled drug delivery. Remarkable difference in tumor uptake between small molecule and biocompatible macromolecules, named SMANC that used in their study was observed. Macromolecule stayed in the body longer and accumulated more, also prolonged body clearance. Additionally, experiments after their collaboration with Prof. K. Ulbrich and Prof. R. Duncan supported previous results.

In the light of this historical background, it is stressed that EPR effect can be used to treat almost all human cancer types. Anatomical and functional abnormalities result in EPR effect. Primary anatomical abnormalities include extensive angiogenesis and high vascular

density, lack of smooth-muscle layer, defective vascular architecture, insufficient lymphatic clearance, and slow venous return. Primary generation of permeability-anhancing factors also are vascular endothelial growth factor (VEGF), nitric oxide (NO),and peroxynitrite (ONOO_) [11].

Tumor cells need oxygen and nutrients to grow and spread. In this connection, angiogenesis is encouraged. Healthy cells are well-ordered and endothelial cells are well-organized, not leaky. However, newly formed vessels around tumor are immature and have irregular shape. Endothelial cells around the tumor are not well ordered and are leaky. In other words, poor lymphatic drainage and wide lumen of tumor vessels form basement of EPR effect. Thanks to poor lymphatic drainage, macromolecules can penetrate and accumulate in tumor, then release drug molecule to show antitumor activity.

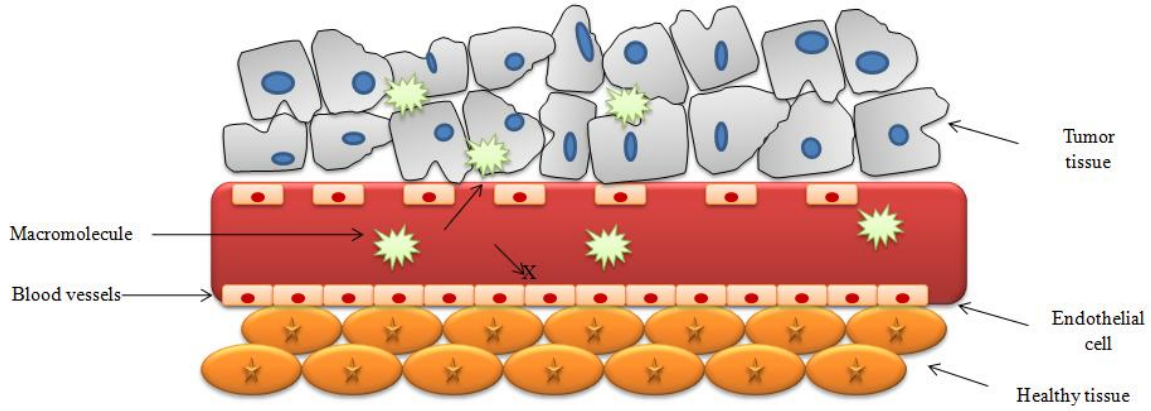

Figure 1.8. Schematic representation of EPR effect [2]

EPR effect offers significant advantages, namely prolonged half-life, stealth-character and non-immunogenicity, enhanced solubility, cellular uptake and stability, receptor-mediated drug targeting, patient compliance and quality of life [6], [11]. That is why conventional chemotherapy starts to be given up.

1.5. Combretastatin A-4

Many angiogenesis inhibitors have been studied to date, yet general issue among them is that selective targeting to endothelial cells is hard. Newly formed irregular shaped vasculatures and tumor vasculatures have an impact on unique proteins. By using this uniqueness, selective pharmacological targeting can be achieved.

Cis-Combretastatin A-4 (CA–4) which is a natural substance was firstly extracted from Combretum Cafrum by Pettit and coworkers in 1982. CA-4 is one of the most powerful antivascular disrupting agents and displays selectivity toward endothelial cell. Structural activity relationship (SAR) of CA-4 is that ethene bridge between the rings provide structural rigidity to required for activity of the compound. Three methoxy group is also very important to display anti-tubulin and cytotoxic activity. Witting reaction and Perkin condensation reaction are two popular methods to synthesize CA-4 but CA-4 is achieved with high yield via Perkin condensation reaction due to predomination of Z isomer of CA-4 [12].

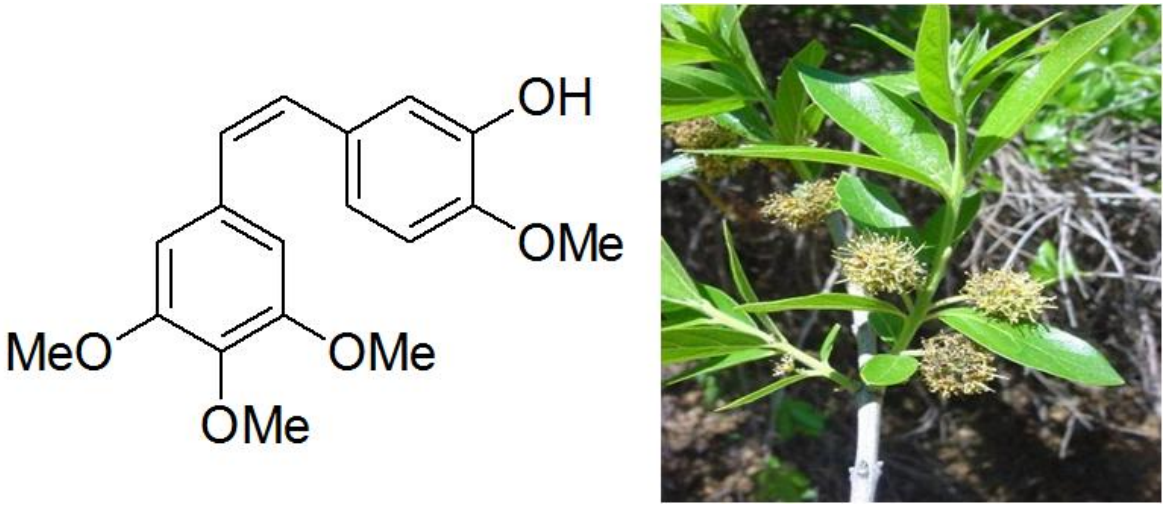

Figure 1.9. Structure of CA-4 (left) and African willow trees Combretum caffrum (right) [13]

Although its exact mechanism of action is unknown, CA-4 binding to tubulin at colchine binding site (α- and β-integrin) tubulin inhibits tubulin polymerzation and tubulin depolymerization results in formation of abnormal mitotic spindle tempting apoptosis.

According to in vitro analysis of cell, cell arrest in G_2 / M phase is observed in short time at concentration close to IC_{50} for cytotoxicity [14].

In other words, CA-4 binds endothelial cells which are inner line of cells and alters their shape from flat to round. Blood flow rate decreases. Hence, vessel shut down and tumor necrosis are displayed [15]. Figure 1.10 depicts potential targets of CA-4 in endothelial cells.

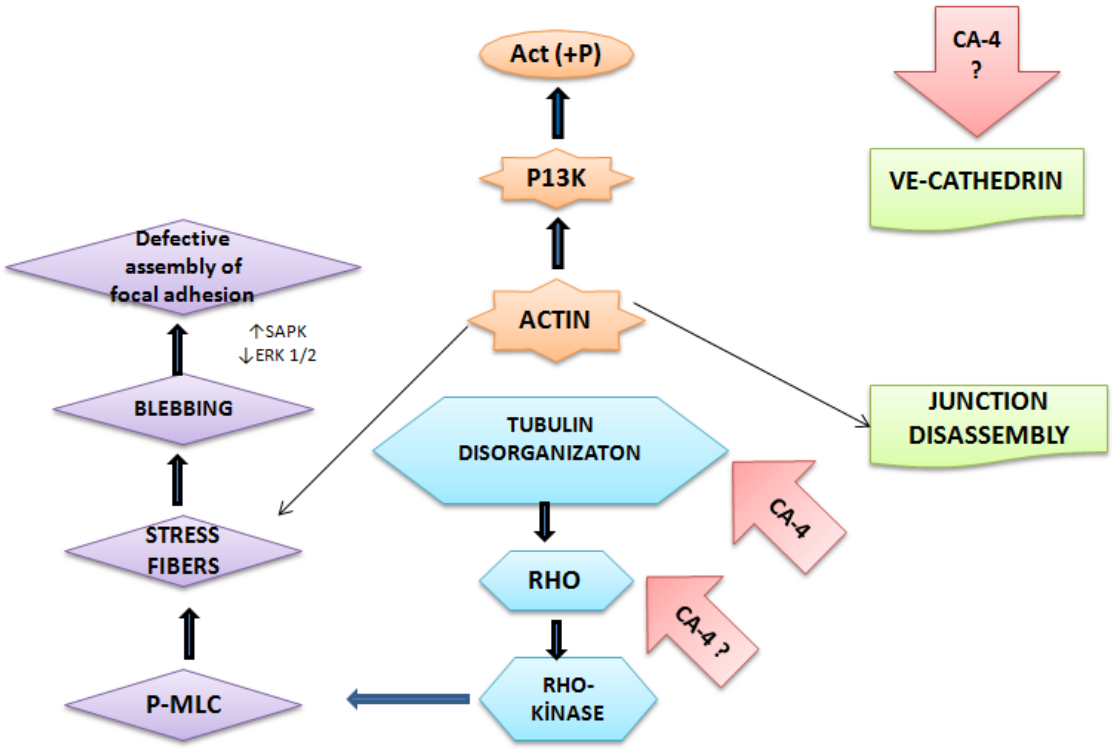

Figure 1.10. Schematic representation of potential targets of CA-4 in endothelial cells: P-LC, phosphorylated myosin light chain; ERK, extracellular receptor kinase; SAPK, stress-activated protein kinase [12]

Although many angiogenesis inhibitors exist such as; paxlitaxel, there are some unprecedented factors which make CA-4 special pharmacodynamically and clinically namely, targeting subpopulation of tubulin in vivo, interplaying between tubulin and CA-4, recognization of undefined target and, disruption of cellular processes in endothelium in vivo [1].

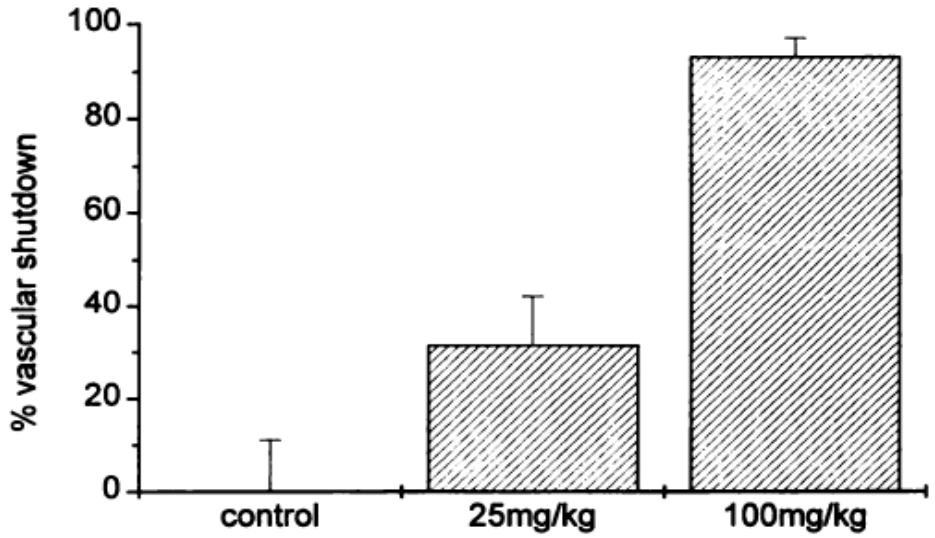

Figure 1.11. Dose effect of CA-4 to vascular volume of mice [16]

Sudha Iyer and coworkers examined dose effect of CA-4 (25 or 100 mg/kg) on mice bearing murine carcinoma. Figure 1.11 displays percentage of vascular shutdown versus mean vascular volume of untreated tumors and are means for 5 to 13 tumors. As a result of experiment, at lower dose, vascular shutdown reached 30 % level 6 h after i.p administration. For higher dose, almost complete vascular shutdown was observed [16].

Furthermore, effects of combretastatin A-4 on staining of HUVECs by Hoechst 33258 also was examined for 6, 16, 24 h to see whether CA-4 stimulates apoptosis or not. After 24 h, fluorescence microscopy displayed that CA-4 triggered apoptosis by exerting chromotin condensation resulting from 15% of HUVECs treated with CA-4 [Figure 1.13] [16].

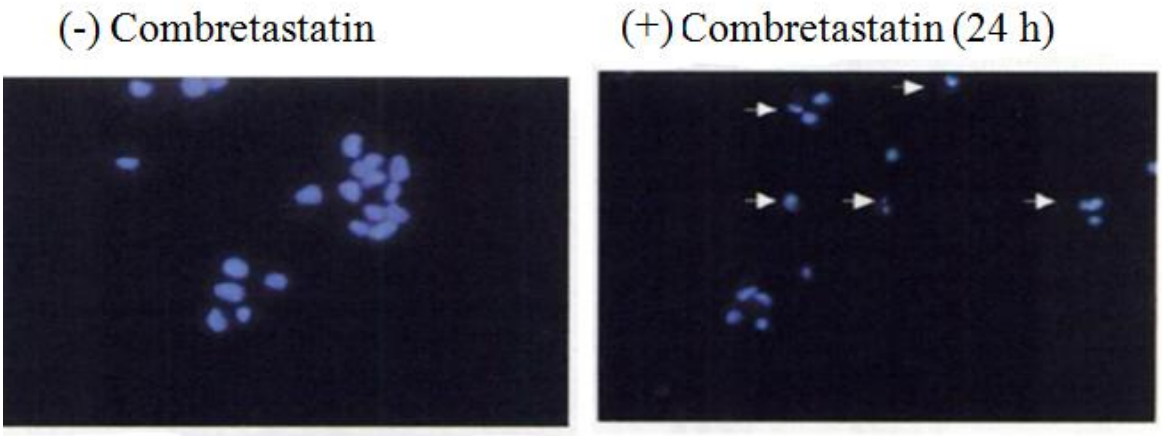

Figure 1.12. Effects of combretastatin A-4 on staining of HUVECs by Hoechst 33258 [16]

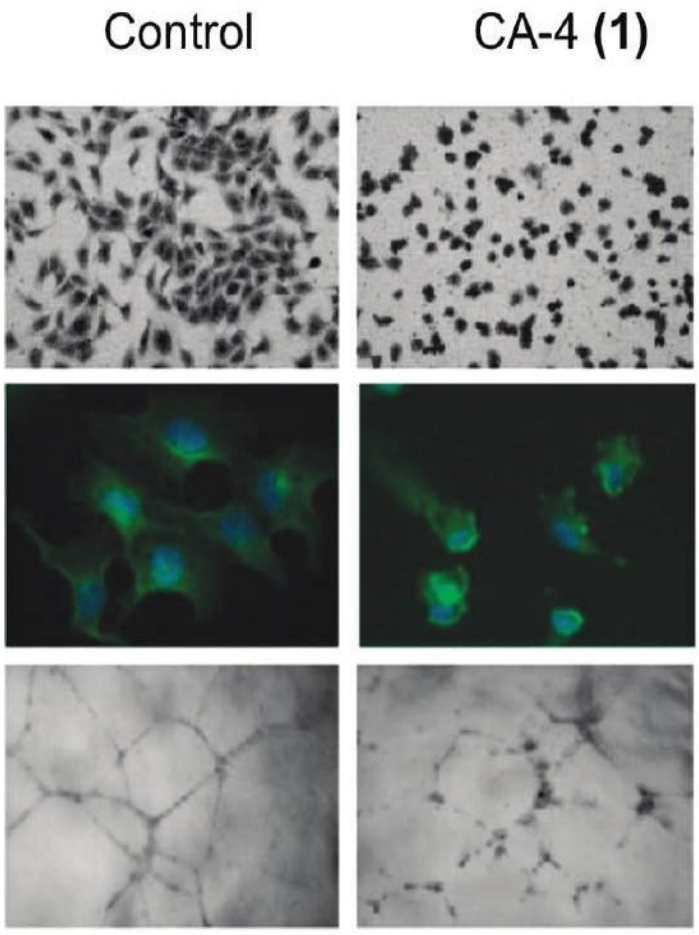

Figure 1.13. Effect of (CA-4) (0.1 μM) on endothelial cell morphology, cytoskeleton organization, and cord formation [17]

Top panel is representative images of HUVEC exposed to the indicated concentration of compounds for 1 h (x100). Middle panel is immunofluorescence analysis of the tubulin cytoskeleton in HUVEC exposed to vehicle or the indicated concentration of compounds for 1 h (x200). Bottom panel is the compounds were added to cords formed by HUVEC on Matrigel, 24 h after seeding. Images (x40) were taken 1 h after addition of the compounds.

As a result of experiment of Bonezzi and coworkers, CA-4 (0.1 μM) disrupts a network of capillary-like structures formed by endothelial cells on a 3D layer of Matrigel. On this permissive matrix, HUVEC spontaneously align forming a network of interconnecting cords reminiscent of immature vessels, complete 24 h after seeding. Formed cord in 1h is disrupted by CA-4 and connection between neighbor cord reduced [Figure 1.13] [17].

1.5.1 Combretastatin A-4 phospate

Zybrestat known as CA-4 phosphate (CA4P) is a water soluble prodrug derivative of CA-4 in phase III clinical trial. According to ongoing clinical experience, survival rate of tumor cell is dramatically declined up to 99 %, 24 h after administration of CA4P (100 mg / kg). Additionally, blood flow reduction, change in endothelial cell morphology and vascular shutdown were observed. Zybrestat is also combined with anticancer therapies to improve anticancer efficacy [18]. Investigation area and phase study of Zybrestat is demonstrated at table 1.1.

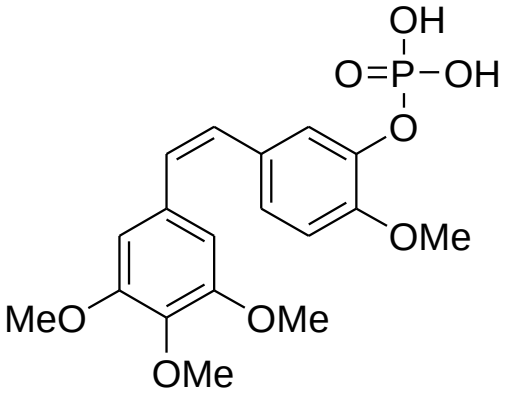

Figure 1.14. Structure of CA4P

Table 1.1. Investigation area and phase study of Zybrestat [19]

Area of investigation	**Phase**
Anaplastic Thyroid Cancer	II / III
Advanced Platinum-Resistant Ovarian Cancer	II
Chemotherapy-Naive Stage IIIB/IV Non-Small Cell Lung Cancer	II
Advanced Solid Tumors in combination with bevacizumab (AVASTIN)	I

2. AIM OF THE STUDY

The study is composed of three steps: Synthesis of reactive polymers (Step 1), synthesis of CA-4 and its analogs (Step 2), conjugation of drug molecules to the reactive polymers (Step 3) [Figure 2.1].

.

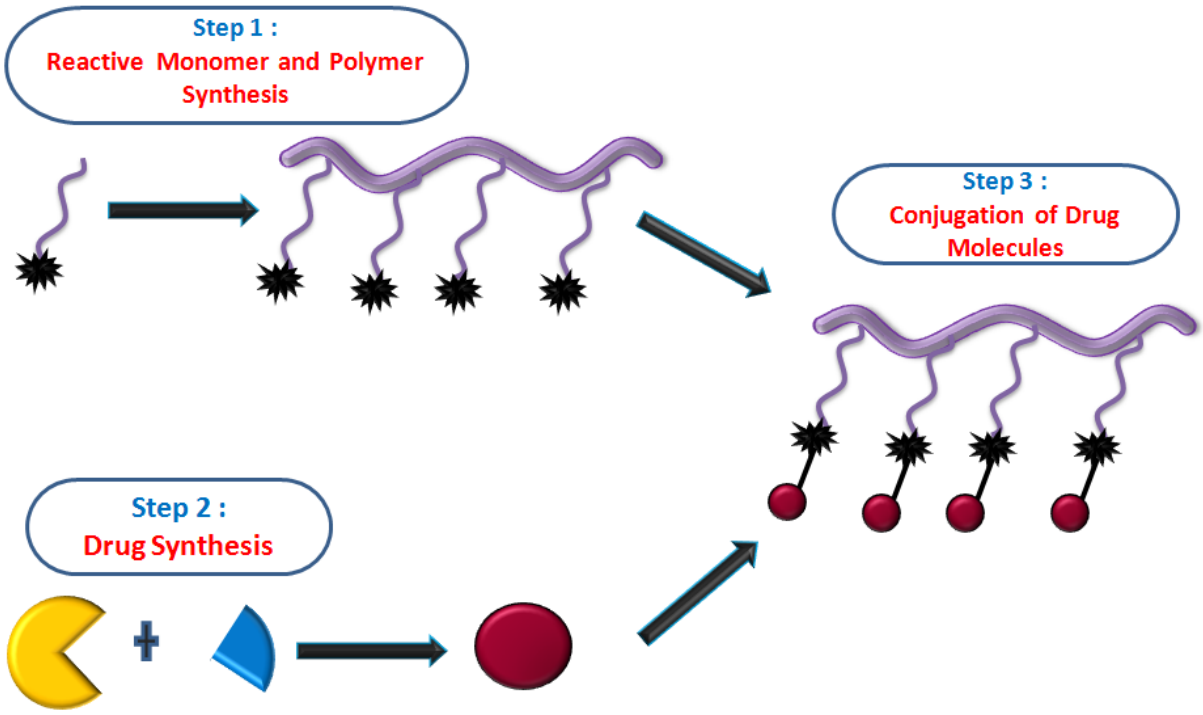

Figure 2.1. Schematic representation of aim of study

Cis - Combretastatin A-4 (CA-4) is one of the most powerful antivascular disrupting agents and displays selectivity toward endothelial cell but need to be solubilized and improved its pharmacokinetic profile. Polymer-drug conjugates which are covalently bounded each other offer significant opportunities due to improved controlled delivery of drug, increased drug efficiency. Moreover, polymer-drug conjugates improve drug solubility, reduce toxicity and undesired side effects, and prolong drug residence in tumor thanks to EPR effect. In addition to them, polymer-drug conjugates provide slow body clearance, increase blood circulation time, and overpass drug resistance. To utilize these remarkable opportunities, CA-4 derivatives was synthesized and covalently conjugated with reactive polymers via Huisgen type ‘click’ reaction.

3. RESULTS AND DISCUSSION

The project consists of three parts:

i. Synthesis of reactive monomer and reactive polymers

ii. Synthesis of cis - combretastatin A-4 and its derivatives

iii. Conjugation of drug molecules on reactive polymers

3.1 Reactive Polymer

Linear PEG polymers have low loading capacity because PEG alone can carry maximum two drug molecules on its periphery. Making copolymer bearing branching unit combats with this drawback. For this reason, azide and alkyne functionalized reactive polymers are synthesized as shown in Figure 3.1. Moreover, functionalization of polymer bearing alkyne or azide groups facilitates the attachment of drug molecules via the Huisgen type 'click' reaction.

3.1.1 Reactive Monomer Synthesis

To obtain azide functionalized polymer (PEG-AHMA, **7**), 6-azidohexylmethaxrylate (**4)** was synthesized in two steps. At first, 6-chlorohexane 1-ol (**1**) was reacted with NaN_3 to obtain 6-azidohexane 1-ol (**2**). Then 6-azidohexyl methacrylate (AHMA, **4**) was synthesized by reacting 6-azidohexane 1-ol with methacryloyl chloride (**4**). Figure 3.1 shows details of this synthesis.

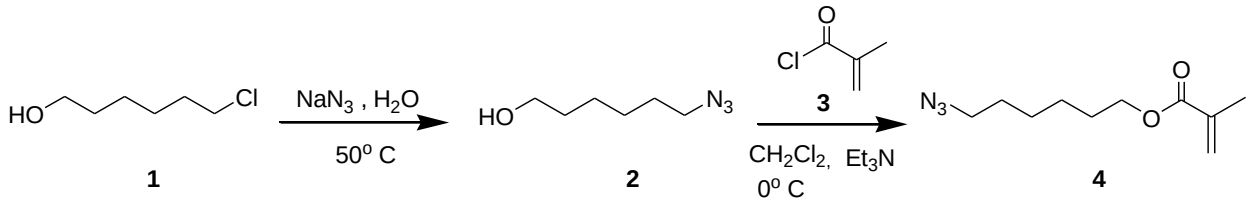

Figure 3.1. Synthesis of AHMA Monomer **4**

After purification, the products **2** and **4** were characterized by FTIR spectrum and product **4** were also characterized by ^{1}H NMR [Figure 3.3 and Figure 3.2 respectively]. For

product **1**, the broad peak at 3332 cm^{-1} is due to alcohol group and the azide group appears at 2095cm^{-1}. For AHMA monomer (**4**)**,** the broad peak coming from alcohol group of product **2** was disappeared, the newly forming peaks at 1715 cm^{-1} and 1638 cm^{-1} was due to the carboxyl group and alkyne group of the product **4** respectively. Additionally, the peaks which were pointed letters at Figure 3.2 proved that product **4** was synthesized successfully.

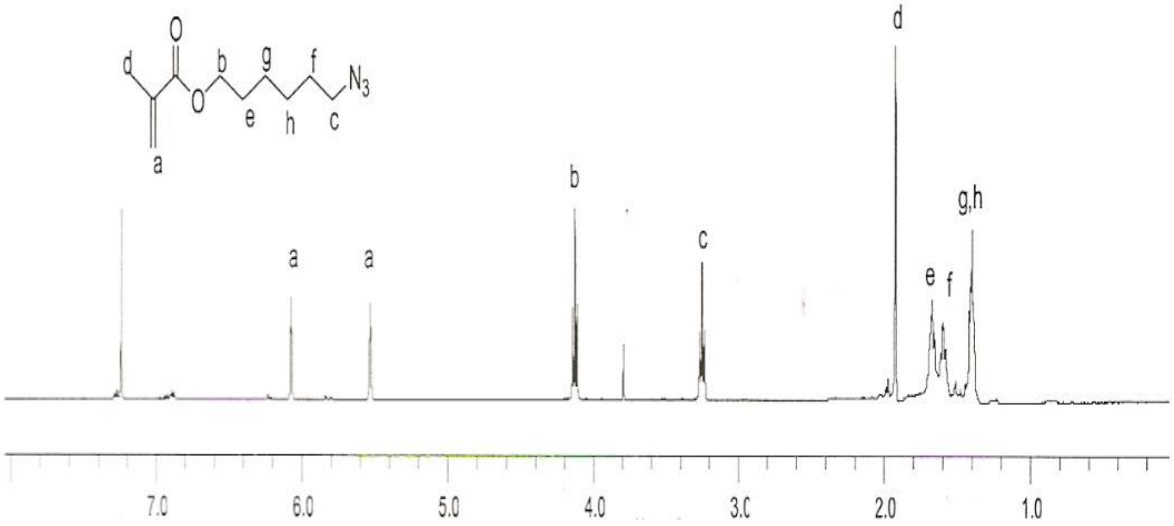

Figure 3.2. ^{1}H NMR spectrum of 6-azidohexyl methacrylate (**4**)

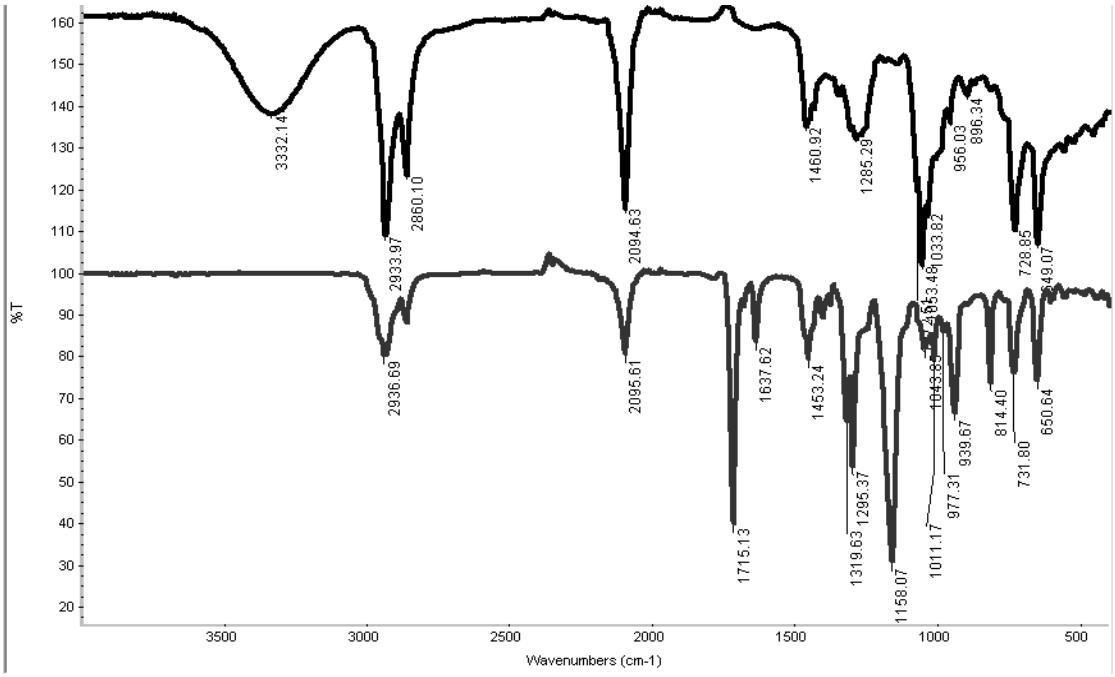

Figure 3.3. IR Comparison between **2** and **4**

3.1.2 Azide Functionalized Reactive Polymer Synthesis

Polymers with narrow dispersity are very essential especially for biological applications. In this study, ATRP method was chosen to obtain desired polymer in a control way. As a controlled living polymerization method, ATRP is initiated by an alkyl halide (ethyl 2-bromoisobutyrate) and catalyzed by a transition metal complex. PEGMA (**5**) and AHMA (**4**) were copolymerized to obtained azide functionalized copolymer (PEG-AHMA, **7**) via ATRP reaction.

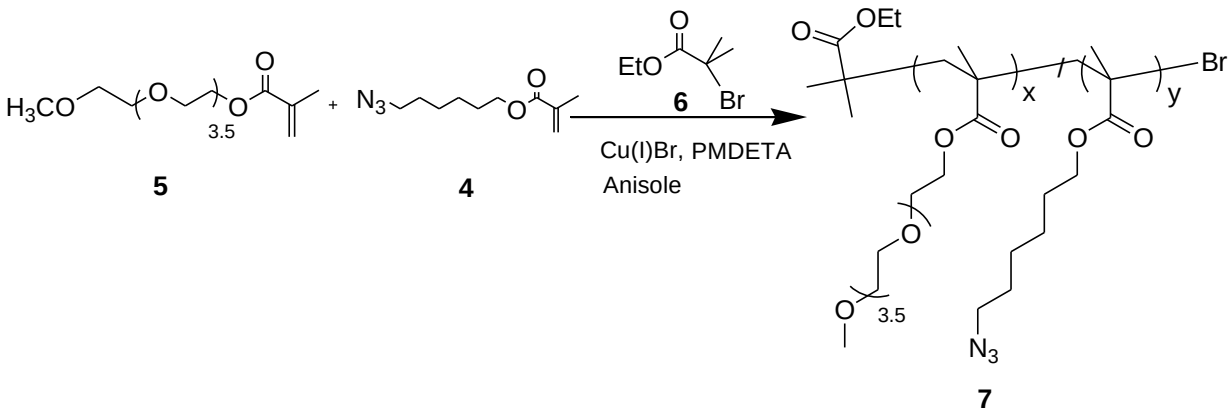

Figure 3.4. Synthesis of Azide Functionalized Copolymer (PEG-AHMA, **7**)

The aim was that 4:1 and 6:1 PEG-AHMA reactive polymers were synthesized. Therefore, ATRP conditions to achieve desired reactive polymers were prepared. Table 3.1 displays ATRP conditions to make 6:1, 20 K-25 K PEG- AHMA copolymers. As a result of the experiment, decrease in anisole amount resulted in increase in MWt and decrease in anisole amount had an impact on precipitation of polymer by improving yield. Mw / Mn value (poly dispersity index, called pDI value) remained nearly the same.

Table 3.1. PEG- AHMA 6:1 Polymer

Entry	PMDETA/ ini / Cu(I)Br	Anisole(mL)	Yield (%)	GPC[a]	
				M_n (g/mol)	M_w/M_n
1	0.5/0.25/0.25	2	17	20100	1.20
2	0.5/0.25/0.25	1.5	19	23190	1.14
3	0.5/0.25/0.25	1	50	25300	1.24

[a] Calibration with linear PS as standard. GPC samples are prepared in THF

3.1.3 Alkyne Functionalized Reactive Polymer Synthesis

PEG-NHS polymer (6:1, 20 K, **9**) was synthesized via ATRP method for using it to obtain PEG- alkne copolymer (6:1, 20 K, **11**) by reacting with PEGMA and NHSMA (**8**). PEG-NHS polymer (**9**) was reacted with propargyl amine (**10**). Conversion of PEG-NHS (**9**) to PEG-alkyne (**11**) was characterized by ^{1}H NMR [Figure 3.6].

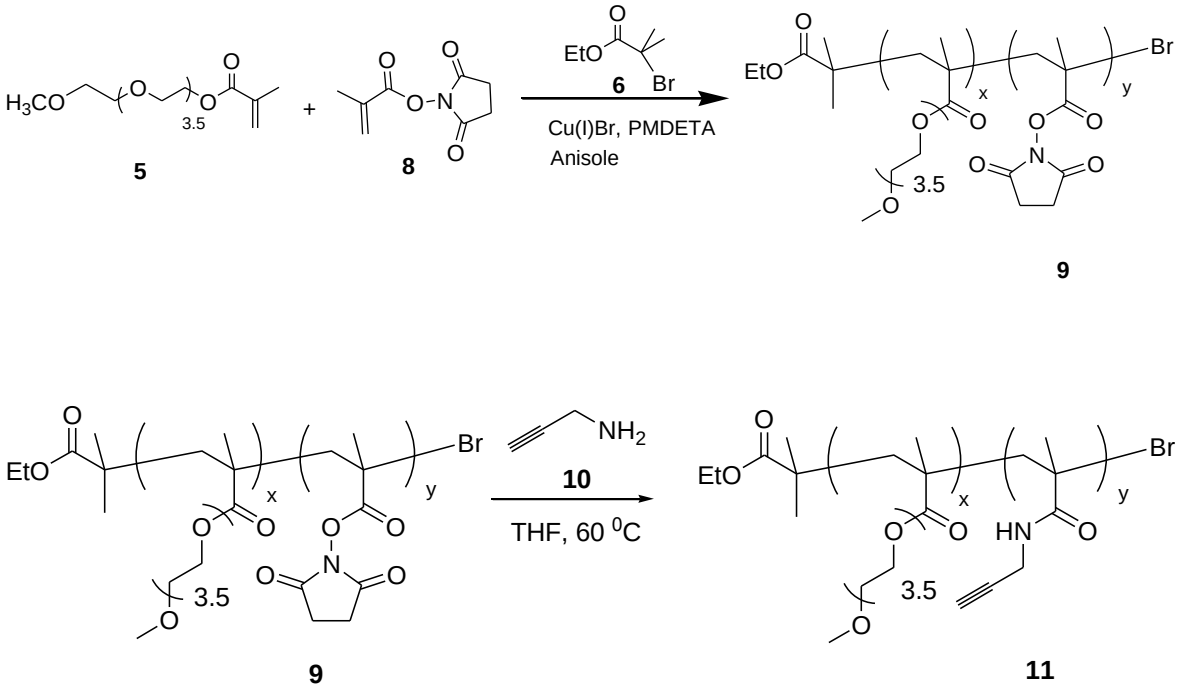

Figure 3.5.Synthesis of PEG-NHS polymer **9** and Alkyne Functionalized Copolymer **11**

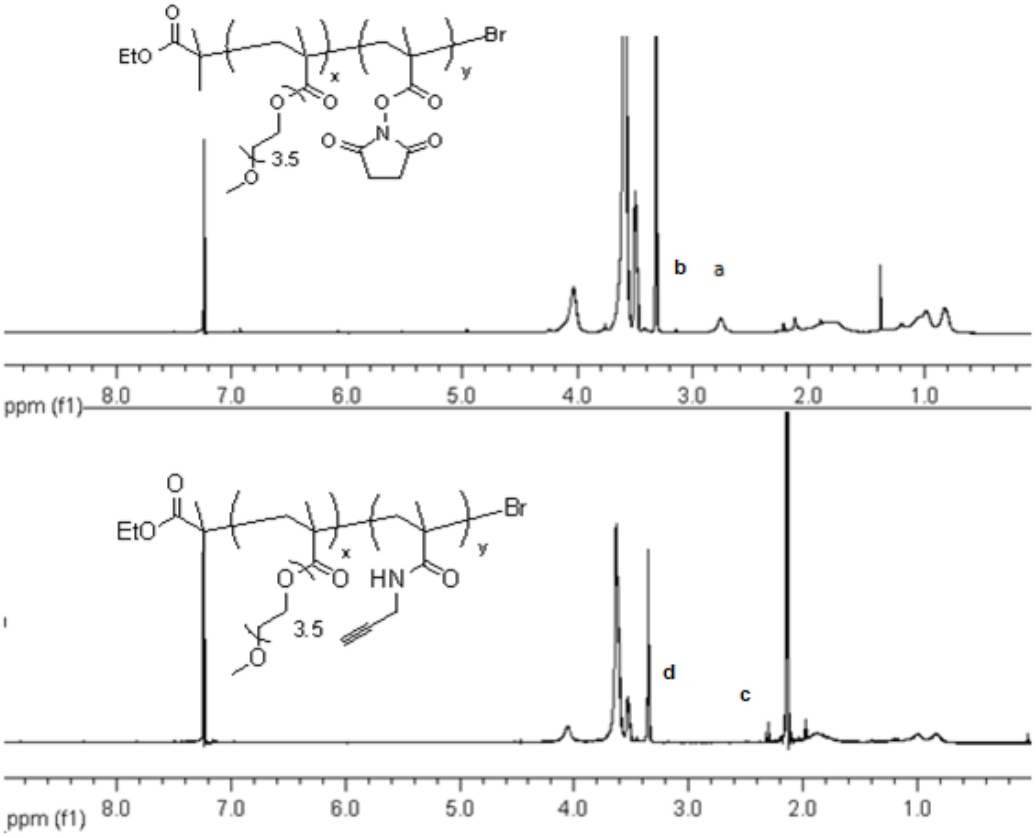

Figure 3.6. ^{1}H NMR Comparison of PEG-NHS (**9**) to PEG-alkyne (**11**)

After integral of b was divided three coming from three H's from PEG-OCH_3 and integral of a was divided four belonging to four H's from NHS part, b: a ratio was calculated as 6:1. Disappearance of the peak at 2.76 ppm coming from NHS (br s, 4 H, CH_2 CH_2C=O, a) and appearance of a new peak at 2.32 pm (s, 1H, HC≡C, c) indicated full conversion of NHS to alkyne Furthermore, d : c integral ratio (-OCH_3 / HC≡C) supported 6:1 PEG-alkyne copolymer (**11**) was obtained successfully [Figure 3.6].

3.2 Synthesis and Functionalization of Cis Combretastatin A- 4

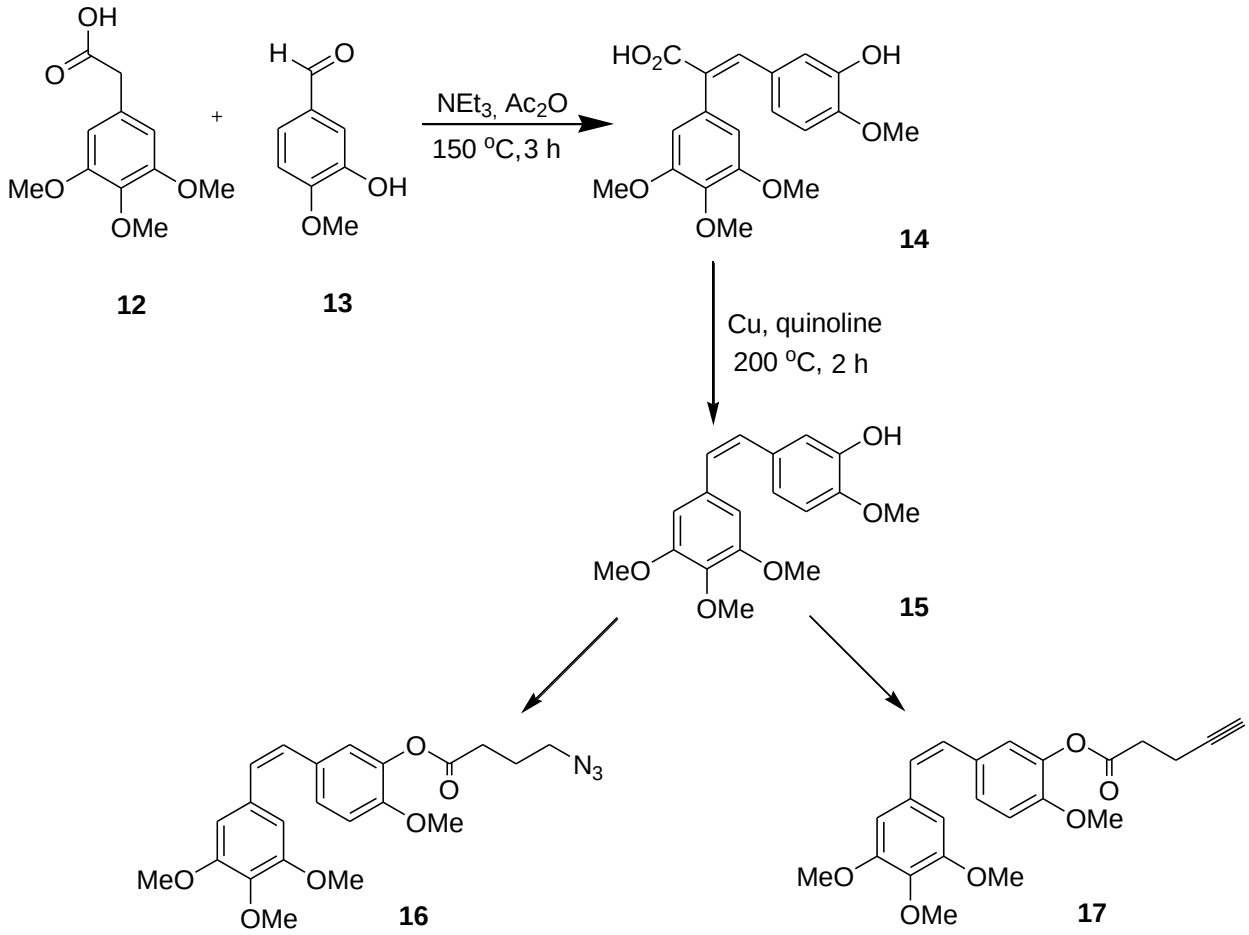

Figure 3.7.Schematic representation of synthesis of CA-4 and its derivatives

3.2.1 Synthesis of Cis-Combretastatin A-4

Propenoic acid **14** was obtained via the reaction of 3-hydroxy-4-methoxybenzaldehyde (**13**) and 3, 4, 5-trimethoxyphenylacetic acid (**12**) in presence of acetic anhydride and triethylamine [Figure 3.8]. Purity of the product was examined with HPLC (95 %) and characterized via ^{1}H NMR spectrum [Figure 3.8 and 3.9 respectively].

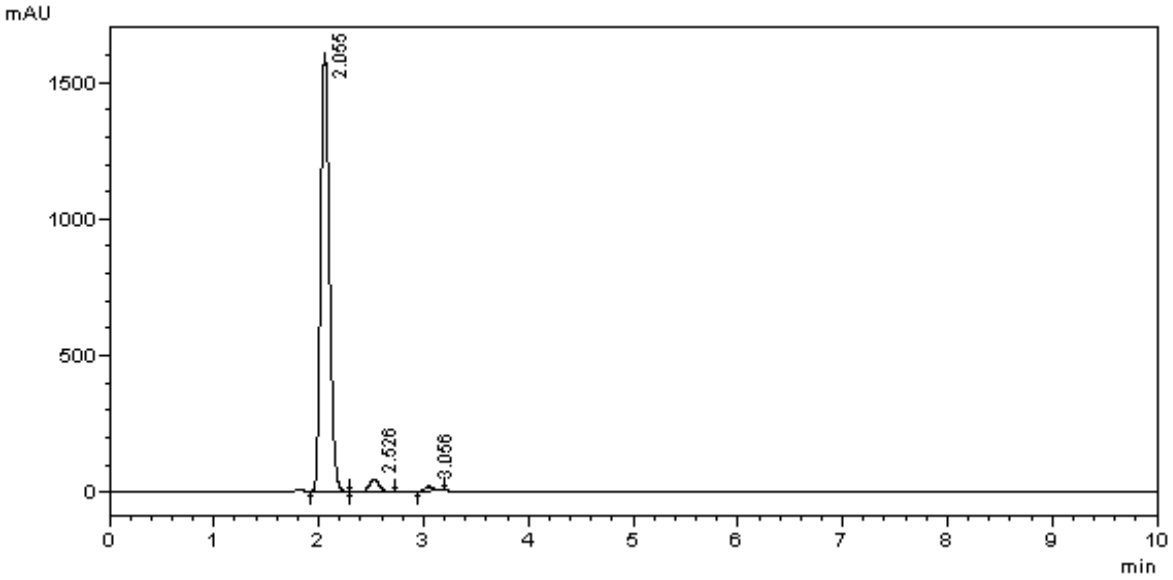

Figure 3.8. HPLC spectrum of propenoic acid **14**

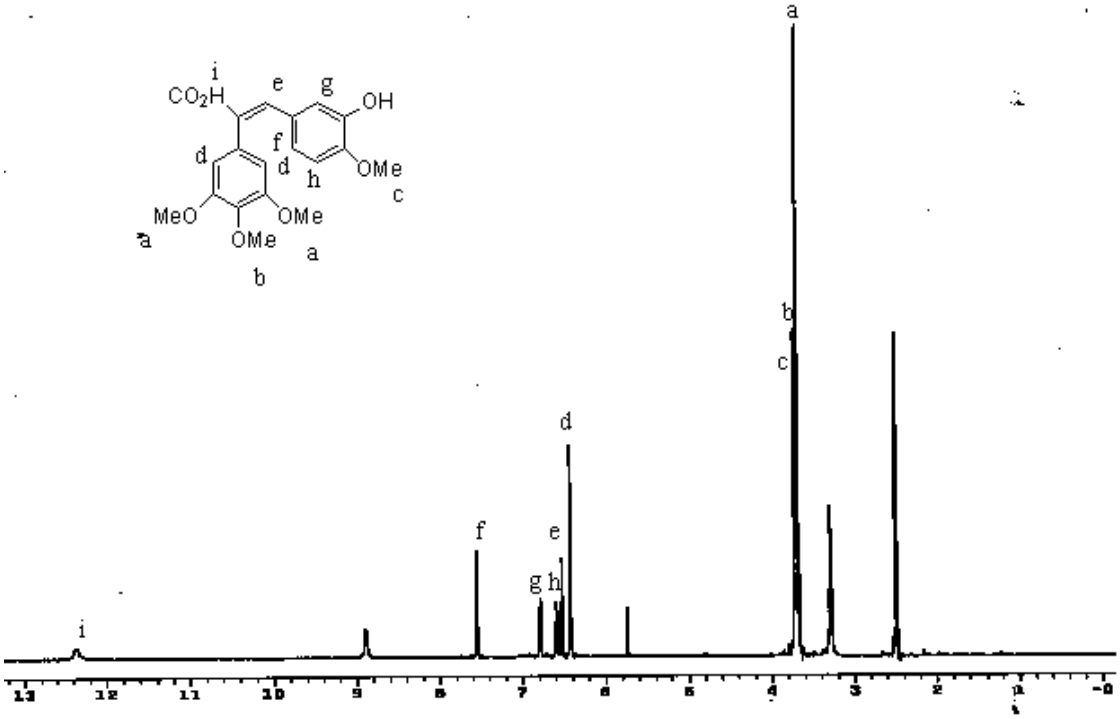

Figure 3.9. ^{1}H NMR spectrum of propenoic acid **14**

There are three different methoxy groups and twelve H's attached to these methoxy groups appear at 3.68, 3.72 and 3.74 ppm. Aromatic protons appear at 6.44, 6.54, 6.80 and 7.58 ppm and the vinylic proton appears at 6.61 ppm. Carboxylic acid proton appears at 12.38 ppm in DMSO-d_6.

Combretastatin A-4 (**15**) was synthesized via the decarboxylation of the propenoic acid (**14**) in the presence of copper and quinoline with 60 percent yield [Figure 3.7]. The product was monitored via ^{1}H NMR spectrum and the purity was examined with HPLC (100 %). To detect and follow the purity of the product, HPLC and ^{1}H-NMR spectra were used [Figure 3.10 and 3.11 respectively].

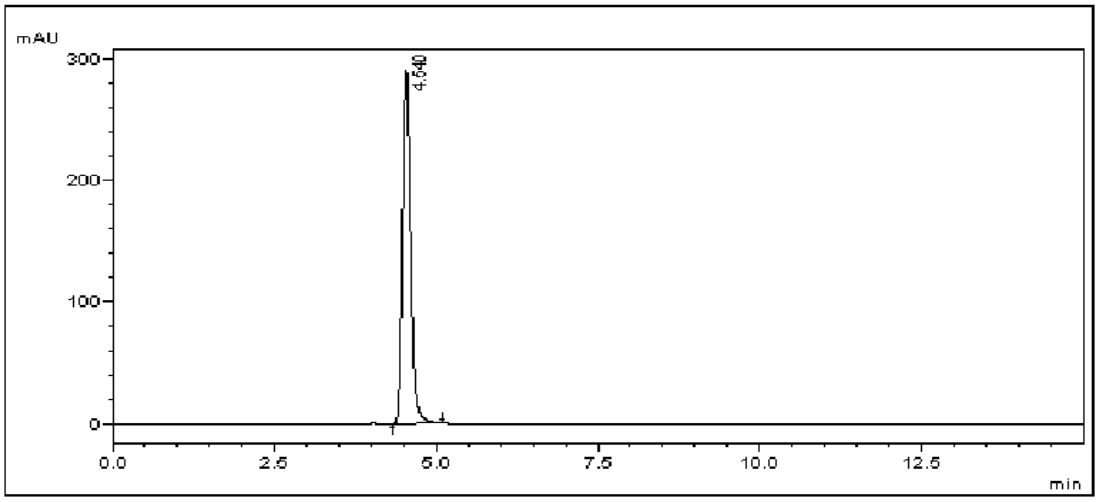

Figure 3.10. HPLC spectrum of CA-4 (**15)**

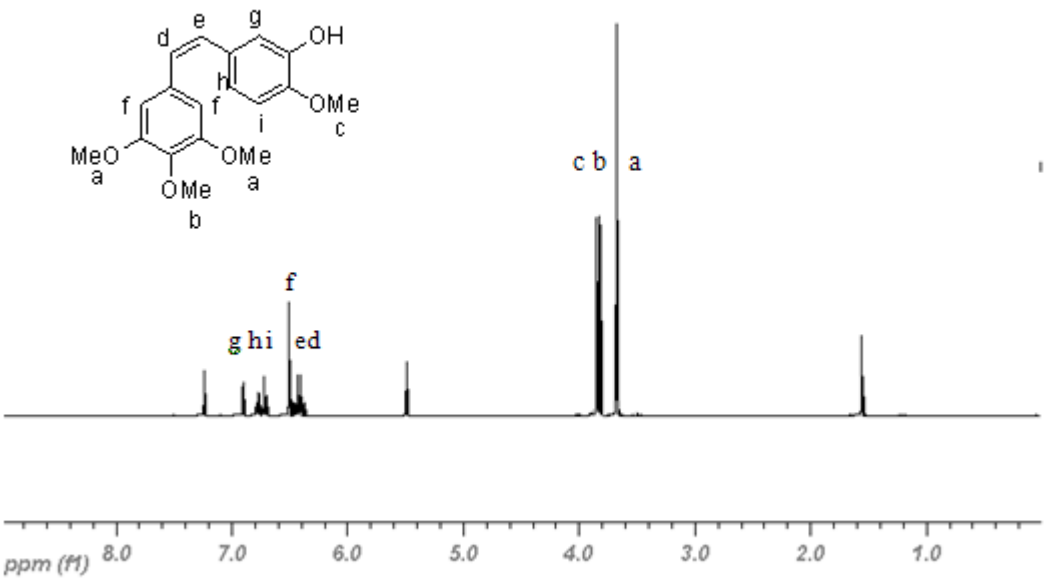

Figure 3.11 ^{1}H NMR spectrum of CA-4 (**15**)

3.2.2 Funtionalization of Combretastatin A-4

Functionalization of CA-4 with alkyne and azide groups facilitates attachment of CA-4 (**15**) on reactive polymer and provides a significant way to apply Huisgen type 'click' reaction.

To begin with, ethyl 4-bromo butyrate (**18**) was reacted with NaN_3 in presence of acetone-water mixture to obtain 4-azidobutyric acid ethyl ester (**19**). 4-azidobutyric acid ethyl ester was hydrolyzed with KOH to get 4-azidobutanoic acid (**20**) according to the literature procedures [24]. Figure 3.12 shows details of the reaction.

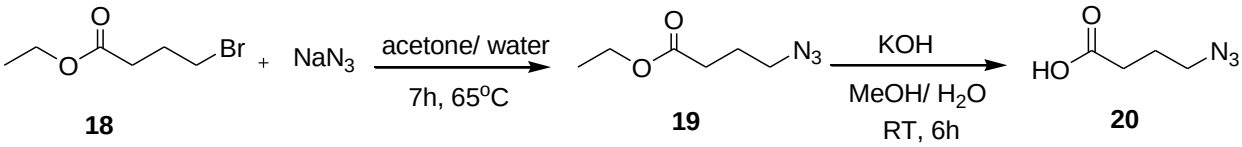

Figure 3.12. Synthesis of 4-azidobutanoic acid (**20**)

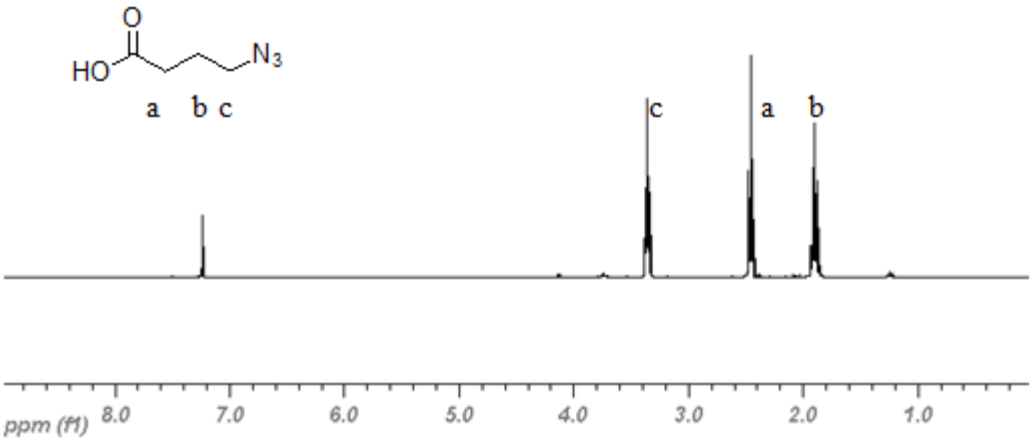

Figure 3.13 ^{1}H NMR spectrum of 4-azidobutanoic acid (**20**)

CA-4 azide derivative (C-N_3, **16**) was synthesized using CA-4 (**15**) and 4-azidobutanoic acid (**20**) via DCC coupling with a high yield (94 %). The reaction was characterized by HPLC, ^{1}H-NMR and, FTIR [Figure 3.15, 3.18, and 3.19 respectively].

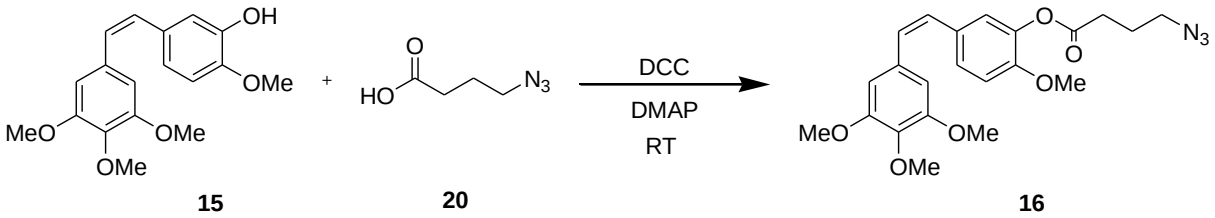

Figure 3.14. Synthesis of CA-4 azide derivative (C-N_3, **16**)

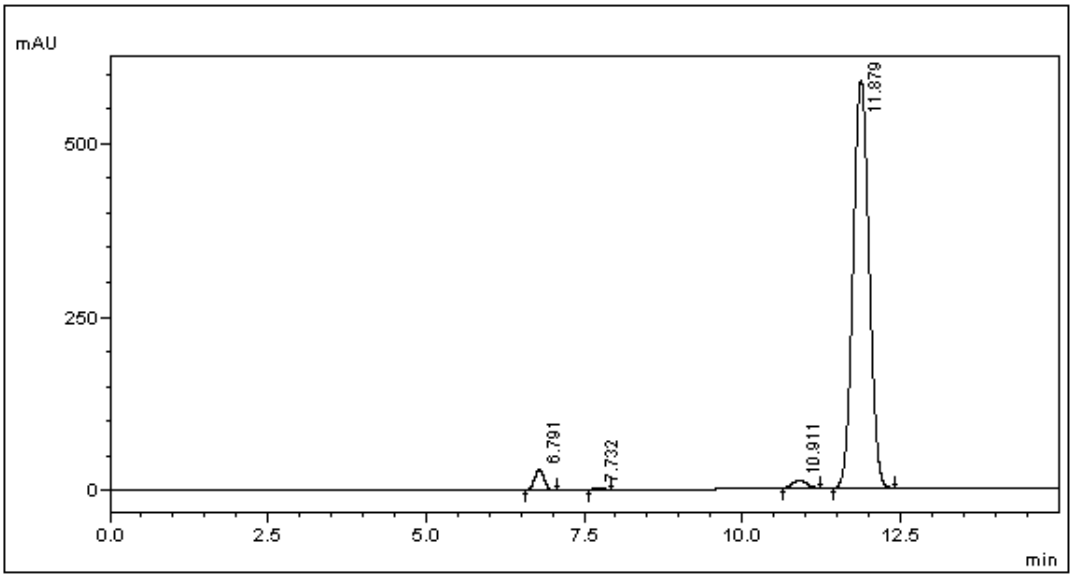

Figure 3.15. HPLC spectrum of CA-4 azide derivative (**16**)

CA-4 alkyne derivative (**17**) was synthesized with the same method of CA-4 azide derivative (**16**). CA-4 (**15**) and 4-pentynoic acid (**21**) underwent DCC coupling reaction. Figure 3.16 displays detail of reaction and CA-4 alkyne derivative (**17**) was obtained with high yield (97%). CA-4 alkyne derivative **10** was characterized with HPLC, ^{1}H-NMR and, FTIR [Figure 3.17, 3.18, and 3.19 respectively].

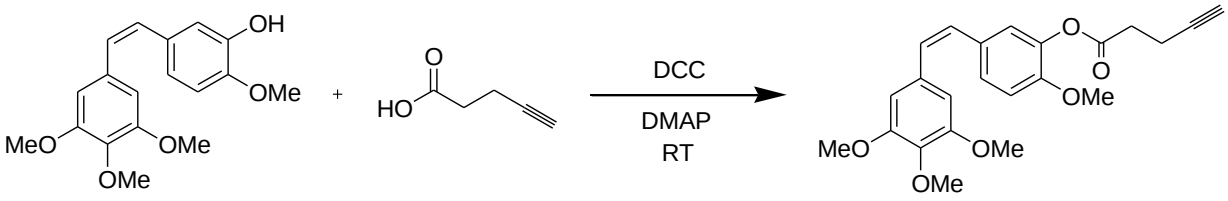

15 **21** **17**

Figure 3.16. Synthesis of CA-4 alkyne derivative (**17**)

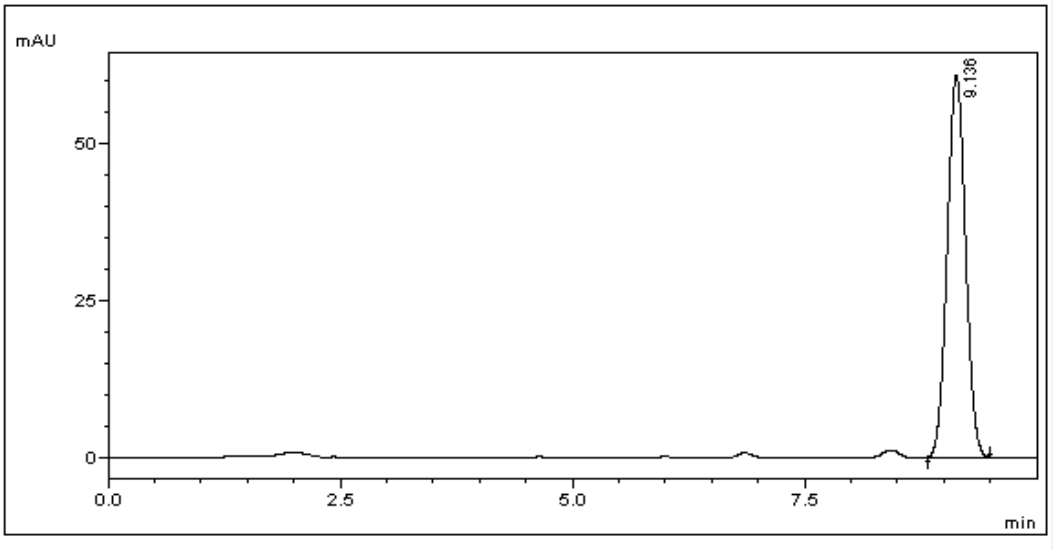

Figure 3.17. HPLC spectrum of CA-4 alkyne derivative (**17**)

^{1}H NMR analysis shows that CA-4 (**15**) and its azide (**16**) and alkyne derivatives (**17**) were successfully achieved [Figure 3.18]. Appearance of new peaks at 3.42 ppm (t, 2H, CH_2N_3), 2,63 ppm (t, 2H, $CH_2C=O$), and 1,98 ppm (m, 2H, CH_2CH_2 N_3) [Figure 3.18] proves the formation of CA-4 azide derivative (**16**). Presence of newly formed peaks belonging to alkyne group after attaching on CA-4 at 2.78 ppm (t, 2H, $CH_2C=O$), 2.59 (dt, 2H, $CH_2C{\equiv}CH$), and 2 ppm (t, 1H, $C{\equiv}CH$) indicate that CA-4 azide derivative is synthesized successfully.

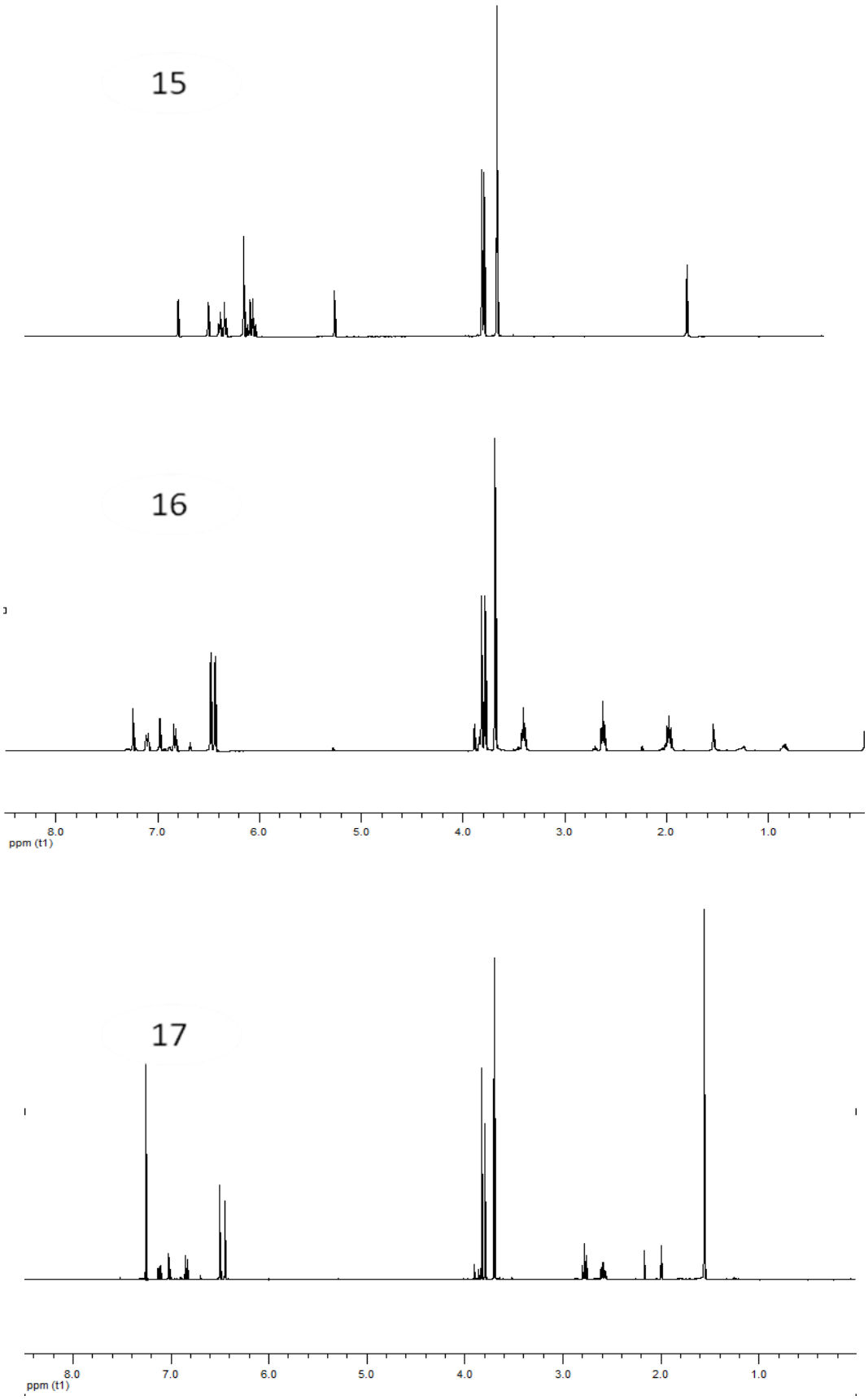

Figure 3.18. ^{1}H NMR comparison of CA-4 (**15**) and its azide **16** and alkyne **17** derivatives

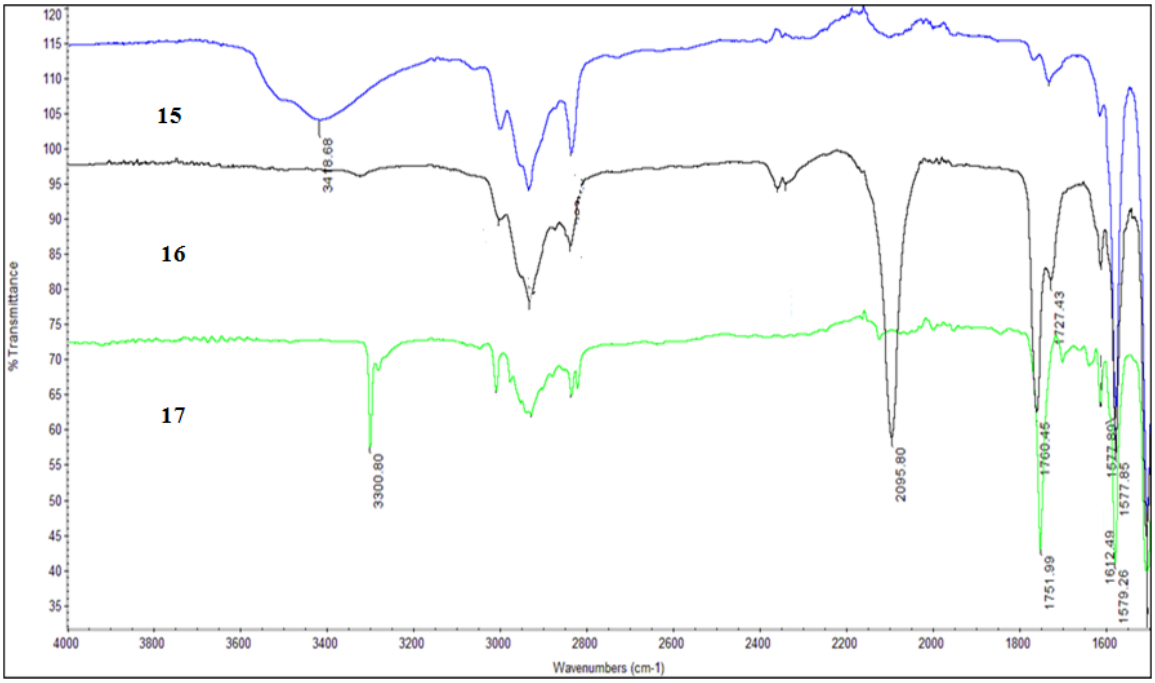

Figure 3.19. IR Comparison of **15**, **16**, **17**

FTIR results also support that CA-4 (**15**) and its azide (**16**) and alkyne derivatives (**17**) were obtained properly [Figure 3.20]. After DCC coupling, the broad peak at 3400 cm^{-1} coming from alcohol group of CA-4 (**15**) was disappeared, the newly forming peaks at 2096 cm^{-1} and 1700 cm^{-1} were due to azide group and the carboxyl group of the product **16**. In the same manner, the broad peak at 3400 cm^{-1} coming from alcohol group of CA-4 (**15**) was disappeared and presence of new peaks at 3301 cm^{-1} and 1752 cm^{-1} were due to alkyne and the carboxyl group of the product **17**.

3.3. Conjugation of Drug Molecules to Reactive Polymers

Conjugation of drug molecules to macromolecules provides many unprecedented advantages such as; increase in accumulation in the tumor via EPR effect, so, increase in the amount of drug in the tumor ,decrease in drug resistance and, reduction of clearance rate. Furthermore, polymer bounded drug molecule is stable in plasma due to the conjugation, after reaching the site of interest, the drug will release from the macromolecule to exhibit the anti-angiogenic effect via pH difference, enzymatically and so on. By this way, the effect of the polymer-bound drug to normal cells is diminished,

decreasing the potential side effects, in other words, decreasing toxicity. For these reasons, in the study, these benefits were utilized to improve therapeutic effects of drug molecules alone. Moreover, drug molecules in the study covalently were attached on polymer.

PEG is a biocompatible polymer but polymer –drug conjugates that are used in the study both biocompatible and biodegradable because ester groups in polymer-drug conjugates make them susceptible to hydrolysis in aqueous media and so, become biodegradable. This gave significant opportunity in terms of clearance rate and release of drug. By taking all these pivotal advantages, conjugation of CA-4 bearing alkyne and azide groups on polymer is achieved via Huisgen type 'click' reaction.

Firstly, PEG-AHMA- C-≡ conjugate (**21**) was prepared using C-≡ (**17**) and PEG-AHMA (**7**) with different molecular weights (10 K and 20 K). General synthesis of Poly-C-N_3 conjugates (**18)** was displayed at Figure 3.20.

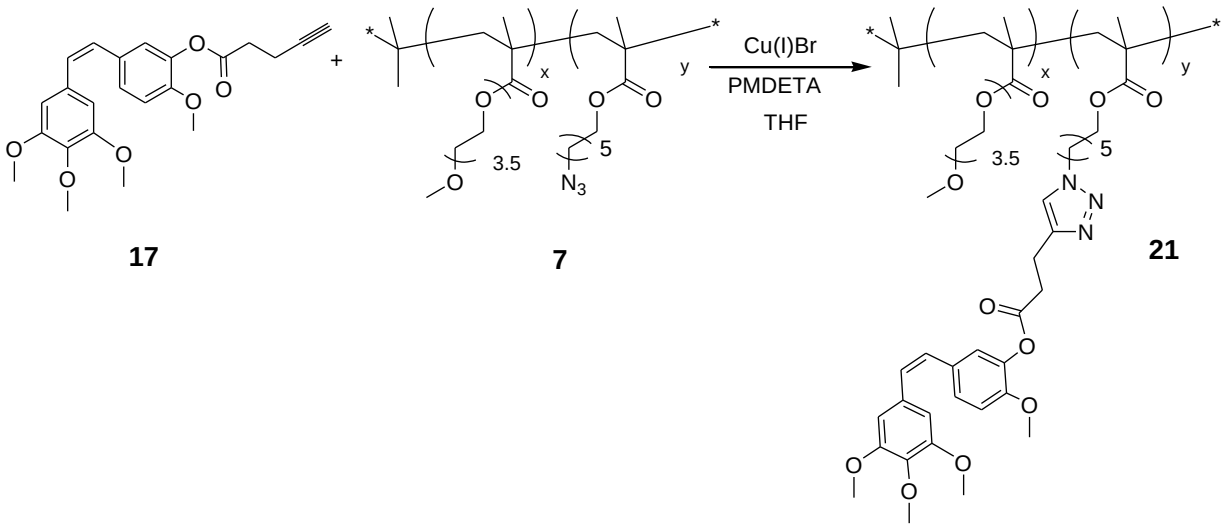

Figure 3.20. Schematic representation of synthesis of Poly- C-≡ conjugates (**21**)

For the first case, it was planned to react only 50 % of the azide functionality of PEG-AHMA polymer (**7**) (MW : 10 K, 1 : 4) with C-≡ (**17**) via Huisgen type 'click' reaction and the rest of the active azide groups on PEG-AHMA polymer (**7**) would be ready for further functionalization. Whether click reaction worked or not was monitored by ^{1}H-NMR. Figure 3.22 exhibits results of conjugation. After conjugation, peak at 3.24 ppm (t, 2H, CH_2N_3) is shifted to down field (4.26 ppm) and integral results showing 45% azide groups are bound with drug, which proves that the click reaction has worked successfully. One of the specific peaks of drug molecule comes at 7.11 ppm shown with letter e at Figure 3.21.

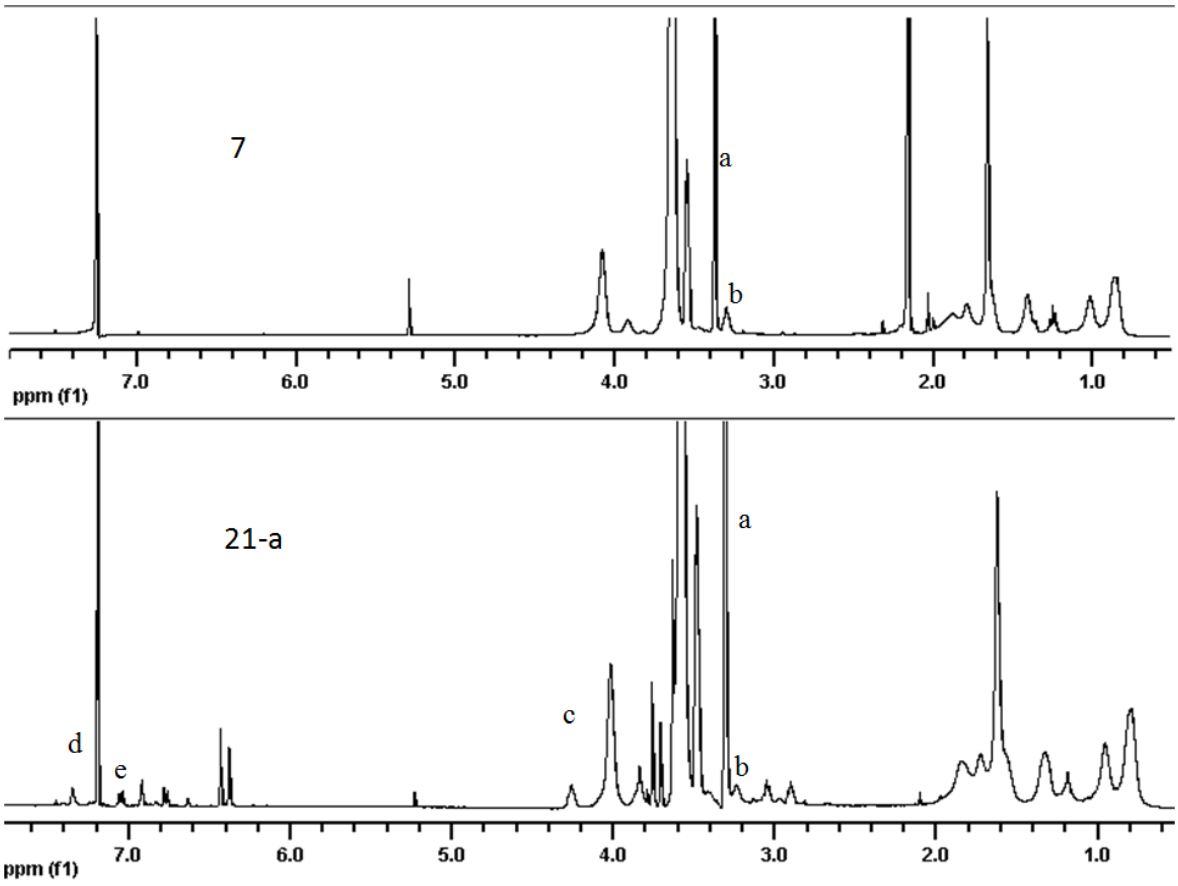

Figure 3.21. ^{1}H-NMR comparison of PEG-AHMA alone (**7**) and PEG-AHMA- C-≡ conjugate (**21-a**)

For the second case, PEG-AHMA polymer with (MW: 20 K, 1:6) was used to 100 % conversion of azide on polymer. Two types of 'click' reaction conditions were used, namely Cu(I)Br and PMDETA in dry THF media and, $CuSO_4$, NaAsc in

$CHCl_3$:EtOH:H_2O . As a result of experiment, Cu(I)Br and PMDETA in dry THF media worked better than $CuSO_4$ / NaAsc click condition, since all drug bounded on PEG-AHMA with high yield. For $CuSO_4$, NaAsc in $CHCl_3$: EtOH: H_2O media, drug bound on polymer but not all. Thus, first click reaction method was used for conjugation. As seen Figure 3.22, after conjugation, peak at 3.28 ppm (t, 2H, CH_2N_3) is shifted to down field (peaks a, h respectively). The peak coming from triazole at 7.4 (br s, NCH=C) and specific peaks belonging to drug molecule (peaks c, d, e, f, g, i, j, k, and l) are evidence for the conjugation of drug molecule on polymer.

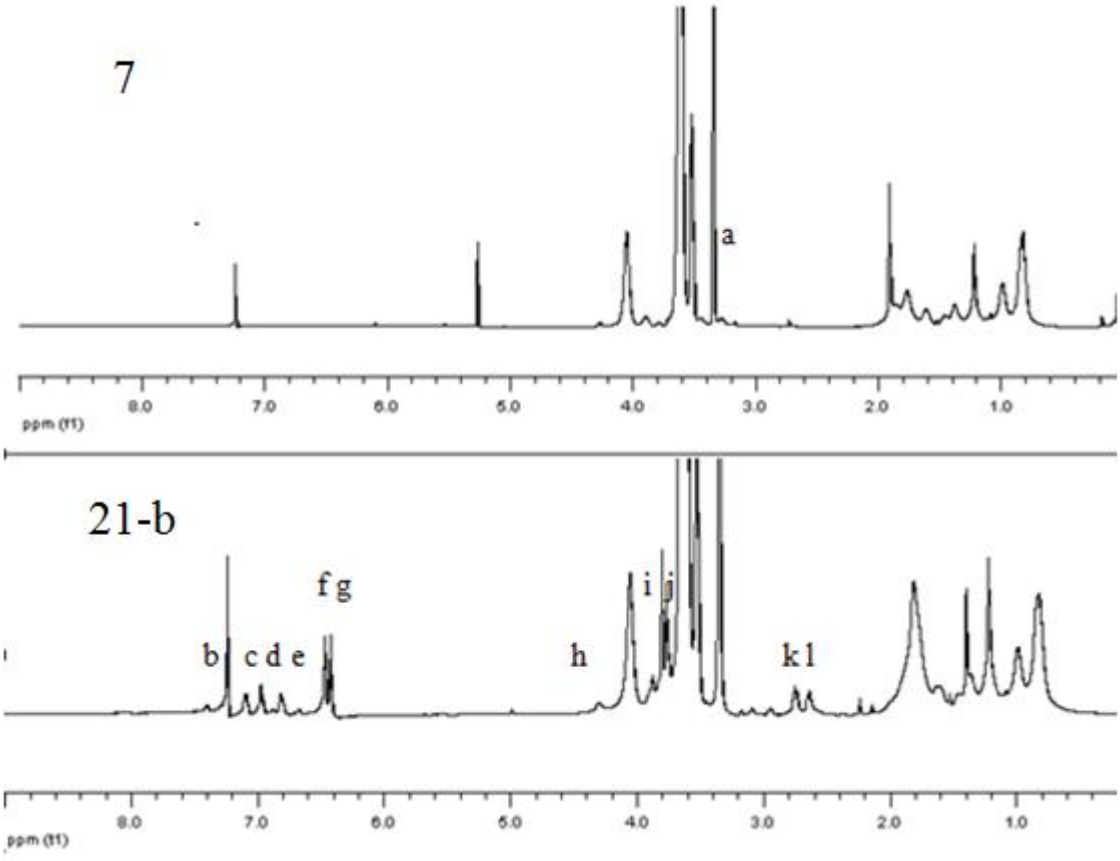

Figure 3.22. ^{1}H-NMR comparison of PEG-AHMA alone (20K, 1:6) (**7**) and PEG-AHMA- C-≡ conjugate (**21-b**)

Secondly, conjugation of CA-4 azide derivative on alkyne functionalized PEGMA was aimed with 100% conversion via Huisgen type ‘click’ reaction. General synthesis

method of Poly- C-N_3 conjugate is shown at Figure 3.23. Click reaction was accomplished in aqueous media using CuSO4, NaAsc in $CHCl_3$: EtOH: H_2O and all alkyne groups on polymer were bound to drug molecules. Reaction which worked successfully was supported by ^{1}H-NMR [Figure 3.24].

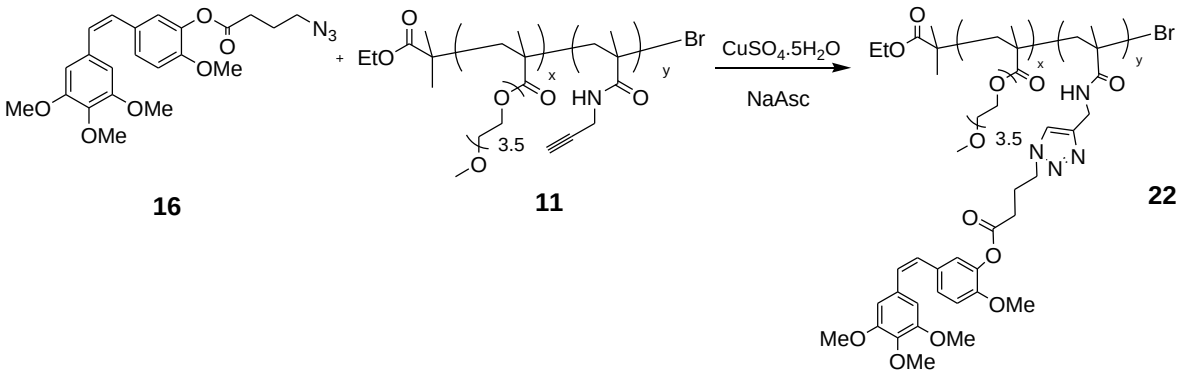

Figure 3.23. Schematic representation of synthesis of Poly- C-N_3 conjugate (**22**)

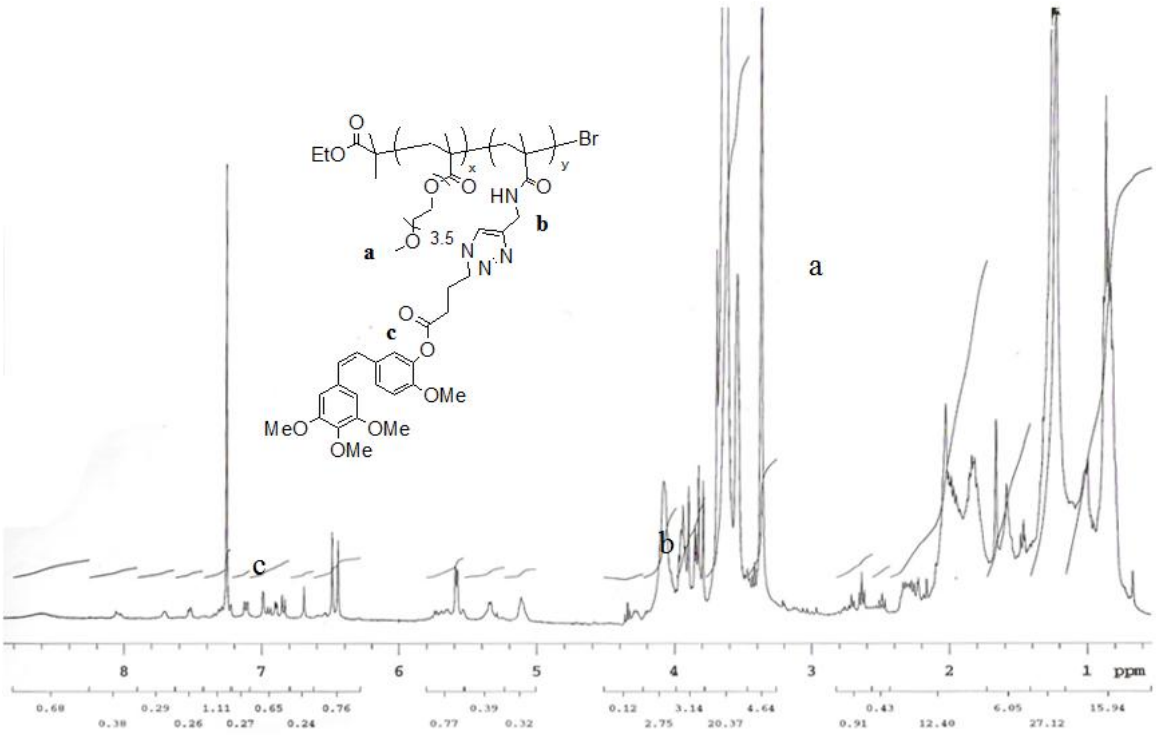

Figure 3.24. ^{1}H-NMR spectrum of Poly- C-N_3 conjugate (**22**)

4. EXPERIMENTAL

4.1. Materials and Methods

All chemicals were used as received from manufacturer (Merck, Aldrich, Alfa Aesar, Riedel de Haen). Dry solvents (CH_2Cl_2, THF) were obtained from ScimatCo Purification System, other solvents were dried over molecular sieves. Column chromatography was performed using silicagel-60 (43-60 nm). Thin layer chromatography was performed using silica gel plates (Kiesel gel 60 F254, 0.2mm, Merck). Plates were viewed under 254 nm UV lamp. High Pressure Liquid Chromatography (HPLC) was performed with Schimadzu LC-20 AT with ACN:Water (65:35) solvent system and preparative HPLC was performed with LC-6 AD. Infrared spectroscopy was carried out on Thermo Scientific Nicolet 380 FT-IR spectrophotometer. ^{1}H NMR (operating at 400 MHz) was recorded on Varian Mercury-MX in $CDCl_3$ and DMSO-d_6 as solvent at the Advanced Technologies Research and Development Center at Boğaziçi University.

Poly(ethylene glycol) methyl ether metacrylate (Mw = 300) (PEGMA, 99%, Aldrich) and *N, N, N', N'', N''*-pentamethyldiethylenetriamine (PMDETA, Aldrich) were passed through basic alumina column to remove inhibitor. The polymer characterizations involved ^{1}H solution NMR spectroscopy (Varian 400 MHz and and Bruker 260 MHz), and Fourier transform infrared (FTIR) spectroscopy (Perkin Elmer 1600 Series). The molecular weights were estimated by gel permeation chromatography (GPC) analysis using a Viscotek GPCmax VE-2001 analysis system. PLgel (length/ID 300 mm 3 7.5 mm, 5 lm particle size) Mixed-C column was caliberated with polystyrene standards, using refractive index detector. THF was used as elutent at a flow rate of 1 mL/min at 30 ^{o}C.

4.2. Synthesis

4.2.1. Synthesis of Reactive Monomer and Reactive Polymers

4.2.1.1. Synthesis of 6-azido hexan-1-ol (2)

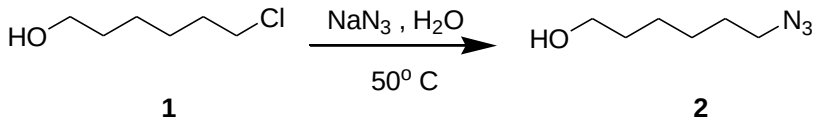

Figure 4.1. Synthesis of 6-azido hexan-1-ol (**2**)

6-chloro 1-hexanol (4 mL, 30mmol) and sodium azide (3.9 g, 60 mmol) are dissolved in distilled water (40 mL). Then, reaction mixture is heated and stirred at 50 ^{o}C for 12 h. The stirred solution is extracted with CH_2Cl_2 (40 mL), dried over Na_2SO_4 and evaporated to obtain transparent liquid (91 % yield). FTIR (cm^{-1}); 3332.

4.2.1.2. Synthesis of AHMA Monomer (4)

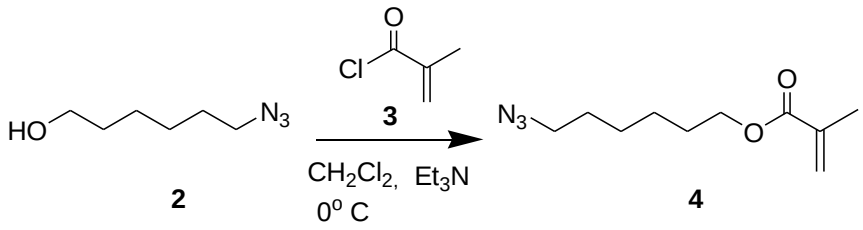

Figure 4.2. Synthesis of AHMA Monomer (**4**)

To a solution of 6-azido hexan-1-ol (1.00 g, 7.69 mmol) and triethylamine (1.28 mL, 9.23 mmol) in CH_2Cl_2 (80 mL) at 0°C, was added methacryloyl chloride (1 mL, 10 mmol) in 0.1 mL portions over 30 min . The clear solution was stirred for 2 h at 0°C under dry condition. To the reaction mixture was added dichloromethane (40 mL) and the mixture was washed with saturated $NaHCO_3$ (2 × 40 mL) and H_2O (2 × 40 mL). The combined organic layers were dried over anhydrous Na_2SO_4 and concentrated to give a yellowish liquid that was purified by flash chromatography on SiO_2 (EtOAc : Hexane 1 : 99) affording 1.20 g (75 % yield) monomer. ^{1}H NMR ($CDCl_3$, δ, ppm); 6.06 (s, 1 H, =CH),

5.52 (s, 1 H, =CH), 4.22 (t, *J* = 6.8 Hz, 2 H, CH_2O), 3.52 (t, *J* = 6.8 Hz , 2 H, CH_2N_3), and 1.91-1.37 (m, 8 H, COO-CH_2-CH_2-CH_2-CH_2-CH_2-CH_2-N_3). FTIR (cm^{-1}); 2096, 1715.

4.2.1.3. Azide Functionalized Reactive Polymer Synthesis (3)

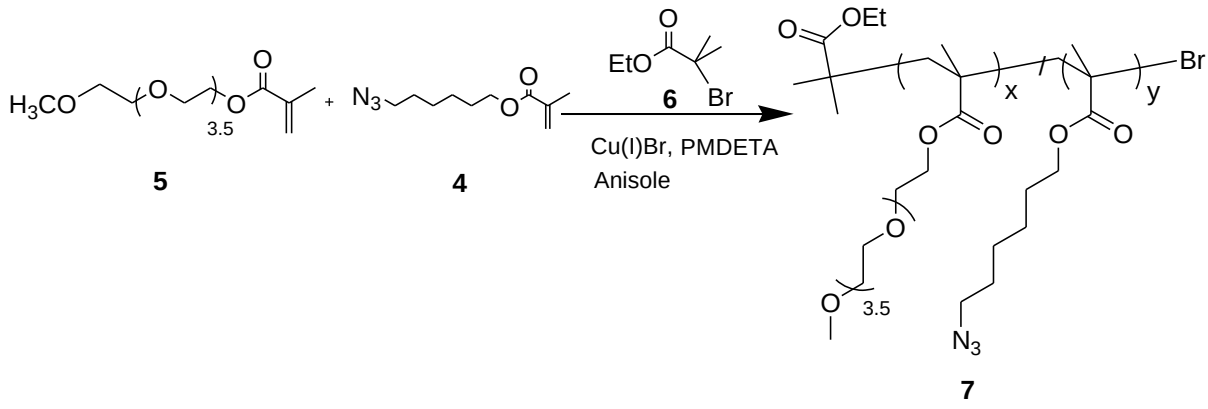

Figure 4.3. Synthesis of Azide Functionalized Copolymer **7**

In a typical polymerization, AHMA (**4**) (0.207 g, 0.98 mmol) and copper (I) bromide (Cu(I)Br) (2.5 mg, 0.018 mmol) were weighed into a dry 10 mL round bottom flask (RBF) equipped with a stir-bar. The flask was sealed and purged with dry nitrogen gas. Then, degassed N,N,N′,N″,N″-Pentamethyldiethylenetriamine (PMDETA) (7.3 μL, 0.035 mmol), PEGMA (1.72 mL, 6.02 mmol) and anhydrous anisole (2 mL) were added to the RBF via syringe and the reaction mixture was stirred for 15 min at room temperature to allow catalyst formation, indicated by a color change to yellow. To the stirring mixture was added ethyl 2-bromoisobutyrate (EBIB) (2.57 μL, 0.0175 mmol) via syringe then the reaction mixture was placed in an 80 ˚C oil bath for 30 min. The reaction ratio was [PEGMA]:[AHMA]:[PMDETA]:[Cu(I)Br]:[EBIB], 86:14:0.5:0.25:0.25. After terminating the polymerization the crude mixture was purified by precipitation into cold diethyl ether and passed through aluminum oxide to remove cupper catalyst. Finally, filtered product was dried under vacuum. ^{1}H NMR ($CDCl_3$, δ, ppm); 4.05-3.80 (m, 4H, COO-C*H*$_2$), 3.63 (br s, 14H, -C*H*$_2$C*H*$_2$O-), 3.51 (br s, 2H, -C*H*$_2$$CH_2$O-), 3.35 (s, 3H, O-C*H*$_3$), 3.28 (t, *J* = 7.6, 2H, CH_2-N_3), 1.91-0.82 (m, 8H, COO-CH_2-CH_2-CH_2-CH_2-CH_2-CH_2-N_3 and CH_2 and CH_3 along polymer backbone).

4.2.1.4. Synthesis of PEG-NHS polymer 9

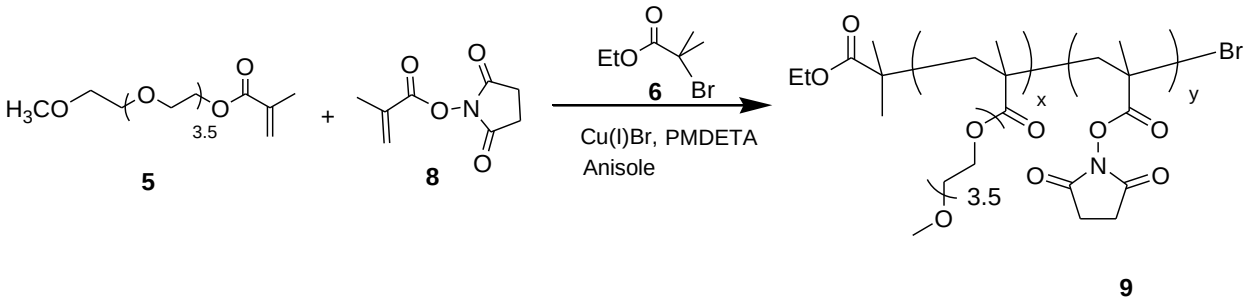

Figure 4.4. Synthesis of PEG-NHS polymer **9**

In a typical polymerization, N-methacryloxysuccinimide (**9**) (179.5 mg, 0.98 mmol) and copper (I) bromide (Cu(I)Br) (2.5 mg, 0.018 mmol) were weighed into a dry 10 mL round bottom flask equipped with a stir-bar. The flask was sealed and purged with dry nitrogen gas. Then, degassed N,N,N′,N″,N″-Pentamethyldiethylenetriamine (PMDETA) (7.3 μL, 0.035 mmol), PEGMA (1.72 mL, 6.02 mmol) and anhydrous anisole (2 mL) were added to the RBF via syringe and the reaction mixture was stirred for 20 min at room temperature to allow catalyst formation, indicated by a color change to blue. To the stirring mixture was added ethyl 2-bromoisobutyrate (EBIB) (2.57 μL, 0.0175 mmol) via syringe then the reaction mixture was placed in an 80 ˚C oil bath for 30 min. The reaction ratio was [PEGMA] : [NHSMA] : [PMDETA] : [Cu(I)Br] : [EBIB], 86 : 14 : 0.5 : 0.25 : 0.25. After terminating the polymerization the crude mixture was purified by precipitation into cold diethyl ether and passed through aluminum oxide to remove cupper catalyst. Finally, filtered product was dried under vacuum. ^{1}H NMR ($CDCl_3$, δ, ppm); 4.09 (br s, 4H, COO-C*H*$_2$), 3.65 (br s, 14H, -CH_2CH_2O-), 3.37 (s, 3H, O-C*H*$_3$), 2.80 (br s, 4H, CH_2CH_2C=ON), 1.72-0.86 (m, 6H, CH_2 and CH_3 along polymer backbone).

4.2.1.5. Alkyne Functionalized Reactive Polymer Synthesis (PEG-alkyne copolymer, 11)

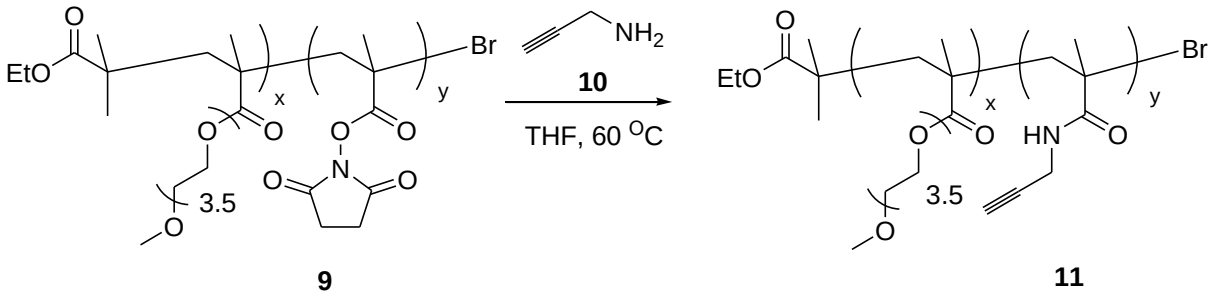

Figure 4.5. Synthesis of Alkyne Functionalized Copolymer **11**

PEG-NHS copolymer **9** (800 mg, 0.037 mmol), propargyl amine (**10**) (257,46 µL, 4.02 mmol) and TEA (280 µL, 2,01 mmol) are put into 10 mL RBF and dissolved in THF under N_2 gas and exposed to N_2 gas for 15 min to keep reaction dry. Then, reaction mixture is refluxed overnight at 60 ^oC. Reaction mixture is precipitated in cold ether until removal of excess propargyl amine (**10**). Product **11** was dried under vacuum. ^1H NMR ($CDCl_3$, δ, ppm); 4.09 (br s, 4H, COO-CH_2), 3.65 (br s, 14H, -CH_2CH_2O-), 3.37 (s, 3H, O-CH_3), 2.29 (br s, 1H, ≡CH), 1.72-0.86 (m, 6H, CH_2 and CH_3 along polymer backbone).

4.2.2. Synthesis of Cis-Combretastatin A-4

4.2.2.1 Synthesis of E-2-(3',4',5'-Trimethoxyphenyl)-3-(3'-hydroxy-4'-methoxyphenyl) prop-2-enoic acid (14)

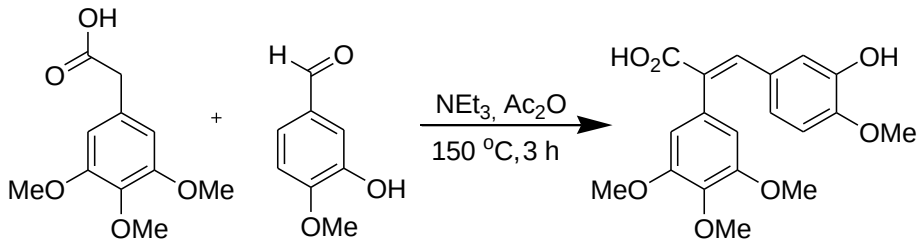

12 **13** **14**

Figure 4.6. Synthesis of propenonic acid **14**

E-2-(3', 4', 5'-Trimethoxyphenyl)-3-(3'-hydroxy-4'-methoxyphenyl) prop-2-enoic acid was synthesized according to the literature procedure [20]. A mixture of 3-hydroxy-4-methoxybenzaldehyde (**13)** (0.67 g, 4.4 mmol), 3, 4, 5-trimethoxyphenylacetic acid (**12)** (2 g, 8.84 mmol) acetic anhydride (4 mL) and triethylamine (2 mL) were heated under reflux for 3 h. After acidification with concentrated hydrochloric acid (6 mL), the resulting solid was filtered off and recrystalized from ethanol to give propenoic acid **14** (1,4 g, 88%) as fine yellow needles. ^1H-NMR (400 MHz, δ, DMSO-d_6): 7.58 (s, 1 H), 6.80 (d, J = 8.3 Hz, 1 H), 6.61 (dd, J = 8.3, 1.9 Hz, 1 H), 6.54 (s, 1 H), 6.44 (s, 2 H), 3.74 (s, 3 H), 3.72 (s, 3 H), 3.68 (s, 6 H).

4.2.2.2. Synthesis of Combretastatin A-4 (15) by Decarboxylation of Cinnamic Acid

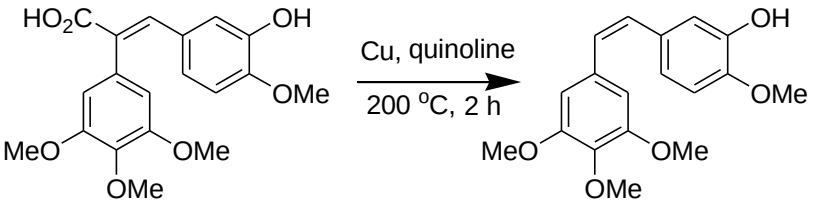

14 **15**

Figure 4.7. Synthesis of Combretastatin A-4 (**15**)

Cis Combretastatin A-4 (**15**) was synthesized according to the literature procedure [20]. (*E*)-3-(3'-Hydroxy-4'- methoxyphenyl)- 2-(3'',4'',5''-trimethoxyphenyl)prop-2-enoic acid (**14)**, (2 g, 5.56 mmol) was added to powdered copper (1.84 g, 28.8 mmol) in quinoline (20 mL, 21.9 g, 0.17 mol), and the resulting mixture was heated at 200 °C for 2 h. Upon cooling, ether was added, and the copper was filtered off through Celite. The filtrate was washed with 1 M hydrochloric acid, and the aqueous layer was separated and extracted with ether. The combined organic layers were washed with saturated aqueous sodium carbonate, water, brine, dried (Na_2SO_4), and concentrated in *vacuum*. Flash column chromatography and recrystalization from ethyl acetate and hexane afforded cis combretastatin A-4 (**15**) as a pale yellow crystalline solid (1.19 g, 68%). ^{1}H NMR($CDCl_3$, δ, ppm); 6.9 (d, *J* = 2 Hz, 1H, CH=COH), 6,8 (dd, *J* = 8,4 Hz, *J* = 2 Hz, 1H, CH-C-CH=COH), 6,71 (d, *J* = 8,4 Hz, 1H, CH=C-C-OH), 6,56 (s, 2H,CH=C-CH), 6,42 (q, *J* = 12.4, 2H, bridged CH=), 3,85 (s, 3H, CH_3-OC-COH), 3,82 (s, 3H, CH_3O-C-CO CH_3), 3,68 (s, 6H, CH_3O-C-C-OCH_3=C-OCH_3). FTIR (cm^{-1}); 3419.

4.2.2.3. 4-azidobutyric acid ethyl ester (19)

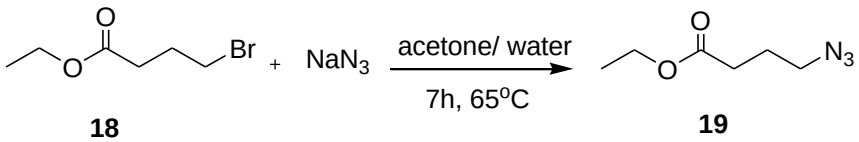

18 **19**

Figure 4.8. 4-azidobutyric acid ethyl ester (**19**)

4-azidobutyric acid ethyl ester (**19**) was synthesized according to the literature procedure [21]. A stirred solution of 4-bromobutyric acid ethyl ester (**18**) (2.21 mL, 15.4 mmol) and

sodium azide (2 g, 30.8 mmol) in acetone/water (22.5/7.5 mL) was heated under reflux for 7 h. The MeOH was removed in vacuo and the residue was partitioned between CH2Cl2 and water. The product was extracted three times with CH2Cl2, and the combined organic extracts were dried over MgSO4 and evaporated to dryness to give the azido ester **19** (2.19 g, 90%) as a colorless oil. FTIR (cm^{-1}); 2095, 1731.

4.2.2.4. 4-azidobutyric acid (20)

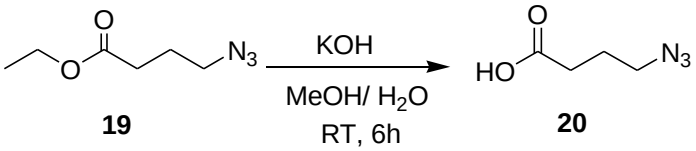

Figure 4.9. Synthesis of 4-azidobutanoic acid (**20**)

4-azidobutyric acid (**20**) synthesized according to the literature procedure [21]. Potassium hydroxide (3.9 g, 69.6 mmol) was added to a solution at 0°C of 4-azidobutyric acid ethyl ester 24 (2.19 g, 13.9 mmol) in a mixture of 32 mL MeOH and 26 mL water. The solution was stirred at room temperature for 6 h and then evaporated. The residue was partitioned between CH2Cl2 and water. The aqueous layer was extracted twice with CH2Cl2, acidified to pH 1 with 1N aqueous HCl and extracted five times with Et2O. The organic extracts were combined, dried over Na_2S0_4 and evaporated to dryness to afford the azido acid **20** (1.77 g, 99%) as a colorless oil. ^{1}H NMR ($CDCl_3$, δ, ppm); 3.37 (t, *J* = 6.8, 2 H, CH_2N_3), 2.46 (t, *J* = 6.8, 2 H, O=C-CH_2), 1.90 (m, 2 H, CH_2- CH_2N_3). FTIR (cm^{-1}); 2940, 2093, 1705.

4.2.2.5. CA-4 azide derivative (C-N_3, 16)

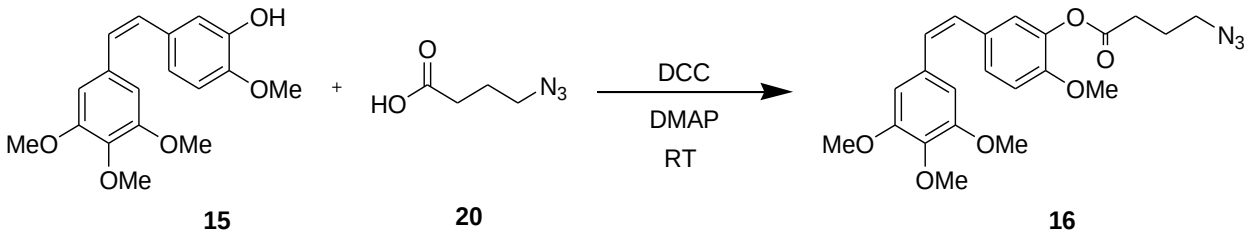

Figure 4.10.Synthesis of CA-4 azide derivative (C-N_3, **16**)

To a stirred solution of 4-azidobutanoic acid (**20**) (82.3 mg, 0.638 mmol) in 5 mL anhydrous CH_2Cl_2 is added DMAP (7.8 mg, 0.0638) and CA-4 (**15**) (182 mg, 0.58 mmol).

DCC (131.64 mg, 0.638 mmol) is added to the reaction mixture at 0 ^{o}C, which is then stirred for 5min at 0°C and 7 h at RT. Precipitated urea is then filtered off and the filtrate evaporated down in vacuo. The residue is taken up in CH_2Cl_2. CH_2Cl_2solution is washed twice with 1 M HCl and with saturated $NaHC0_3$ solution, and then dried over Na_2S0_4. The solvent is removed by evaporation and product **16** is obtained in pure form by flash column chromatography from EtOAc: CH_2Cl_2: Hexane mixture.(94 % yield). ^{1}H NMR($CDCl_3$, δ, ppm); 7,10 (dd, *J* = 8,4 Hz, *J* = 2,1 Hz, 1 H, CH=COH), 6,98 (d, *J* = 2,1 Hz, 1 H, CH-C- CH=COH), 6,83 (d, *J* = 8,4 Hz, 1H, CH=C-C-OH), 6,48 (s, 2 H,CH=C-CH), 6,44 (s, 2 H, bridged =CH), 3,82 (s, 3 H, CH_3O-C-CO CH_3), 3,78 (s, 3 H, CH_3-OC-COH), 3,69 (s, 6 H, CH_3O-C-C-OCH_3=C-OCH_3), 3,40 (t, *J* = 7.1 Hz, 2 H, CH_2N_3), 2,63 (t, *J* = 7,1 Hz, 2 H, O=C-CH_2), 1,98 (m, 2 H, CH_2- CH_2N_3). FTIR (cm^{-1}); 2095, 1760.

4.2.2.6. CA-4 alkyne derivative (10)

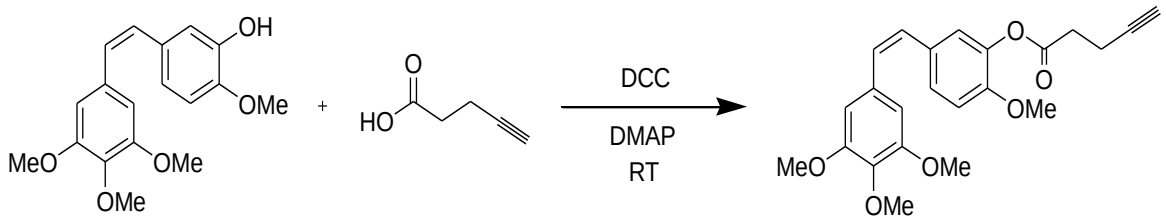

15 **21** **17**

Figure 4.11.Synthesis of CA-4 alkyne derivative (**10**)

To a stirred solution of 4-pentynoic acid (**21**) (17 mg, 0.174 mmol) in 5 mL anhydrous CH_2Cl_2 is added DMAP (2 mg, 0.0174) and CA-4 (**15**) (50 mg, 0.158 mmol. DCC (36 mg, 0.174 mmol) is added to the reaction mixture at 0 ^{o}C, which is then stirred for 5min at 0°C and 7 h at RT. Precipitated urea is then filtered off and the filtrate evaporated down in vacuo. The residue is taken up in CH_2Cl_2. CH_2Cl_2solution is washed twice with 1 M HCl and with saturated $NaHC0_3$ solution, and then dried over Na_2S0_4. The solvent is removed by evaporation and the residue was purified by silica gel column chromatography ($CHCl_3$). The residue was purified by flash column chromatography (EtOAc: CH_2Cl_2: Hexane mixture) to obtain pure product **17** (61 mg, 97 % yield). ^{1}H NMR($CDCl_3$, δ, ppm); 7,12 (dd, J_1 = 8,4 Hz, J_2 = 2,1 Hz, 1 H, CH=COH), 7,02 (d, *J* = 2,1 Hz, 1 H, CH-C- CH=COH), 6,84 (d, *J* = 8,4 Hz, 1H, CH=C-C-OH), 6,5 (s, 2 H,CH=C-CH), 6,45 (s, 2 H, bridged

=CH), 3.83 (s, 3 H, CH_3O- C-CO CH_3), 3,79 (s, 3 H, CH_3-OC-COH), 3,704 (s, 6 H, CH_3O-C-C-OCH_3=C-OCH_3), 2,78 (t, *J* = 7,6 Hz, 2H ,CH_2C=O), 2,59 (dt, J_1=7,6 Hz, J_2 = 2,8 Hz, 2H, CH_2-C≡), 2,00 (t, *J* = 2,8 Hz, 1H, C≡H). FTIR (cm^{-1}); 3301, 1752.

4.2.3. Conjugation of Drug Molecules on Reactive Polymers

4.2.3.1. PEG-AHMA- C-≡ conjugate for 50 % conversion

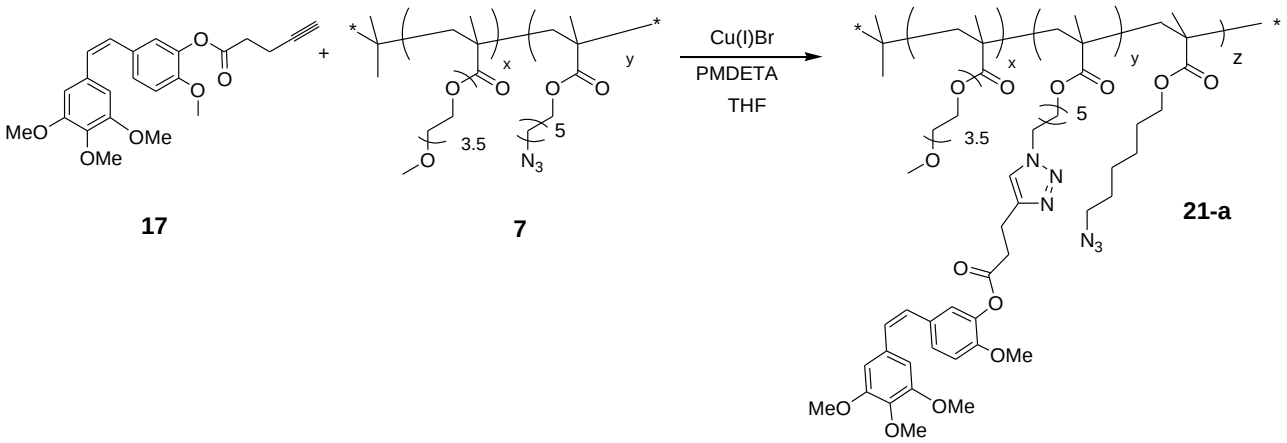

17 **7**

Figure 4.12. Synthesis of Poly- C-≡ conjugates **21-a**

C-≡ (**17**) (7.8 mg, 0.02 mmol) and copper (I) bromide (Cu(I)Br) (1.14 mg, 0.008 mmol) are weighed into a 10 mL RBF equipped with a stir-bar. The flask is purged with dry nitrogen gas adding 1 mL degassed THF into the flask. PEG-AHMA copolymer **7** (1:4, 10 K) (50 mg, 0.005 mmol) in 2 mL THF is added into the flask. After that, degassed N,N,N′,N″,N″-Pentamethyldiethylenetriamine (PMDETA) (1.14 μL, 0.002 mmol) is added into reaction mixture. The reaction mixture was stirred for 24 h at RT. To purify the product **21-a** membrane dialysis (1000 K) is made in MeOH. ^{1}H NMR ($CDCl_3$, δ, ppm); 7,39 (s, 1H, CH from triazole), 7,10 (d, *J* = 8,4 Hz, 1 H, CH=COH), 6,96 (s, 1 H, CH-C-CH=COH), 6,82 (d, *J* = 8,4 Hz, 1H, CH=C-C-OH), 6,48 (s, 2 H,CH=C-CH), 6,42 (s, 2 H, bridged =CH), 4.3 (br s, 2H, CH_2N), 4,02-3.88 (m, 4H, COO-CH_2), 3,81 (s, 3 H, CH_3O-C-CO CH_3), 3,71 (s, 3 H, CH_3-OC-COH), 3,64 (br s, 20 H, CH_3O-C-C-OCH_3=C-OCH_3 and -CH_2CH_2O from polymer), 3.53 (br s, 2H, -C*H*$_2CH_2O$-), 3,36 (s, 3H, O-C*H*$_3$), 3,28 (br s, 2H, C*H*$_2$-N_3), 3,10 (t, *J* = 7,4 Hz, 2H ,CH_2C=O), 2,95 (t, *J* = 7,4 Hz, 2H, CH_2-C≡), 1,84-

0,96 (m, 8H, COO-CH_2-CH_2-CH_2-CH_2-CH_2-CH_2-N_3 and CH_2 and CH_3 along polymer backbone).

4.2.3.2 PEG-AHMA- C-≡ conjugate

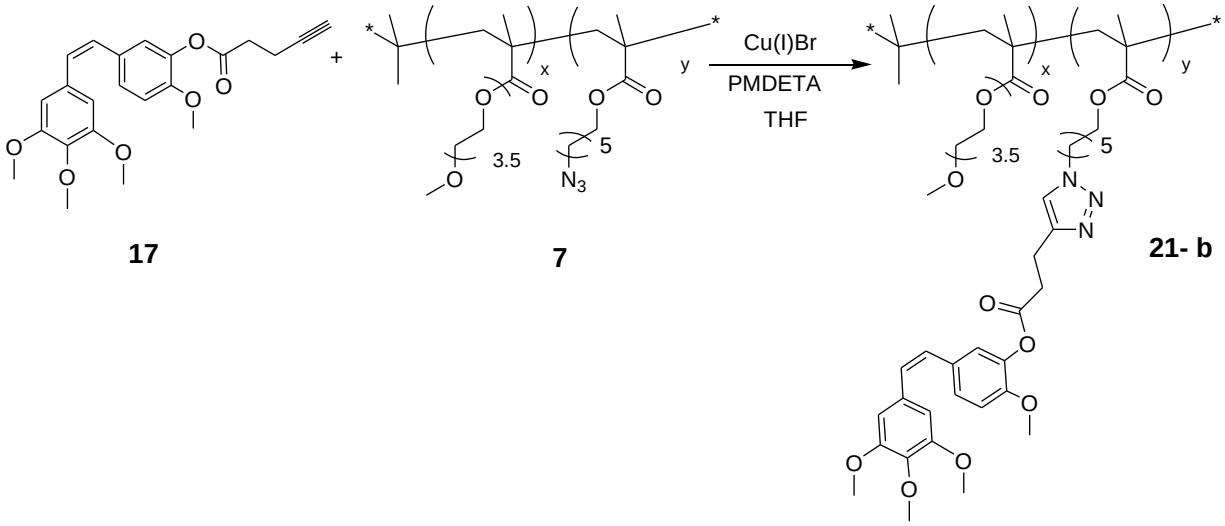

Figure 4.13. Synthesis of Poly- C-≡ conjugates **21-b**

Comb alkyne derivative **17** (18.69 mg, 0.047 mmol) and copper (I) bromide (Cu(I)Br) (2.7 mg, 0.02 mmol) are weighed into a 10 mL RBF equipped with a stir-bar. The flask is purged with dry nitrogen gas adding 1 mL degassed THF into the flask. PEG-AHMA copolymer **7** (1:6, 19 K) (60 mg, 0.003 mmol) in 2 mL THF is added into the flask. After that, degassed N,N,N′,N″,N″-Pentamethyldiethylenetriamine (PMDETA) (4 μL, 0.002 mmol) is added into reaction mixture. The reaction mixture was stirred for 24 h at RT. To purify the product **21-b** membrane dialysis (3500 K) is made in THF. ^{1}H NMR($CDCl_3$, δ , ppm); 7,1 (d, J = 8, 1 H, CH=COH), 6,98 (s, CH-C- CH=COH), 6,81 (1H, d, J = 8, 1H, CH=C-C-OH), 6,47 (s, 2 H,CH=C-CH), 6,42 (s, 2 H, bridged =CH), 4,3 (br s, 2H, CH_2N), 4,06 (br s, 4H, COO-CH_2), 3,80 (s, 3 H, CH_3O-C-CO CH_3), 3,77 (s, 3 H, CH_3-OC-COH), 3,63 (br s, 20 H, CH_3O-C-C-OCH_3=C-OCH_3 and -CH_2CH_2O from polymer), 3.53 (br s, 2H, CH_2CH_2O-), 3,35 (s, 3H, O-CH_3), 2,75 (2H, t, J = 7,2), 2,64 (2H, t, J = 7,2), 1,81 – 0,82 (m, 8H, COO-CH_2-CH_2-CH_2-CH_2-CH_2-CH_2-N and CH_2 and CH_3 along polymer backbone).

4.2.3.3. Poly- C-N_3 conjugate

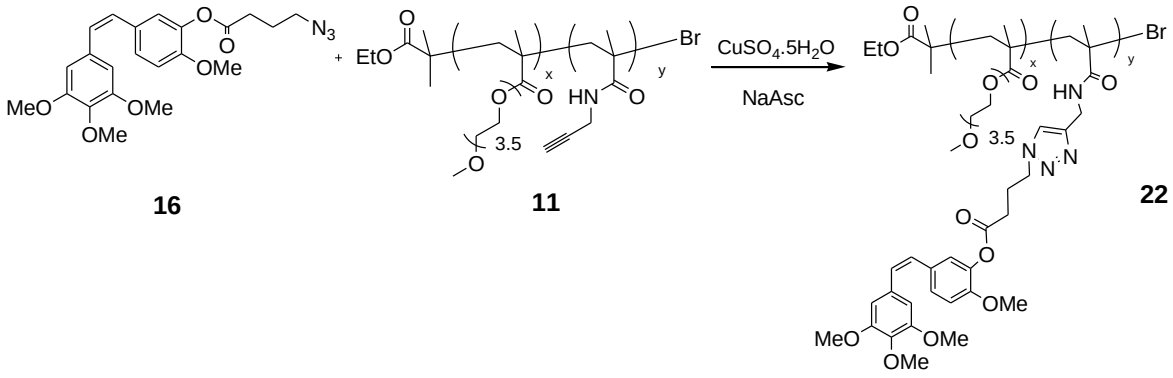

Figure 4.14. Synthesis of Poly- C-N_3 conjugate **22**

A solution of the compound **16** (12,45 mg, 0.029 mmol), compound **11** (42.2 mg, 0.0194 mmol), sodium ascorbate (NaAsc) (2.32 mg, 0.0012 mmol), and CuSO4 (1.5 mg, 0.006 mmol) in a mixture of CHCl3, EtOH and water (1:0.8:0.8 mL) was stirred at room temperature for 50 h. After evaporation of the solvents, the crude product **22** was purified by Sephadex G-25 (H2O) to get rid of free drug. ^{1}H NMR($CDCl_3$, δ, ppm) ; 7,5 (s, 1H, CH-triazole), 7,1 (d, *J* = 8, 1 H, CH=COH), 6,97 (s, 1 H, CH-C- CH=COH), 6,83 (d, *J* = 8, 1H, CH=C-C-OH), 6,47 (s, 2 H,CH=C-CH), 6,43 (s, 2 H, bridged =CH), 4,34 (t, *J* = 6,8, 2H, CH_2-N), 4.09 (br s, 4H, COO-CH_2)3,81 (s, 3 H, CH_3O-C-CO CH_3), 3,78 (s, 3 H, CH_3-OC-COH), 3,64 (s, 20 H, CH_3O-C-C-OCH_3=C-OCH_3 and CH_2CH_2O from polymer), 3,36 (s, 3H, O-CH_3), 2,62 (t, *J* = 7,1 Hz, 2 H, O=C-CH_2), 1,65 -0,85 (m, 6H, CH_2 and CH_3 along polymer backbone).

5. CONCLUSIONS

Synthesis of reactive monomer and reactive polymers, cis - combretastatin A-4 and its derivatives, and conjugation of drug molecules on reactive polymers were achieved successfully. Reactive polymers bearing azide and alkyne functionality enhance the drug loading capacity of PEG polymer. CA-4 containing azide functionality was reacted with alkyne groups of the copolymer via Huisgen type ‘click’ chemistry or vice versa. It is also expected that the drug will show higher water solubility and improved pharmacokinetic properties.

APPENDIX

^{1}H NMR and FTIR spectra of the synthesized products are included.

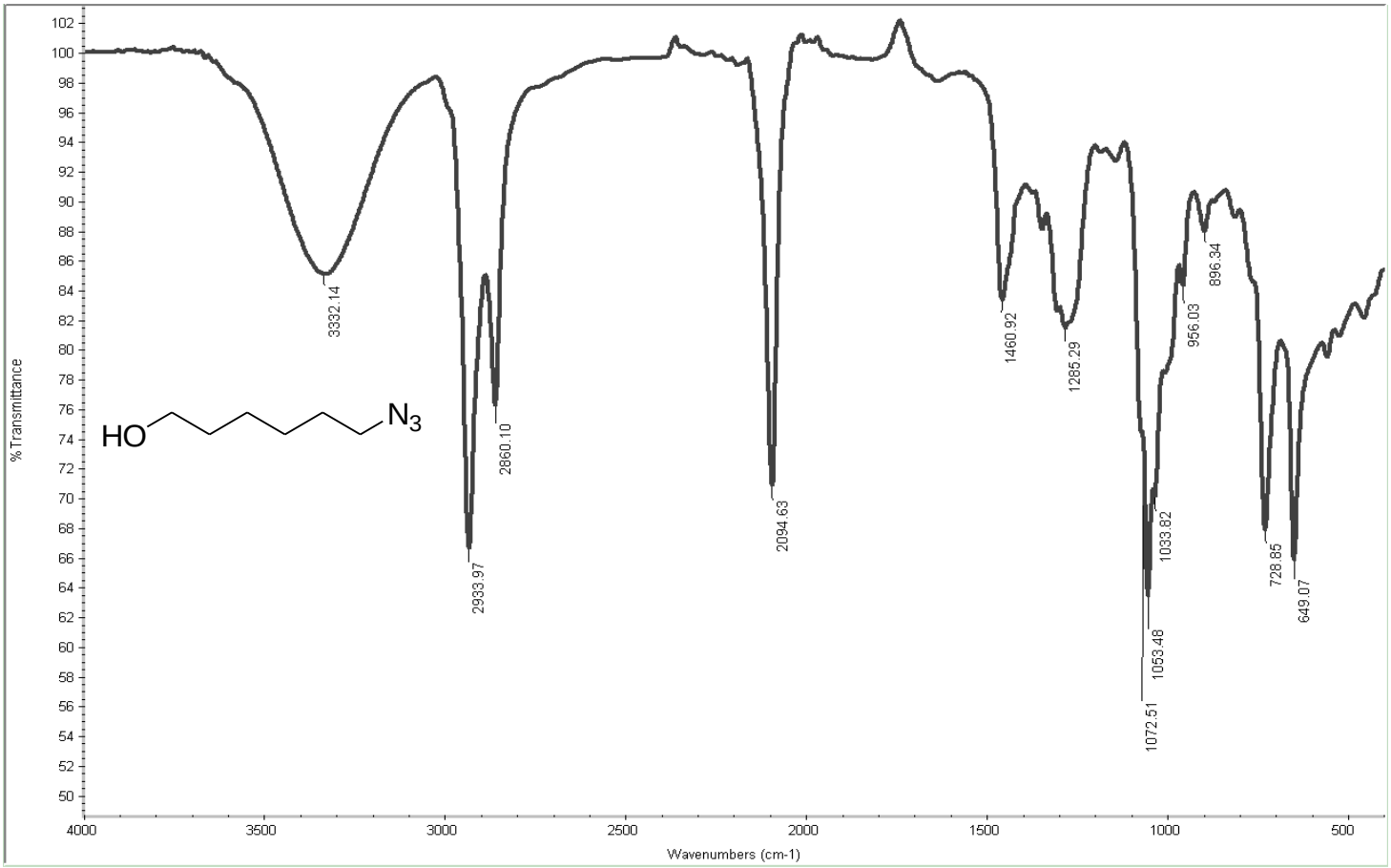

Figure A.1. IR spectrum of 6-azidohexane 1-ol (**2**)

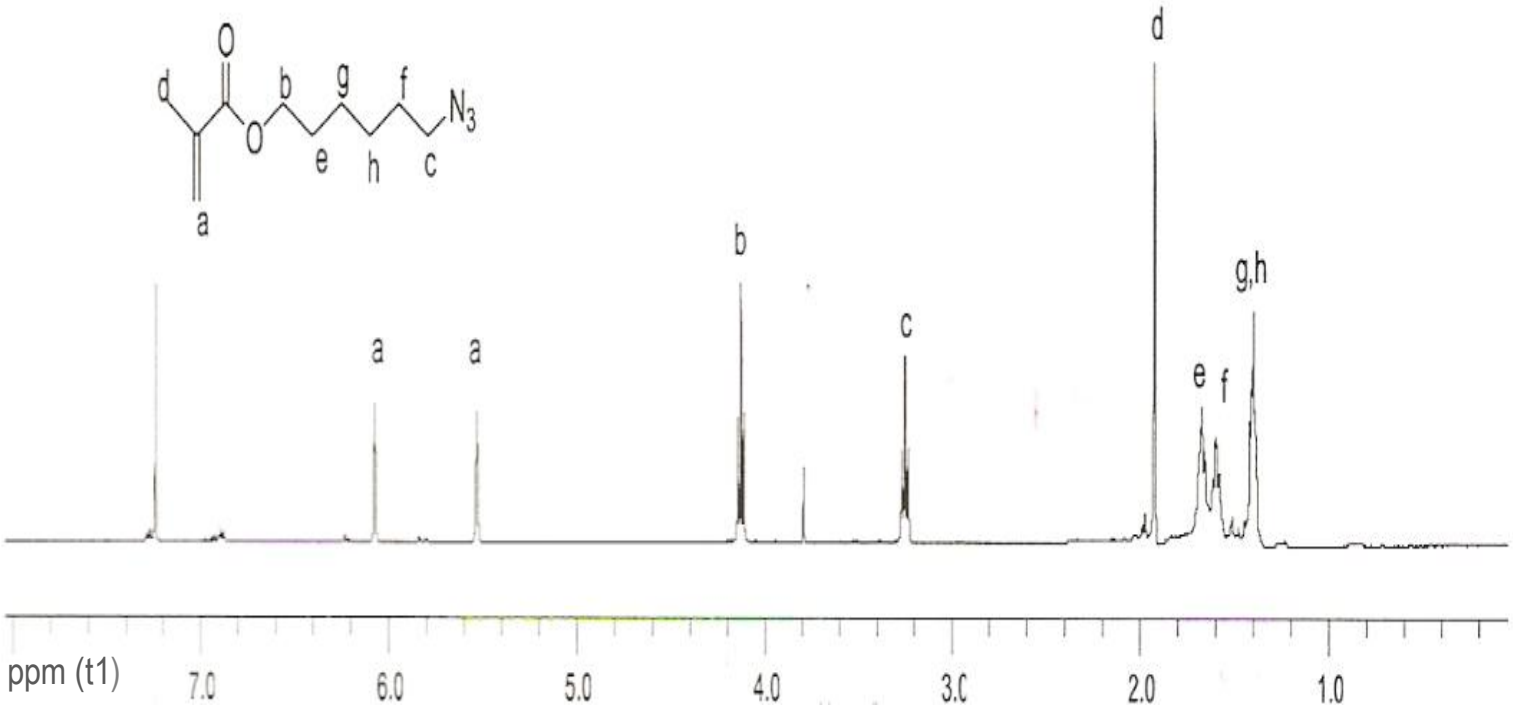

Figure A.2. ^{1}H NMR spectrum of 6-azidohexyl methacrylate (**4**)

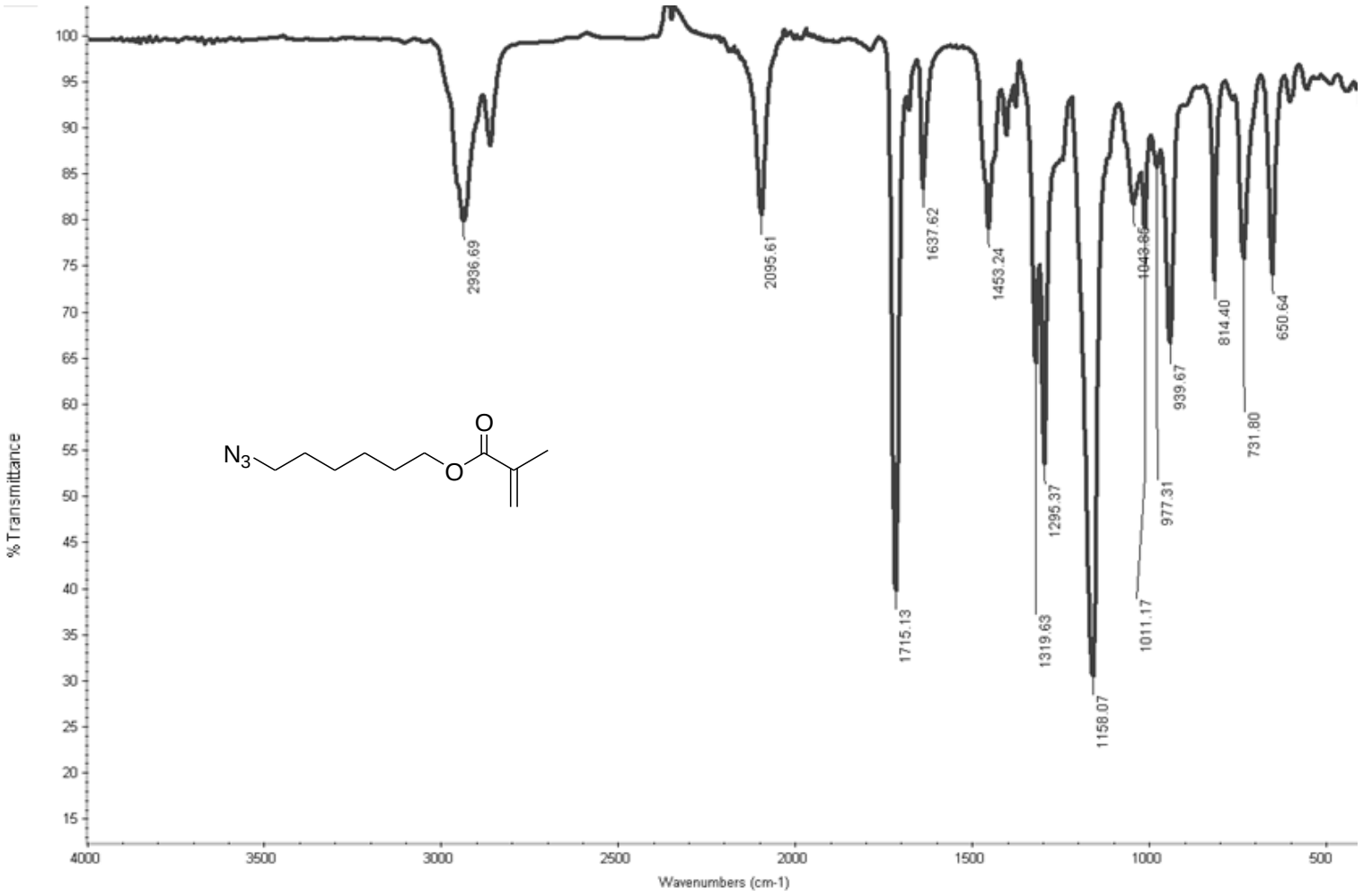

Figure A.3. IR spectrum of 6-azidohexyl methacrylate (**4**)

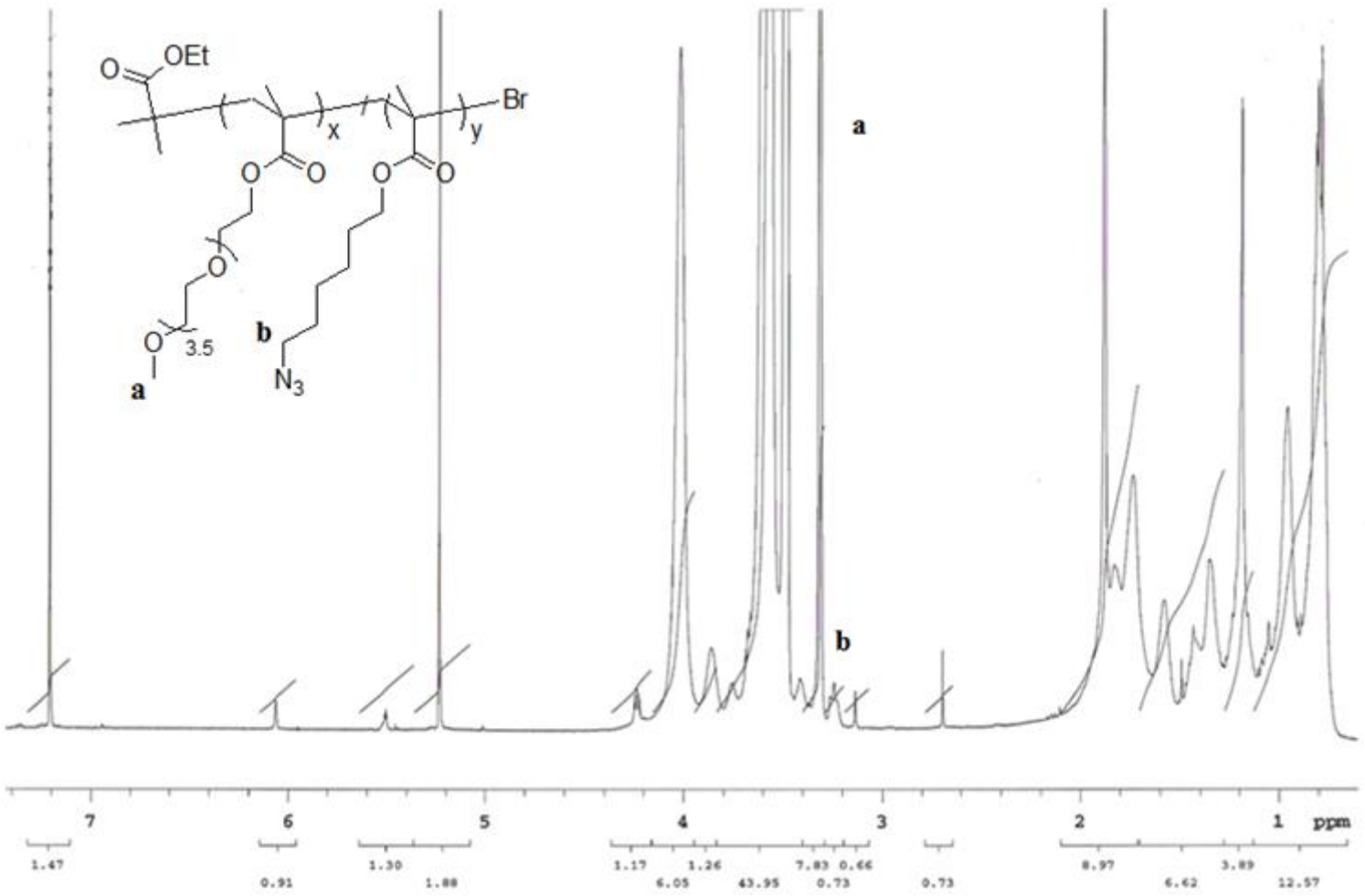

Figure A.4. ^{1}H NMR spectrum of PEG-AHMA **7**

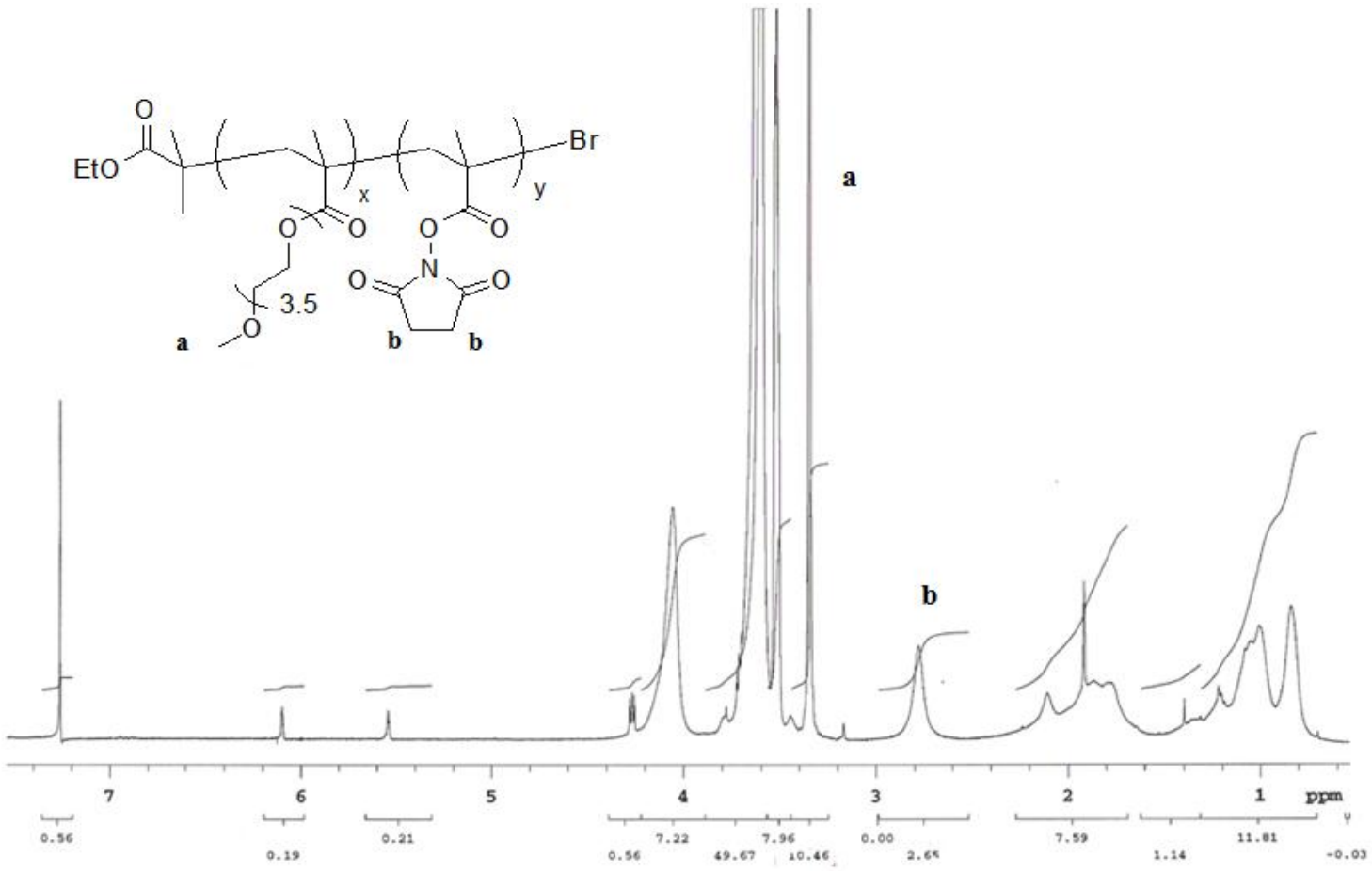

Figure A.5. ^{1}H NMR spectrum of PEG-NHS **9**

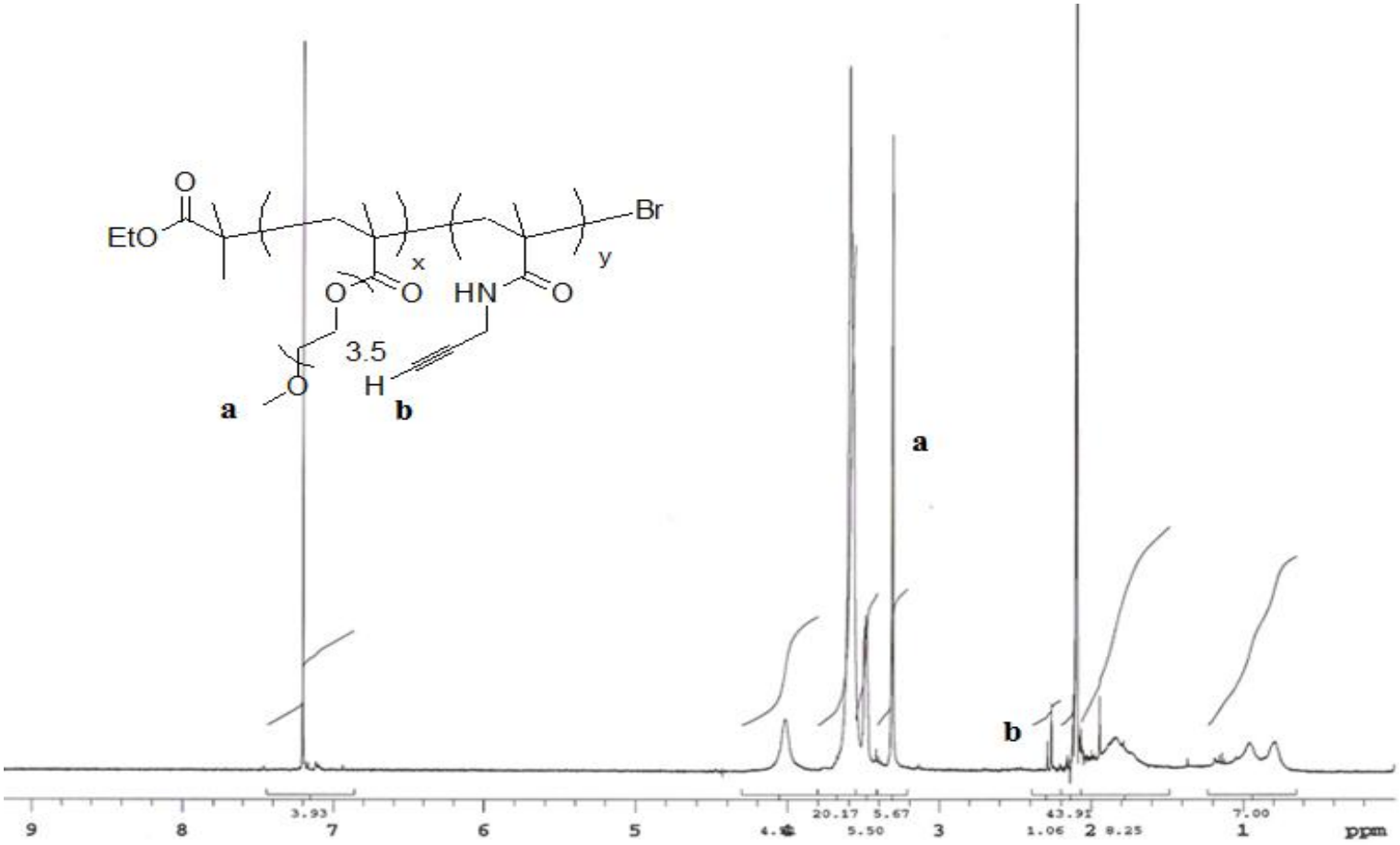

Figure A.6. ^{1}H NMR spectrum of PEG-alkyne **11**

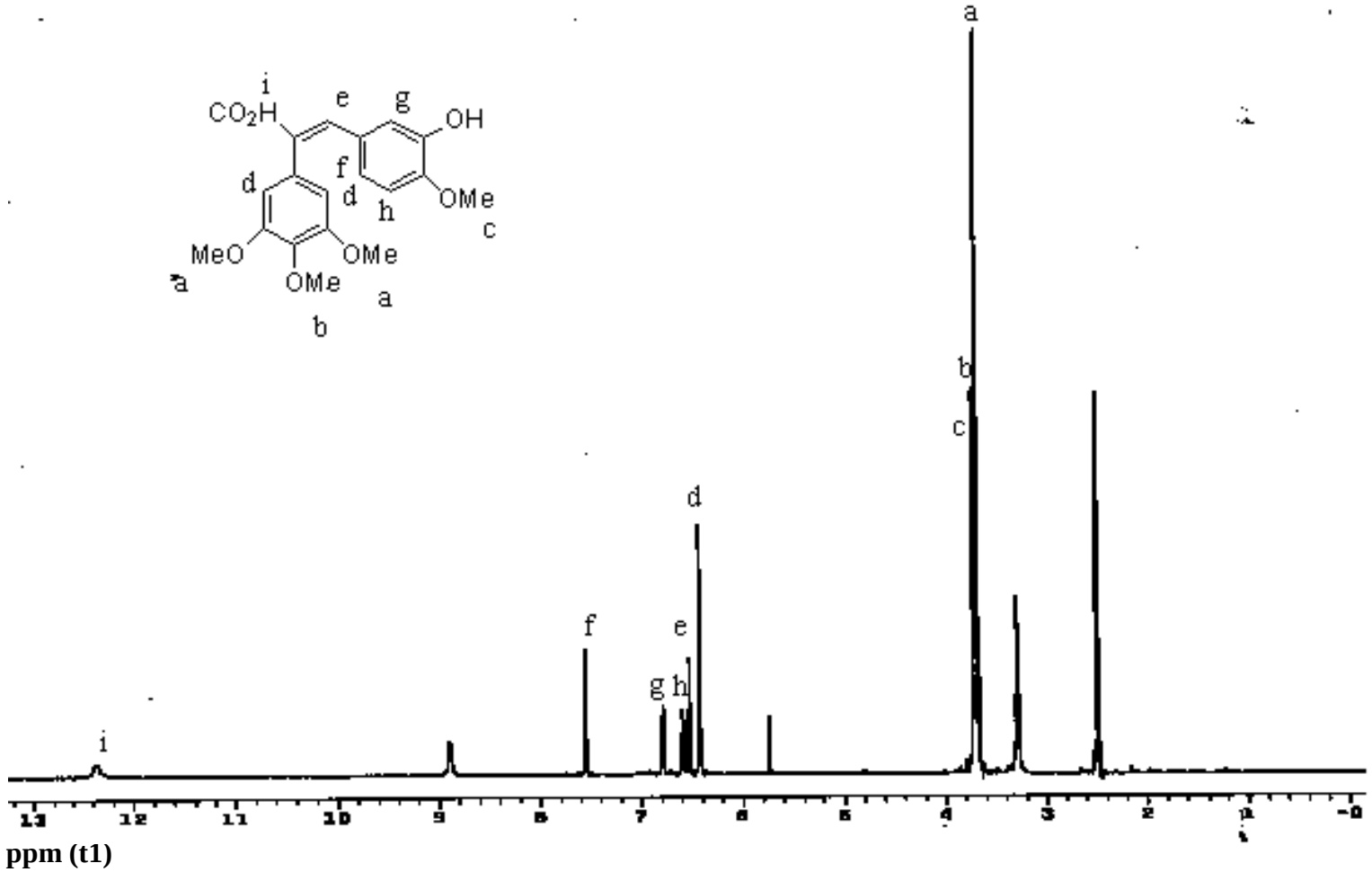

Figure A.7. ^{1}H NMR spectrum of propenoic acid **13**

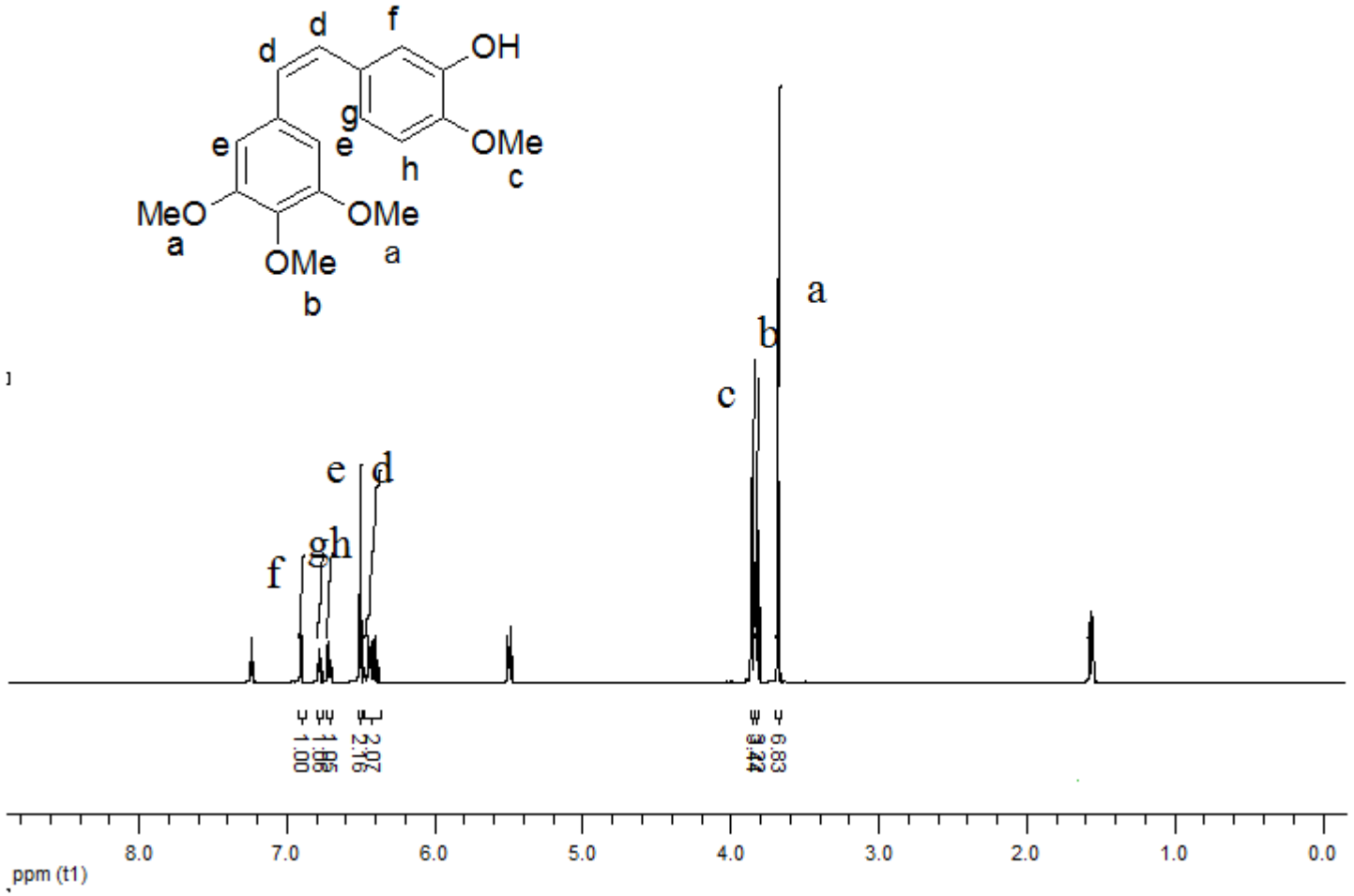

Figure A.8. ^{1}H NMR spectrum of CA-4 (**15**)

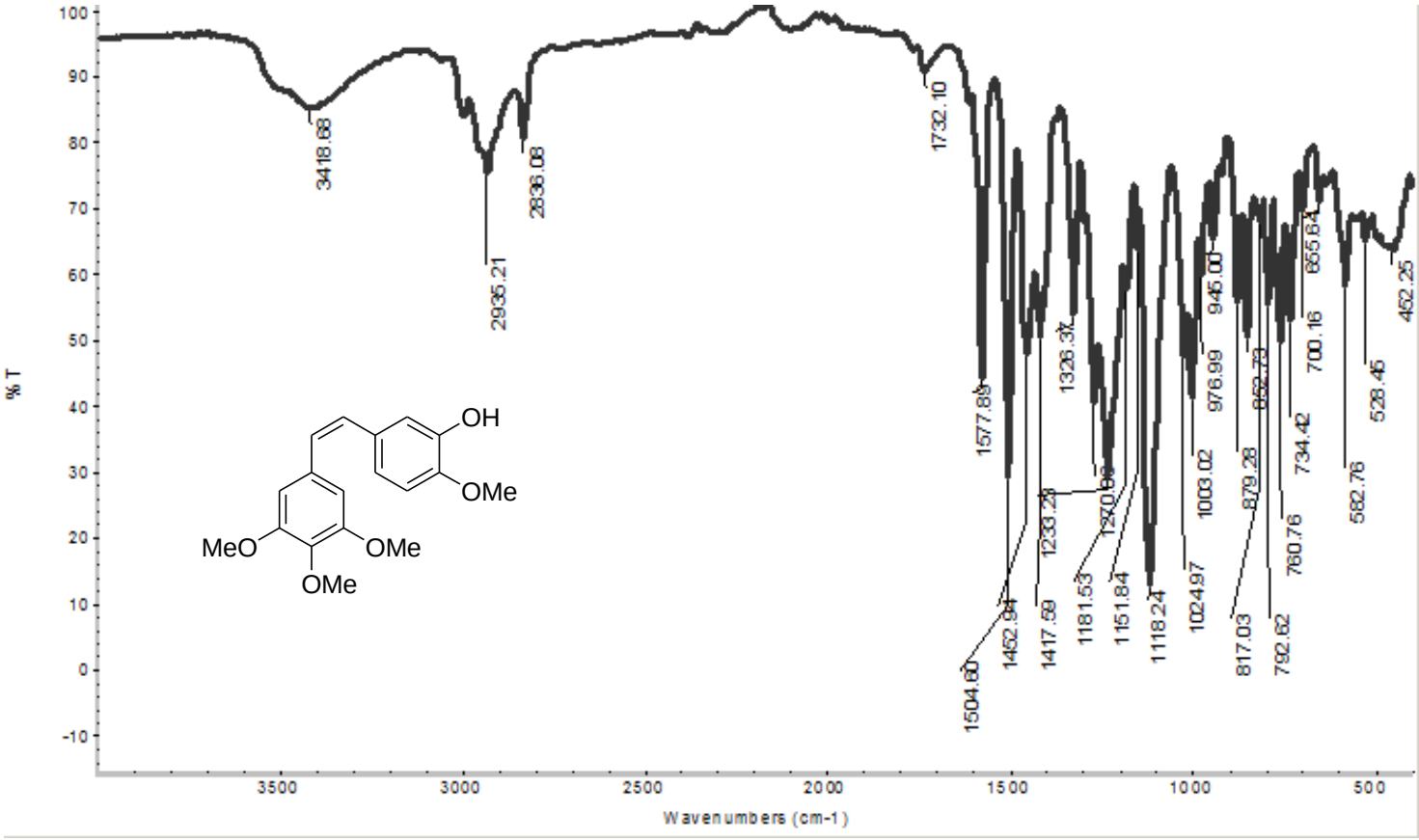

Figure A.9. IR spectrum of CA-4 (**15**)

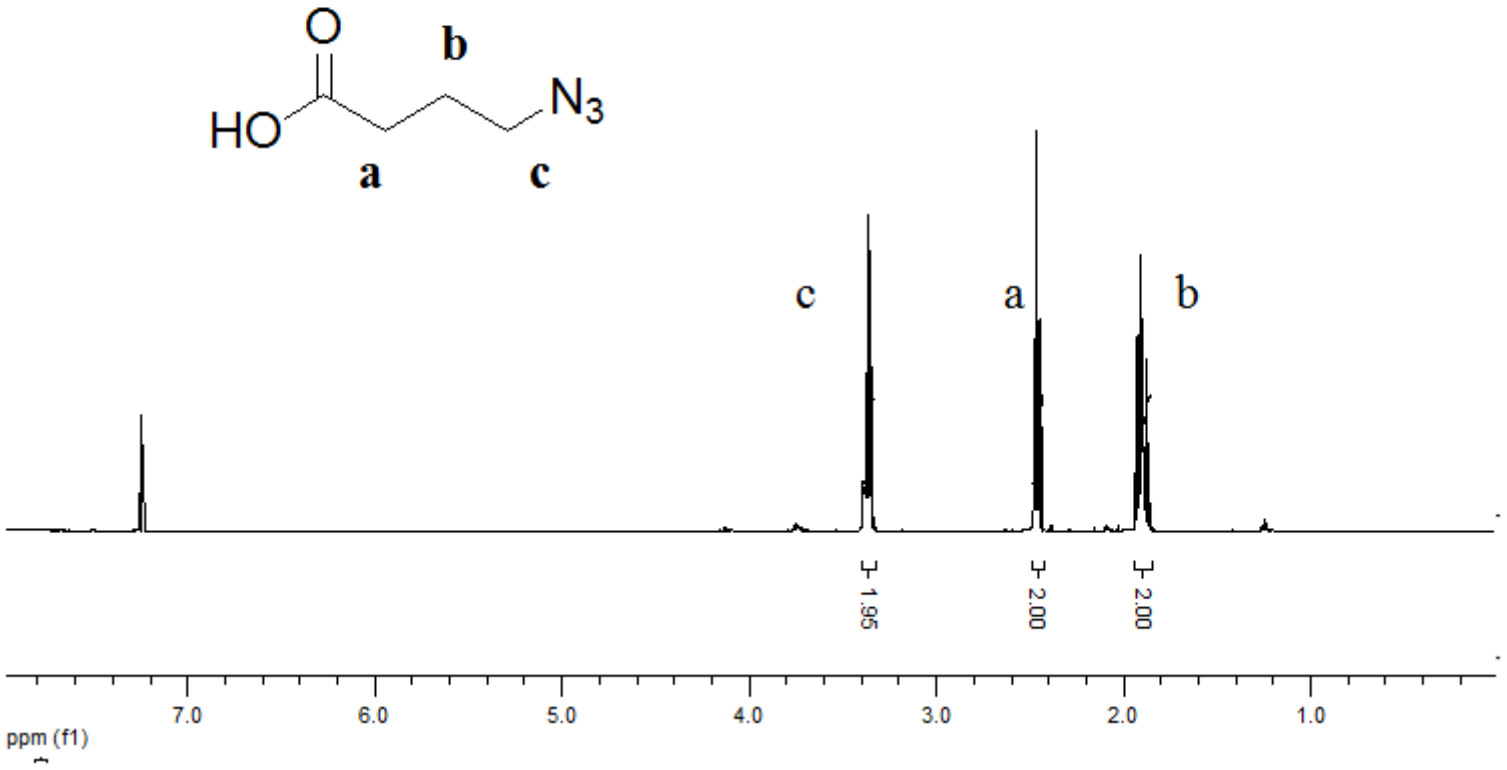

Figure A.10. ^{1}H NMR spectrum of 4-azidobutanoic acid (**20**)

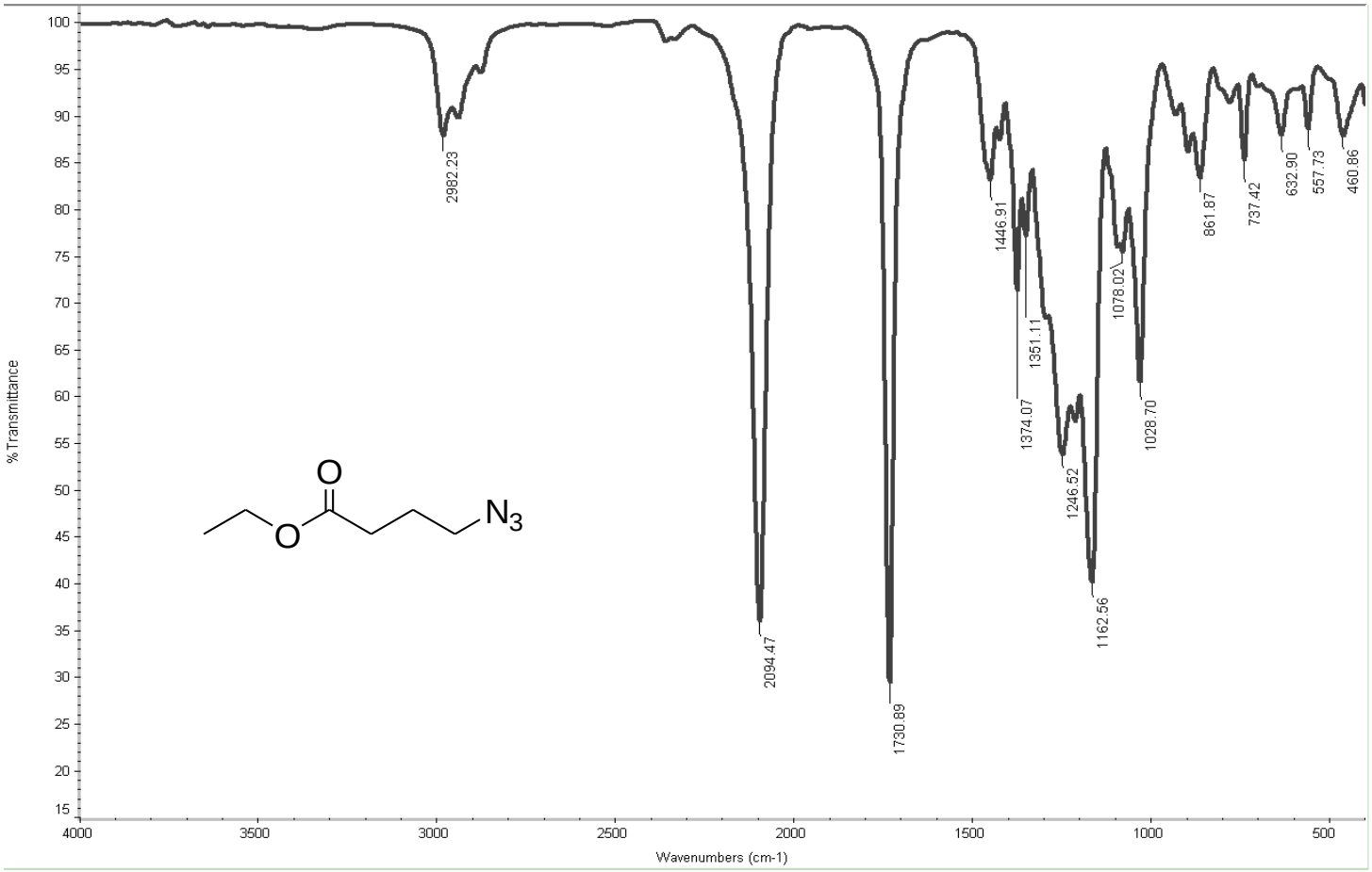

Figure A.11. IR spectrum of 4-azidobutyric acid ethyl ester (**19**)

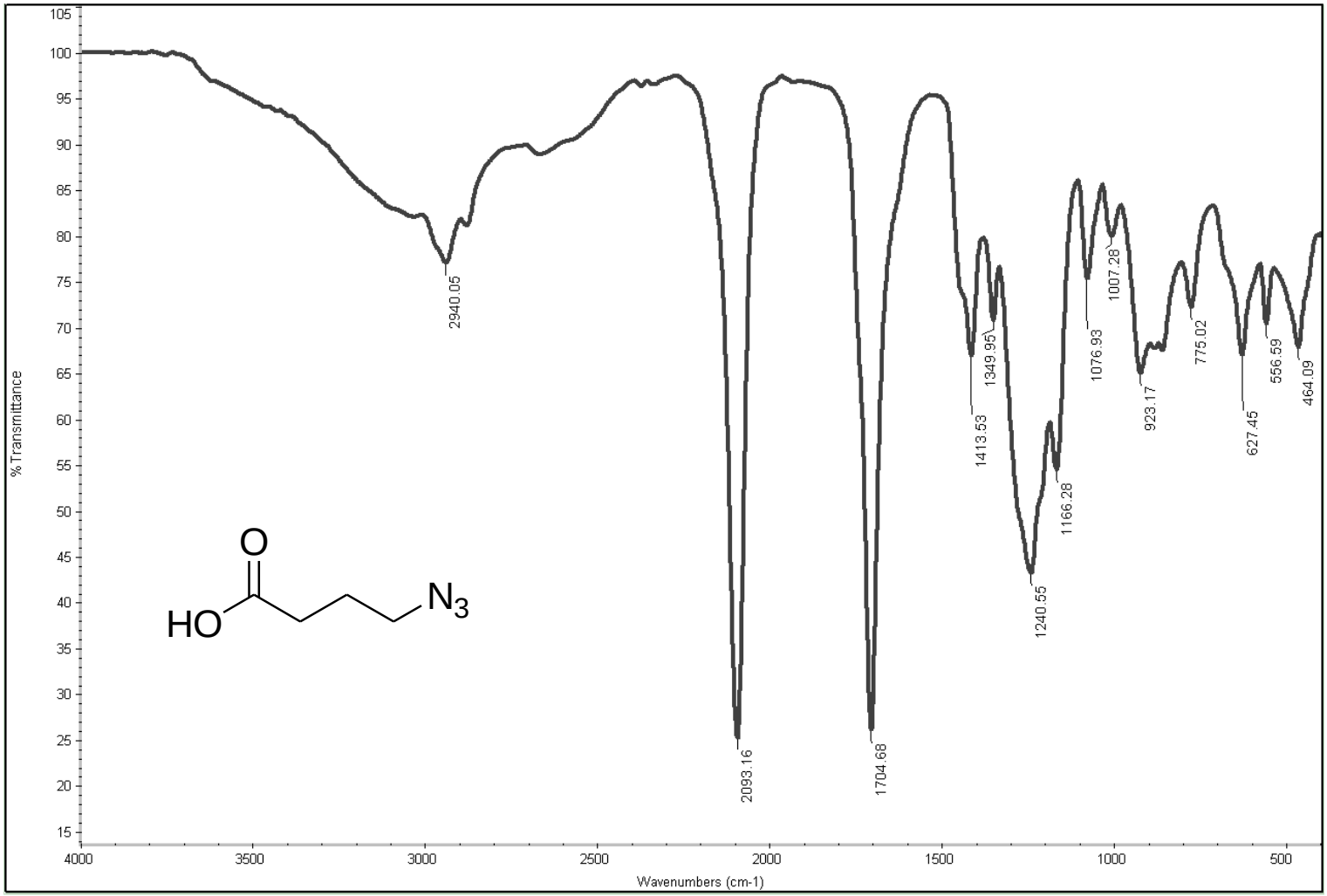

Figure A.12. IR spectrum of 4-azidobutanoic acid (**20**)

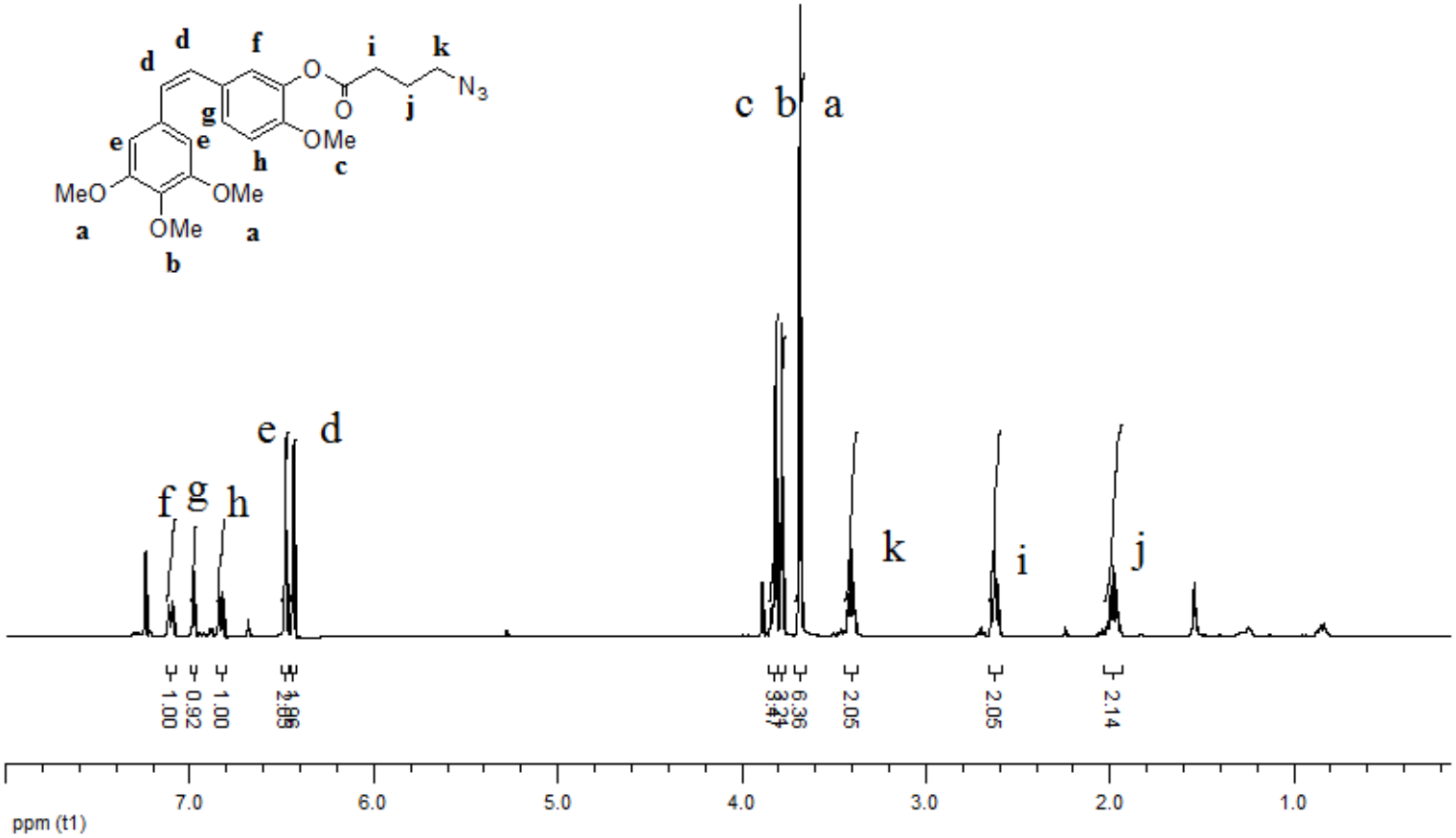

Figure A.13. ^{1}H NMR spectrum of C-N_3 **16**

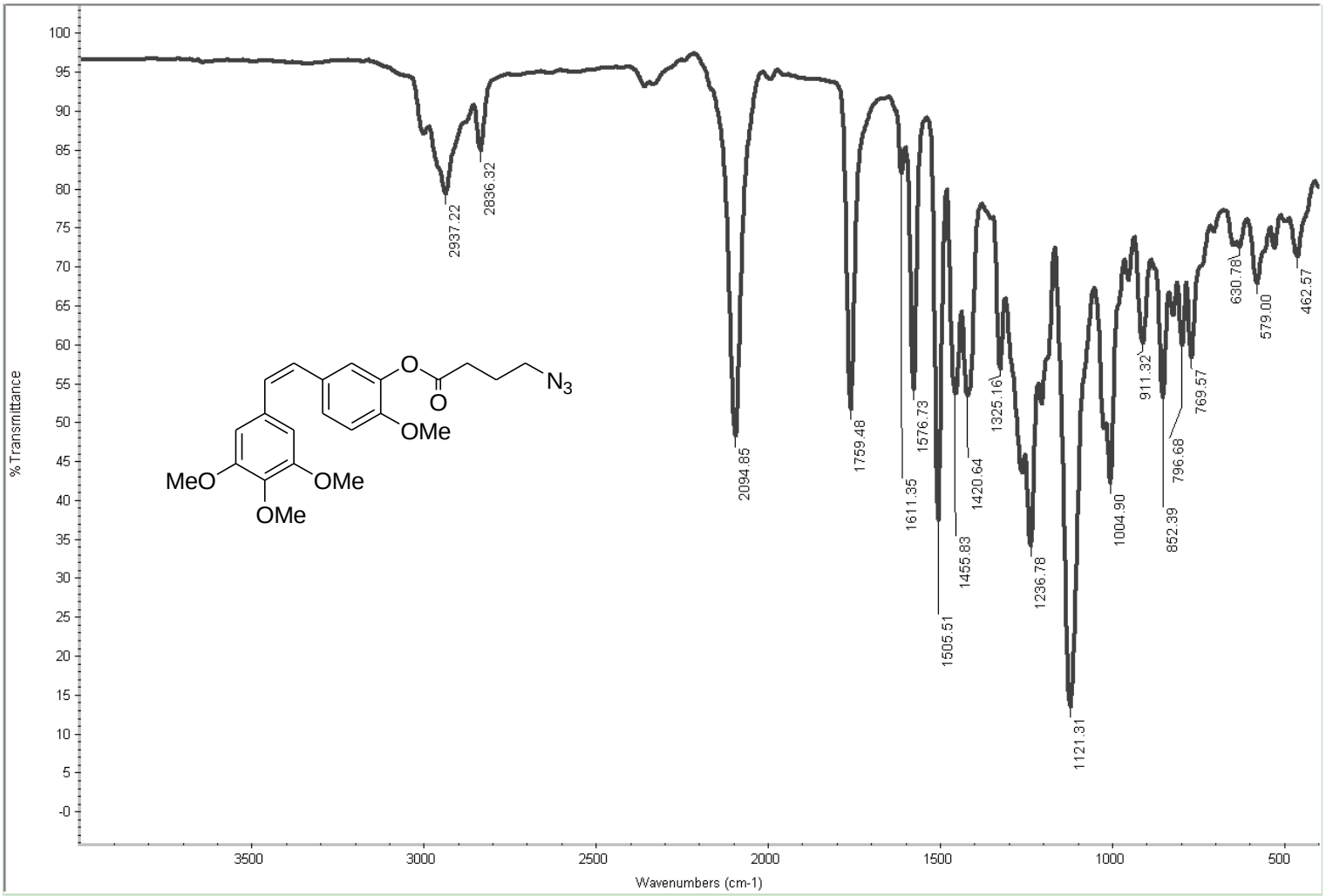

Figure A.14. IR spectrum of C-N_3 **16**

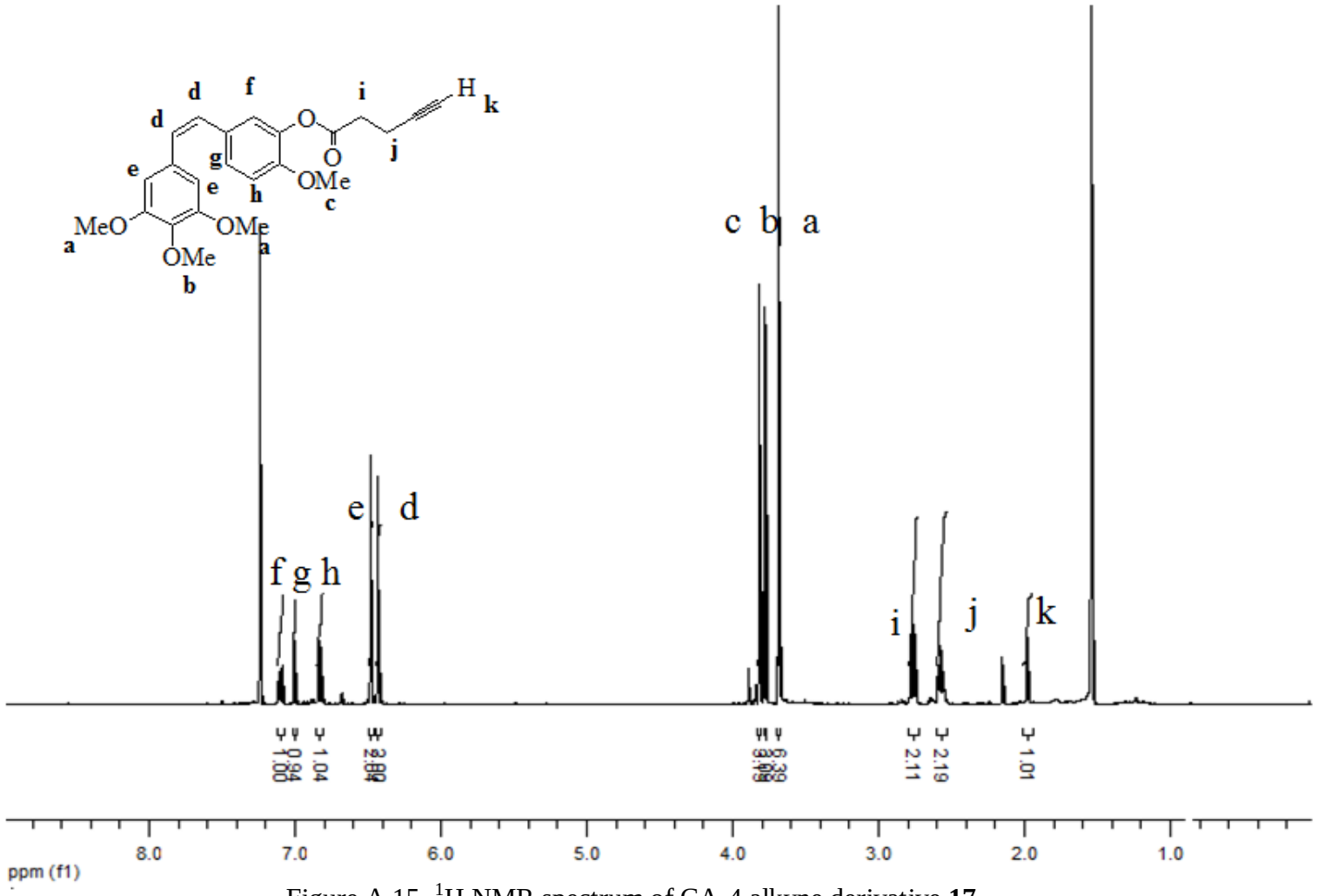

Figure A.15. ^{1}H NMR spectrum of CA-4 alkyne derivative **17**

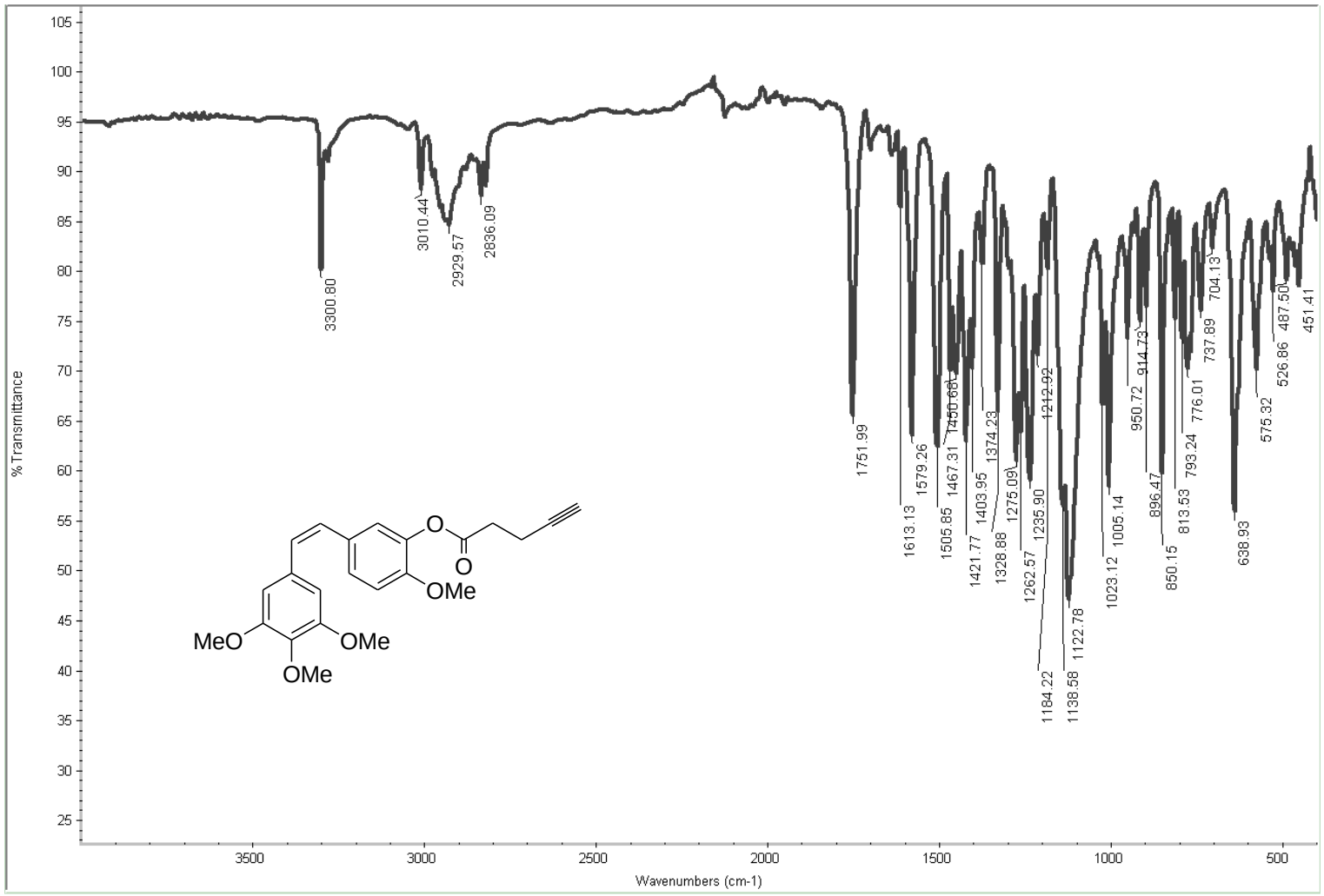

Figure A.16. IR spectrum of CA-4 alkyne derivative **17**

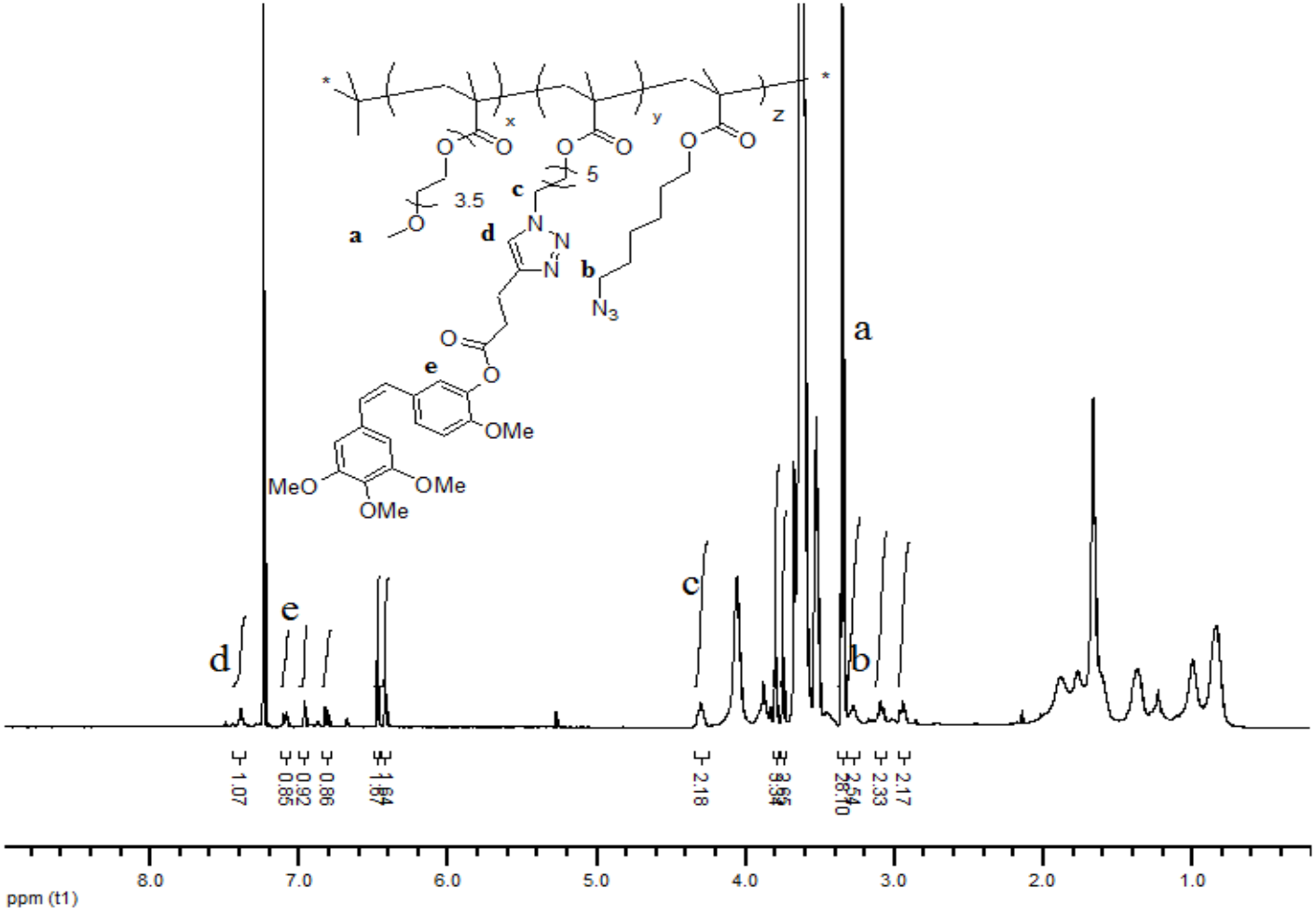

Figure A.17. ^{1}H NMR spectrum of PEG-AHMA- C-≡ conjugate **21-a**

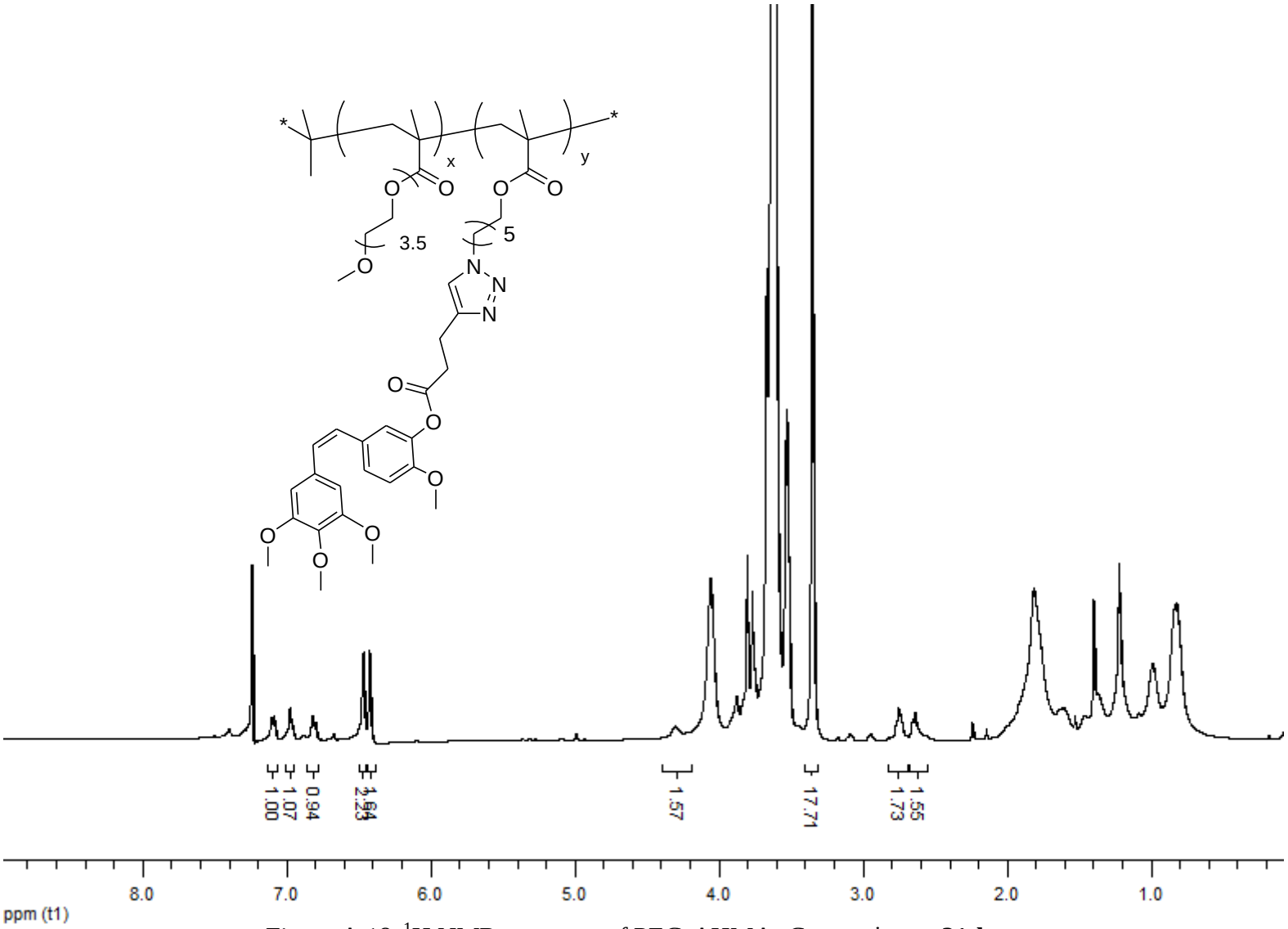

Figure A.18. ^{1}H NMR spectrum of PEG-AHMA- C-≡ conjugate **21-b**

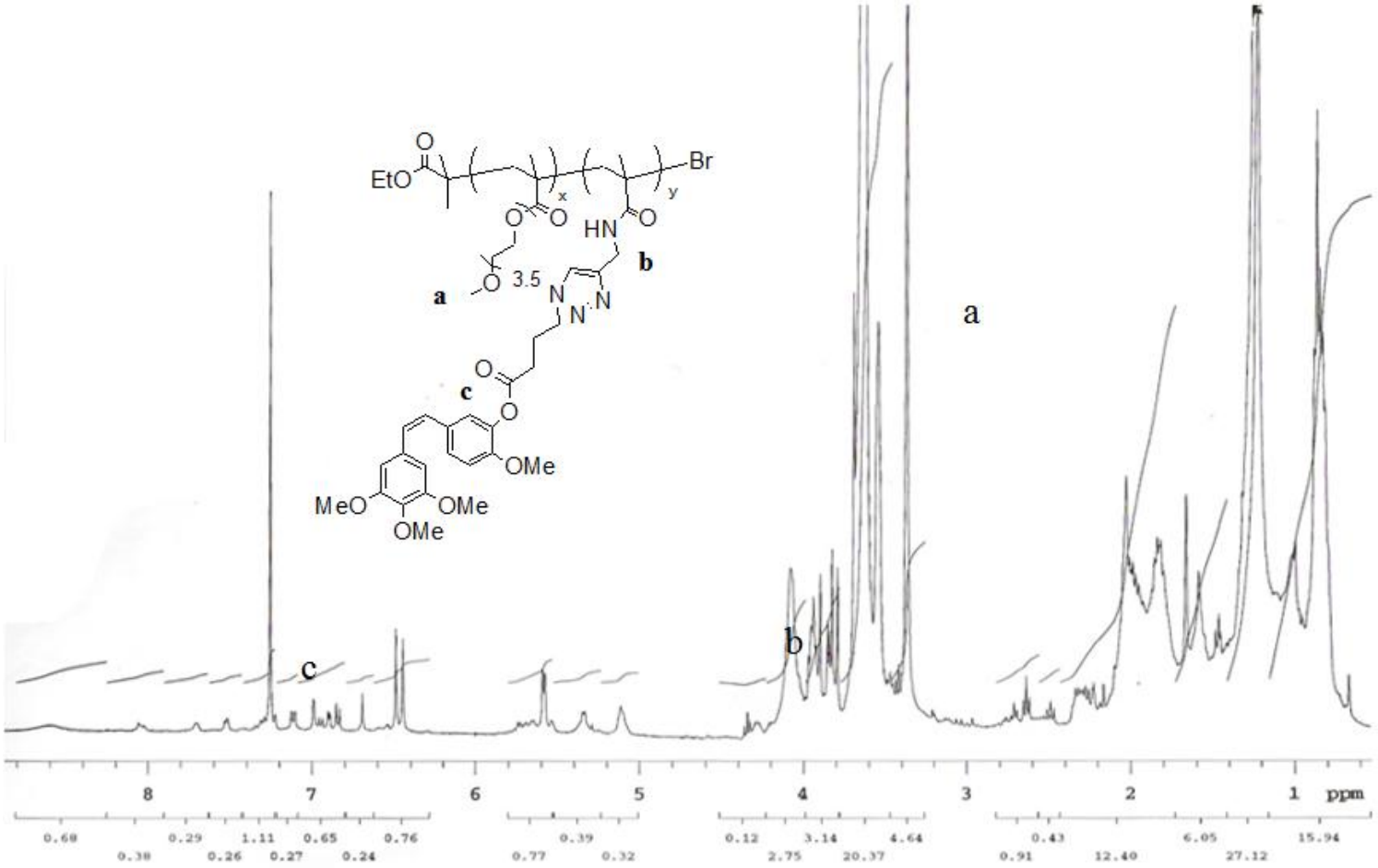

Figure A.19 ^{1}H-NMR spectrum of Poly- C-N_3 conjugate **22**

REFERENCES

1. http://www.cancer.gov/cancertopics/cancerlibrary/what-is-cancer, 2010.

2. Segal E., Satchi-Fainaro R., *Advanced Drug Delivery Reviews*, 61, 1159–1176, 2009.

3. Liekens S., Clercq E. D., Neyts J., *Biochemical Pharmacology*, 61, 253–270, 2001.

4. http://onctalk.com/wp-content/uploads/2008/01/angiogenesis-summary.jpg., 2010.

5. Fox M. E., Szoka F. C., and Fr´echet. J. M., *Accounts of Chemical Research*, Vol. 42, No. 8 1141-1151, August 2009.

6. Iyer A. K., Khaled G., Fang J. and Maeda H., *Drug Discovery Today*, Volume 11, Numbers 17/18, September 2006.

7. Liu S., Maheshwari R., and Kiick K. L., *Macromolecules*, 42, 3-13, 2009.

8. Duncan R., *Nature reviews - Drug Discovery*, Volume 2, May 2003.

9. Greco F., Vicent M. J., *Advanced Drug Delivery Reviews*, 61, 1203–1213, 2009.

10. Singer, J. W., *Journal of Controlled Release*, Vol. 109, pp. 120–126, 2005.

11. H. Maeda et al., *European Journal of Pharmaceutics and Biopharmaceutics*, Vol. 71, pp. 409–419, 2009.

12. Tron G. C., Pirali T., Sorba G., Pagliai F., Busacca S., and Genazzani A. A., *Journal of Medicinal Chemistry*, Vol. 49, No. 11, 2006.

13. http://www.drugdevelopmenttechnology.com/projects/anticancerdrug/anticancer drug1. html, jpg, 2010.

14. Anurag, Roy R. K., Sharma P. P., *Int.J. PharmTech Res.*, Vol. 1, No. 4, 1462-1469, 2009.

15. http://oxigene.com/our_science/how_our_drugs_work/, 2010.

16. Iyer S., Chaplin D. J., Rosenthal D. S., Boulares A. M., Li L.Y., and Smulson M. E., *Cancer Research*, Vol. 58, pp. 4510-4515, 1998.

17. Bonezzi K., Taraboletti G., Borsotti P., Bellina F., Rossi R., and Giavazzi R., *Journal of Medicinal Chemistry*, 4000, Vol. 300, No. 20, 2009.

18. Sieman D. W., Chaplin D. J., Walicke P. A., *Expert Opin. Investig. Drugs*, 2009.

19. http://www.oxigene.com/pipeline/clinical_trials, 2010.

20. Gaukroger K., Hadfield J. A., Hepworth L. A, Lawrence N. J, Mc Gown. A. T., *J.Org.Chem*, Vol. 66, No. 24, 2001.

21. Reux B., Weber V., Galmier M-J., Borel M., Madesclaire M., Madelmont J. C., Debiton E., and Coudert P., *Bioorg. Med. Chem.*, 16, 5004-5020, 2008.